CHAPTER

4

Dynamics

4.1 INTRODUCTION

Biped locomotion is a complex dynamical motion/force phenomenon. Healthy humans can keep balance while walking due to skills acquired by learning. Under such skills, proper force/moment components can be impressed on the stance foot during the single-leg support phase, or at both feet, during the double-leg support phase. The respective reaction force/moments are used then to propel the body in a desired way. The impressed force/moment components stem from the force of gravity and the inertial force/moments generated by the acceleration of the total CoM and the angular accelerations of the body segments. Friction forces at the foot contacts and impact forces at foot landing have to be considered as well. During walking, the stability of the gait is the main concern. Fortunate enough, though, walking on regular ground is a periodic phenomenon. Thus, despite its complexity, biped locomotion can be modeled with simplified dynamical models such as the linear inverted pendulum (LIP) or the table-cart models [54].

The situation changes dramatically, however, when the cyclic motion process is subjected to irregular inputs. Recently, research has focused on the role of external disturbances during walking or while standing upright. Avoiding a fall, e.g. by modifying the length of the step or by making a side step in the direction of the disturbance, is highly desirable. The robot should also be able to walk over unknown and varying irregular terrain, e.g. as in disaster-related environments. This obviously cannot be done with a perfect periodic gait. Research results suggest that in these cases, the simple dynamical models mentioned above are insufficient. Enhanced simplified models may still be used for motion generation in the presence of such external perturbations [146], but for stabilization purposes a complete dynamical model might be needed [149]. Such a model is also advantageous in multifinger and dual-arm object manipulation, as well as in whole-body motions like jumping, kicking a ball, and so on.

This chapter discusses dynamical models of biped humanoid robots. Such models are used in the analysis and model-based control. The chapter is organized in fourteen sections. In the following Section 4.2, the focus is on the characterization of humanoid robots as underactuated systems with a "floating" base. Simple underactuated models on the plane and in 3D are discussed in Section 4.3 and Section 4.4, respectively. The dynamic modeling of fixed-base manipulators is highlighted in Section 4.5. In Section 4.6, the first-order differential motion relations of a free-floating manipulator in zero gravity are analyzed from the viewpoint of spatial momentum. In Section 4.7, the concept of the Reaction Null Space (RNS) is introduced. The equation of motion of a free-floating manipulator is discussed in Section 4.8. A solution

https://doi.org/10.1016/B978-0-12-804560-2.00011-0

to the inverse dynamics is derived with the help of the RNS in Section 4.9. The spatial momentum of a humanoid robot is discussed in Section 4.10. In Section 4.11, the equation of motion of a humanoid robot is represented in terms of different types of quasivelocities. Constraint elimination methods for constrained multibody systems are introduced in Section 4.12. Reduced-form representations of the equation of motion of a humanoid robot are discussed in Section 4.13. Section 4.14 explores inverse dynamics solutions.

It is assumed that the reader is familiar with the basic concepts of rigid-body mechanics in 3D space, such as mass and inertia characteristics of a rigid body, the CoM and rotational dynamics, the concepts of momentum and angular momentum, and the equation of motion. Also, knowledge about fixed-base robot dynamical relations in 3D space, including analytical and recursive methods of forward and inverse robot dynamics, is a prerequisite.

4.2 UNDERACTUATED ROBOT DYNAMICS

Mechatronic systems having fewer actuators than the number of generalized coordinates are called *underactuated systems*. There is a variety of such systems, including humanoid robots. Underactuated systems can be classified into two main groups [167]. The first one is characterized by passive DoFs *distributed* throughout the kinematic chain. Flexible-link manipulators composed of slender, light-weight links are one representative example. Their joints are actuated, the passive DoFs stemming from elastic deflections in the links. These manipulators were the first underactuated manipulators to be studied extensively, since the mid-1970s [13,63]. Another representative example are manipulators with flexible joints, comprising the so-called series-elastic actuators. Each joint is actuated but there is an elastic element (e.g. a torsional spring) that yields the passive DoF [75]. Flexible-joint manipulators have drawn a lot of attention due to their potential for ensuring safety in physical human/robot interaction tasks. Successful implementations have been reported in [48,2]. More recently, implementations in humanoid robots have appeared as well [34,150,30]. Furthermore, there are underactuated manipulators with distributed passive DoFs that comprise active as well as fully passive joints. These type of underactuated manipulators were studied in the beginning of the 1990s, motivated by "minimalism" [4,88]. Finally, there is a class of underactuated manipulators comprising passive joints exclusively. Motion is induced by reaction wheels (the so-called torque-unit manipulator) [111,110], or by control momentum gyros [17]. These type of underactuated manipulators have been considered for use in microgravity environments as space robots. Similarly, motion of the so-called "Gyrobot" is induced by a gyrating link [38]. The desired configuration is attained with the help of brakes at the passive joints.

The second major group of underactuated systems is characterized with passive DoFs *concentrated* at the root (base) link of the kinematic chain. Such systems can be modeled by connecting the base link via a virtual rigid-body (6-DoF) joint to inertial ground. Hence, there is a "floating" base, as in the case of a humanoid robot. Other representative examples within this subclass include spacecraft and free-flying space robots, aerial (vertical take-off and landing [VTOL] aircraft), and marine vehicles (surface and underwater), as well as manipulators mounted on a flexible base. The "floating" property of the base depends on the type of environment and the respective interaction forces. Apparently, the environment conditions are

quite different. This complicates the development of a uniform modeling and control approach.

Assuming a total of $n = n_p + n_a$ DoFs, where the p and a subscripts denote quantities related to the passive and active joints, respectively, the equation of motion representing a "generic" underactuated system can be written as

$$\begin{bmatrix} \boldsymbol{M}_p & \boldsymbol{M}_{pa} \\ \boldsymbol{M}_{pa}^T & \boldsymbol{M}_a \end{bmatrix} \begin{bmatrix} \ddot{\boldsymbol{q}}_p \\ \ddot{\boldsymbol{q}}_a \end{bmatrix} + \begin{bmatrix} \boldsymbol{c}_p \\ \boldsymbol{c}_a \end{bmatrix} + \begin{bmatrix} \boldsymbol{g}_p \\ \boldsymbol{g}_a \end{bmatrix} = \begin{bmatrix} \boldsymbol{0} \\ \mathcal{F}_a \end{bmatrix}, \tag{4.1}$$

where $\boldsymbol{q}_p \in \Re^{n_p}$ and $\boldsymbol{q}_a \in \Re^{n_a}$ denote the generalized coordinates, $\mathcal{F}_a \in \Re^{n_a}$ stands for the generalized force, $\boldsymbol{M}_p \in \Re^{n_p \times n_p}$, $\boldsymbol{M}_a \in \Re^{n_a \times n_a}$, and $\boldsymbol{M}_{pa} \in \Re^{n_p \times n_a}$ are submatrices of the system inertia matrix, $\boldsymbol{c}_p \in \Re^{n_p}$ and $\boldsymbol{c}_a \in \Re^{n_a}$ denote the nonlinear velocity-dependent forces, and $\boldsymbol{g}_p \in \Re^{n_p}$ and $\boldsymbol{g}_a \in \Re^{n_a}$ are the gravity-dependent forces. Note that no other external forces than gravity are taken in consideration at this point.

The matrix-vector form of the above equation of motion clearly displays the passive/active DoF structure of an underactuated manipulator with concentrated passive-joint disposition, e.g. a free-floating space robot or a humanoid robot (without elasticity in the joints). Especially, the explicit appearance of the inertial coupling between the passive and active DoFs via submatrix $\boldsymbol{M}_{pa}$ is important. This matrix is referred to as the *coupling inertia matrix* [96]. The inertial coupling property plays an important role in control law design as shown in [140]. Input/output *partial feedback linearization* (PFL) is possible, either w.r.t. the actuated coordinates (collocated PFL) or w.r.t. the passive coordinates (noncollocated PFL). The latter is especially interesting since then the internal system dynamics become explicit. These dynamics are quite useful, e.g. for generating *reactionless motion*. The method was first developed for reactionless manipulator control of a free-floating space robot [97,94] and later applied in the balance control of a humanoid robot in response to external disturbances [101]. Further details will be discussed in Section 4.6 and Section 7.6. The above matrix-vector form representation of the equation of motion will be preferred throughout this text in lieu of an often used notation involving a "selection" matrix for the active coordinates (cf. (2.102)). The latter is more compact, but the passive/active structure is hidden.

It is important to emphasize that the behavior of the above-mentioned underactuated systems, stemming from their unforced dynamics, is quite distinctive. Take as an example the subclass of underactuated manipulators with distributed active and fully passive joints. A simple planar 2R manipulator with a passive joint at the root and an active joint at the elbow (the so-called "Acrobot" [46]) behaves quite differently from that of a similar 2R manipulator obtained by exchanging the passive/active roles of the joints (known as the "Pendubot" [137,31]). Furthermore, these two types of passive-joint robots operate within the vertical plane and hence under gravity. If they were to operate on the horizontal plane, and hence under zero gravity, completely different types of behavior would be obtained [53,4,88].

Fewer actuators than the number of generalized coordinates means also fewer control inputs. This is the reason why classic methods of linear control theory, such as continuous time-invariant feedback control for example, cannot be applied to underactuated systems [15]. Efforts made since the 1990s have led to the development of a variety of new control methods. The PFL approach mentioned above is one of them; others are based on nonlinear state feedback, passivity, and energy control, as well as hybrid and switching control

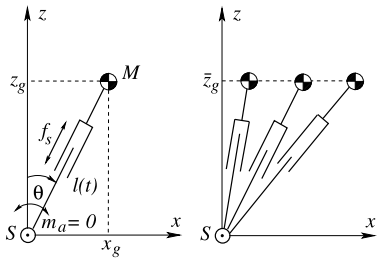

FIGURE 4.1 The motion of the support leg is modeled in the plane (sagittal or frontal). (A) Left: Inverted pendulum with massless leg and varying length. (B) Right: Linear inverted pendulum. The CoM is constrained to move along a line (in this case, a horizontal one): $z_g = \bar{z}_g = \text{const}$ or $z_g = kz_x$, $k = \text{const}$. The ankle joint S is assumed passive. The stroke force f_s is actively controlled.

[53,136,123,104]. The reason for such diversity in control methods is that control law design for underactuated manipulators relies on a deeper understanding of their distinct dynamics, as explained above. Humanoid robots are no exception.

4.3 SIMPLE UNDERACTUATED MODELS ON THE PLANE

The dynamics of humanoid robots are essential for their control. Multi-DoF dynamic models are quite complex though. Therefore, control law design has always relied on simplified models. For instance, for gait pattern generation and control within a restricted environment, e.g. walking on a level ground, very simple models on the plane have proven useful. These will be introduced below.

4.3.1 The Linear Inverted Pendulum Model

The linear inverted pendulum (LIP) and cart-on-table are simple models used to design balance controllers for a number of humanoid robots [54]. The availability of a closed-form solution for these models facilitates analysis and cyclic motion generation for gaits on level ground, as well as control law design for gait stabilization. Real-time implementation can also be ensured. The underlying model is an inverted pendulum (IP) with point mass M at the end of a massless leg of variable length $l(t)$, as shown in Fig. 4.1A. The IP is used as a model of the support leg during gait in the sagittal plane. The varying leg length, actively controlled with stroke force f_s, accounts for the motion in the knee joint. The mass point represents the total mass of the robot concentrated at the hip joint. The pendulum is pivoted at the ankle joint which is assumed to be passive (nonactuated). Thus, the model represents a simple underactuated system.

To derive the equation of motion, it is convenient to use polar coordinates as generalized coordinates; such coordinates are in full harmony with the physical system. Denote by $\theta(t)$ the angular displacement from the vertical. The angular coordinate is passive by assumption; hence, the respective generalized force component (moment m_a at support point S) is zero.

The other generalized force component is the leg stroke force f_s. The equation of motion is

$$\begin{aligned} Ml^2\ddot{\theta} + 2Ml\dot{l}\dot{\theta} - Mlg\sin\theta = 0, \\ M\ddot{l} + Ml\dot{\theta}^2 + Mg\cos\theta = f_s, \end{aligned} \tag{4.2}$$

where g denotes the gravity acceleration. The vector matrix form of this equation is:

$$\begin{bmatrix} M_p & 0 \\ 0 & M_a \end{bmatrix} \begin{bmatrix} \ddot{\theta} \\ \ddot{l} \end{bmatrix} + \begin{bmatrix} c_p \\ c_a \end{bmatrix} + \begin{bmatrix} g_p \\ g_a \end{bmatrix} = \begin{bmatrix} 0 \\ f_s \end{bmatrix}, \tag{4.3}$$

where $M_p = Ml^2$ and $M_a = M$ stand for the inertia/mass properties, $c_p = 2Ml\dot{l}\dot{\theta}$ and $c_a = Ml\dot{\theta}^2$ are the nonlinear velocity-dependent forces, and $g_p = -Mlg\sin\theta$ and $g_a = Mg\cos\theta$ are the gravity force terms, g denoting the acceleration of the gravity force. The passive/active structure, revealed with (4.1), is immediately apparent.

Note that in the above equation, there is no *inertial coupling* between the generalized coordinates, i.e. $M_{pa} = M_{ap} = 0$. Hence, under linearization, two decoupled differential equations would be obtained. The *linear* IP model, however, does not rely upon linearization. Instead, the following *task-based motion constraint* is applied [146]: keep the vertical position of the CoM constant, so $z_g \equiv \bar{z}_g = \text{const}$. This constraint yields the important advantage of having a closed-form solution to the nonlinear system.

To impose the $\bar{z}_g = \text{const}$ constraint, it is convenient to rewrite the equation of motion in Cartesian coordinates, so we have

$$\begin{aligned} M\ddot{x}_g = |f_s|\sin\theta, \\ M(\ddot{z}_g + g) = |f_s|\cos\theta. \end{aligned} \tag{4.4}$$

Here x_g is the projection of the CoM on the ground, henceforth referred to as the *gCoM*. The two terms on the r.h.s. represent the components of a vector, denoted as $\boldsymbol{f}_r$. This vector is referred to as the Ground Reaction Force (GRF) vector.

Furthermore, with $\ddot{z}_g = 0$, the stroke force f_s can be eliminated from the above equations to obtain the following linear ordinary differential equation (ODE):

$$\ddot{x}_g = \bar{\omega}^2 x_g, \tag{4.5}$$

where $\bar{\omega} = \sqrt{g/\bar{z}_g}$ is the (constant) natural angular frequency of the LIP. The closed-form solution to this equation is [54]

$$x_g(t) = x_{g0}\cosh(\bar{\omega}t) + \frac{v_{g0}}{\bar{\omega}}\sinh(\bar{\omega}t), \tag{4.6}$$

$x_{g0} = x_g(0)$, $v_{g0} = \dot{x}_g(0)$ denoting the initial values. The above equation of motion facilitates gait generation on level ground with the appropriate timing [58,54]. It should be noted, though, that the resulting gait is with bent knees. Such gait lacks efficiency in terms of energy [25]. Also, the appearance of the gait is "ape-like," i.e. it is quite different from the erect human gait.

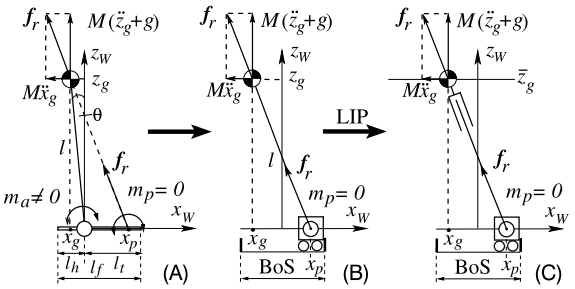

FIGURE 4.2 IP type models with BoS constraint $l_f = l_h + l_t$ (the foot length). (A) Nonlinear (constant-length) IP-on-foot model. The ankle torque ($m_a \neq 0$) alters the GRM, thereby displacing the CoP and accelerating/decelerating the CoM. (B) Nonlinear (constant-length) IP-on-cart model. The CoM horizontal motion is determined by the displacement of the cart, associated with that of the CoP. (C) Variable-length, constant-height LIP-on-cart model. In all models, the GRF acts along the line connecting the CoP and the CoM.

4.3.2 Foot Modeling: CoM Dynamics Driven by the Center of Pressure

The LIP model can be improved by adding a model of the foot. It is assumed that the foot is in multipoint/line contact with the supporting ground. The foot serves as an interface for the impressed/reaction forces that act via the contact points. Note that the resultant force is the GRF, $\boldsymbol{f}_r$. This force is applied at a specific point called Center of Pressure (CoP). This situation is depicted in Fig. 4.2A, where x_p denotes the CoP. In the case of multiple links in contact with the environment, CoPs are defined for each link. These CoPs exist only within the Base-of-Support (BoS) boundaries of the links in contact.

A number of studies in the field of biomechanics have clarified the important role of the CoP in human balance control [85,10,162]. The importance stems from the fact that the tangential components of the Ground Reaction Moment (GRM) are zero at this point. Thus, the location of the CoP within the BoS can be used as an indicator of contact stability. Assuming an unknown external disturbance, the contact will be more stable when the CoP is in the vicinity of the BoS center rather than in that of the BoS boundaries. Further insight into stability issues are presented in Chapter 5.

In the special case of feet support on flat ground, i.e. such as with a double-stance posture, a *net CoP* is defined [162]. The net CoP is not necessarily located within the BoS of a single foot; it may be located between the feet. Nevertheless, such location still falls within the double-stance BoS, which is defined as the convex hull of all contact points on the flat ground [39,120,54]. It is worth noting that in the early studies on humanoid robots, the special case of flat ground was exclusively considered and the term "zero-moment point" (ZMP) was coined [158]. On flat ground, the ZMP is identical to the CoP/net CoP (in the cases of single/double stance). On nonflat ground, though, these points do not coincide [120]. In the following discussion, whenever ambiguity is avoidable, the terms CoP and ZMP will be used alternatively.

Linearized IP-on-Foot Model

A constant-length (nonlinear) IP model attached to a foot is shown in Fig. 4.2A. The GRF $\boldsymbol{f}_r$ acts at the CoP, x_p, along the line determined by the CoP and the CoM. The two components

of this force result from gravity and the CoM acceleration. Note that the moment at the CoP is zero. Note also that the ankle joint is not anymore passive, as it was with the LIP model. The ankle torque $m_a \neq 0$ alters both, the CoM acceleration and the CoP. The equation of motion of the simple IP is

$$Ml^2\ddot{\theta} = Mgl\sin\theta + m_a. \tag{4.7}$$

The CoP is determined from the GRM balance equation as

$$x_p = -\frac{m_a}{M(g+\ddot{z}_g)} \overset{(4.7)}{=} \frac{gl\sin\theta - l^2\ddot{\theta}}{g - l\dot{\theta}^2\cos\theta - l\ddot{\theta}\sin\theta}. \tag{4.8}$$

Furthermore, since the foot length, l_f, (the BoS) is limited, the pendulum cannot deviate significantly from the vertical. Otherwise, the foot will begin to rotate and the pendulum will eventually tip over. In the following discussion it is assumed that the deviation is limited, s.t. the foot remains always in full contact with the ground. The equation of motion can then be linearized around the vertical as

$$\ddot{\theta} = \omega^2\theta + \frac{m_a}{Ml^2}. \tag{4.9}$$

Here $\omega \equiv \omega_{IP} = \sqrt{g/l}$ denotes the natural angular frequency of the pendulum.

The linearized IP-on-foot model has been employed for human balance stability analysis in the field of biomechanics [162,113]. The equation of motion (4.9) has also been used in the field of humanoid robotics [6]. Most works make use, however, of a representation in Cartesian coordinates. Since the aim is to gain insight into the role of the CoP, the focus is on the component in the horizontal direction, i.e.

$$\ddot{x}_g = \omega^2(x_g - x_p), \tag{4.10}$$

or

$$\ddot{x}_g - \omega^2 x_g = -\omega^2 x_p. \tag{4.11}$$

Apparently, the CoP plays the role of a forcing term for the gCoM dynamics.

In the special case of a fixed CoP, denoted as $\bar{x}_p$, the solution to the above equation can be obtained in closed-form. We have

$$x_g(t) = \left(x_{g0} - \bar{x}_p\right)\cosh(\omega t) + \frac{v_{g0}}{\omega}\sinh(\omega t) + \bar{x}_p \tag{4.12}$$

$$= \frac{1}{2}\left(x_{g0} - \bar{x}_p + \frac{v_{g0}}{\omega}\right)e^{\omega t} + \frac{1}{2}\left(x_{g0} - \bar{x}_p + \frac{v_{g0}}{\omega}\right)e^{-\omega t} + \bar{x}_p. \tag{4.13}$$

This equation plays an important role in balance stability analysis (cf. Chapter 5).

IP-on-Cart Model

The ODE (4.11) clarifies that the CoM motion trajectory can be controlled via the forcing term, i.e. by appropriate position control of the CoP. This approach resembles the way of

balancing a stick on the palm. The respective model is shown in Fig. 4.2B. This model is widely used in the field of control under the name "IP-on-cart model." Note that the distance between the CoM and the cart (the CoP) is assumed constant. The equation of motion in the horizontal direction is of the same form as (4.11). Note, however, that the coefficient ω^2 is not anymore constant; now we have

$$\omega(t) = \sqrt{\frac{\ddot{z}_g + g}{z_g - z_p}}. \tag{4.14}$$

The vertical CoP coordinate z_p is usually assumed constant (e.g. zero on a level ground). Solving (4.11) for the CoP with the above expression for ω, one obtains

$$x_p = x_g - \frac{\ddot{x}_g}{\ddot{z}_g + g} z_g = x_g - \frac{f_{rx}}{f_{rz}} z_g. \tag{4.15}$$

Here f_{rx} and f_{rz} denote the two components of the GRF. This equation is used for balance control under the name "ZMP manipulation" or "indirect ZMP" control [80,144], as explained in Section 5.4.

LIP-on-Cart Model

A variable ω, as in (4.14), complicates the analysis since the solution cannot be obtained in such a simple form as that for the linearized IP model. To alleviate this problem, the task-based (LIP) constraint

$$z_g = \bar{z}_g = \text{const} \Rightarrow \omega \equiv \bar{\omega} = \sqrt{g/\bar{z}_g} = \text{const} \tag{4.16}$$

is imposed. The resulting model is shown in Fig. 4.2C. Note that the form of the equation of motion, (4.11), will be preserved. Thus, any displacement of the cart (or equivalently, the CoP) will alter the horizontal CoM acceleration via the term $\bar{\omega}^2 x_p$. This also implies respective changes in the direction of the GRF. We have

$$\frac{f_{rx}}{Mg} = \frac{x_g - x_p}{\bar{z}_g} \tag{4.17}$$

and hence, of the GRM, i.e. $(x_g - x_p)Mg = \bar{z}_g f_{rx}$. Note that with this model, the vertical component of the GRF equals the gravity force; $f_{rz} = Mg$. Furthermore, using (4.8) with $\ddot{z}_g = 0$, the equation of motion can be represented as

$$\ddot{x}_g = \omega^2 x_g + \frac{m_a}{M\bar{z}_g}. \tag{4.18}$$

The LIP-on-cart model is used in numerous studies on balance control. Further details will be presented in Chapter 5.

The LIP constraint is also used in the so-called "cart-on-table" model [55,54], shown in Fig. 4.3. The equation of motion of the cart-on-table model is identical to that of the IP models, (4.11). The difference lies only in the interpretation, when used in controller design. In

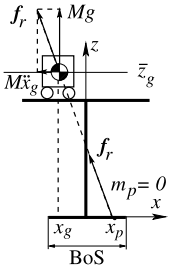

FIGURE 4.3 Cart-on-table model: the CoP location is determined by the horizontal acceleration component of the CoM.

fact, all these models demonstrate that *balance control can be based on the relative CoP-CoM motion*. In the table-cart model, the CoM motion trajectory is used as the input while the CoP position is subject to control. This is in contrast to the IP models, where the CoP is used as control input, as clarified above.

CoP manipulation via CoM acceleration has also been exploited under the so-called "angular momentum inducing IP model" (AMPM) [62]. Through the CoP relation, an additional moment (a controllable feedforward component) stemming from the rate of change of the *moment of momentum* of the pendulum is imposed on the foot. It is important to note that with this enhancement, a closed-form solution is still available to facilitate gait planning and control with the capability of dealing with external disturbances. Note also that the term "moment of momentum" is deliberately introduced here to distinguish this type of angular momentum from the "intrinsic" (cf. [32], p. 31) or "centroidal" angular momentum. The latter can be used to control the imposed moment on the foot as well. This will be addressed in Section 4.3.3.

4.3.3 Linear Reaction Wheel Pendulum Model and Centroidal Moment Pivot

With the LIP model, a feedforward control component to be used in CoP-based gait generation can be obtained. Then, an appropriate balance of the reactive force components at the foot that result from the gravity and inertia forces imposed by the vertical and horizontal acceleration of the CoM, respectively, can be ensured. The inclusion of the CoP into the model leads to the desirable property of a controllable moment at the foot, as already explained with the cart-on-table model. It should also be noted that this property can be obtained in an alternative way, via a controlled change of *centroidal* angular momentum. The simplest way to accomplish this is with the *reaction wheel pendulum* (RWP) model. The RWP is a simple pendulum with a massless leg of constant length, comprising a reaction wheel (RW) at the CoM. Controllable angular acceleration/deceleration of the RW induces a variation in the joint rate of the passive pivot joint, via inertial coupling. In this way, the stability of the system can be improved.

The RWP was introduced in the beginning of the century [138] and studied extensively as a landmark underactuated example in nonlinear control [12]. The RWP has been adopted in humanoid robotics as well, e.g. as a means to determine appropriate foot locations for a

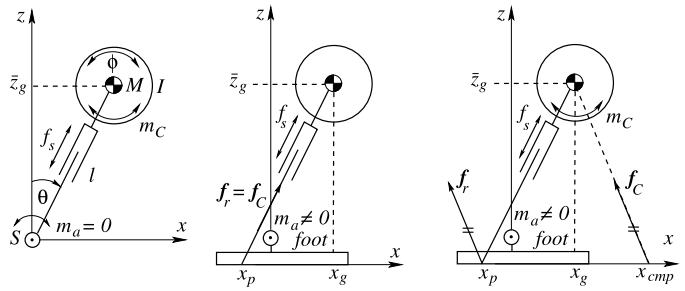

FIGURE 4.4 Linear RWP models. (A) Left: Ankle joint as passive joint. (B) Middle: The linear RWP-foot model is identical to the LIP when the RW torque is zero. (C) Right: A nonzero RW moment m_C alters the direction of the GRF $\boldsymbol{f}_r$ so that its line of action deviates from the CoM. The centroidal (reaction) force $\boldsymbol{f}_C$ is in the same direction as the GRF but its line of action passes through the CoM. The application point of $\boldsymbol{f}_C$ defines the centroidal moment pivot (CMP) [40,120].

reactive-step strategy, the so-called "Capture point" [121]. As with the LIP model, the leg length of the RWP is made variable (cf. Fig. 4.4A). The general form of the equation of motion for such system is

$$\begin{bmatrix} M_p & \boldsymbol{M}_{pa} \\ \boldsymbol{M}_{pa}^T & \boldsymbol{M}_a \end{bmatrix} \begin{bmatrix} \ddot{q}_p \\ \ddot{\boldsymbol{q}}_a \end{bmatrix} + \begin{bmatrix} c_p \\ \boldsymbol{c}_a \end{bmatrix} + \begin{bmatrix} g_p \\ \boldsymbol{g}_a \end{bmatrix} = \begin{bmatrix} 0 \\ \mathcal{F}^a \end{bmatrix}. \tag{4.19}$$

Here, $q_p = \theta$, $\boldsymbol{q}_a = \begin{bmatrix} l & \phi \end{bmatrix}^T$ denote the generalized coordinates, $\mathcal{F}^a = \begin{bmatrix} f_s & m_c \end{bmatrix}^T$ is the generalized force, $M_p = Ml^2$, $\boldsymbol{M}_{pa} = \begin{bmatrix} 0 & I \end{bmatrix}$, $\boldsymbol{M}_a = \text{diag}\begin{bmatrix} m & I \end{bmatrix}$ are the inertia matrix components, I denotes the RW moment of inertia, $c_p = 2Ml\dot{l}\dot{\theta}$, $\boldsymbol{c}_a = \begin{bmatrix} Ml\dot{\theta}^2 & 0 \end{bmatrix}^T$ are the nonlinear velocity-dependent forces, and $g_p = -Mgl\sin\theta$, $\boldsymbol{g}_a = \begin{bmatrix} Mg\cos\theta & 0 \end{bmatrix}^T$ are the gravity-dependent forces. Denote by l_y the angular momentum w.r.t. the CoM, i.e. the *centroidal angular momentum*. The RW torque, m_c, alters the centroidal angular momentum as $\frac{d}{dt}l_{cy} = \frac{d}{dt}I\dot{\phi} = m_c$. Note that the RW rotation angle ϕ represents a *cyclic* or *ignorable* generalized coordinate. It is known that the Lagrangian is independent of such coordinates and that the respective momentum will be conserved [65]. This is the essence of the inertia coupling. As already explained, according to the partial-feedback linearization approach, the (linear) inertia coupling for the passive coordinate (pendulum rotation θ) is essential for stability. As apparent from the coupling inertia matrix (row matrix $\boldsymbol{M}_{pa}$), the coupling is realized via the RW moment $I\ddot{\phi}$.

To impose the task-based LIP constraint, rewrite the equation of motion in Cartesian coordinates, i.e.

$$M\ddot{x}_g = |f_s|\sin\theta - \frac{m_c}{l}\cos\theta = f_{cx},$$
$$M(\ddot{z}_g + g) = |f_s|\cos\theta + \frac{m_c}{l}\sin\theta = f_{cz}, \tag{4.20}$$
$$I\ddot{\phi} = m_C. \tag{4.21}$$

The vector $\boldsymbol{f}_C = \begin{bmatrix} f_{cx} & f_{cz} \end{bmatrix}^T$, thus defined, acts in the same direction as the GRF vector $\boldsymbol{f}_r$ (cf. Fig. 4.4C). The application points however are different. This follows from the fact that the line of action of the GRF does not pass anymore through the CoM; the direction of $\boldsymbol{f}_r$ depends on the centroidal moment, m_C. The line of action of $\boldsymbol{f}_C$, on the other hand, always passes through the CoM. The point of application of this vector will be clarified in short.

Next, apply constraint $\dot{z}_g = \ddot{z}_g = 0$ to reduce the dimension of the system, i.e.

$$\begin{aligned} \ddot{x}_g &= \omega^2 x_g - \frac{1}{M\bar{z}_g} m_C, \\ \ddot{\phi} &= \frac{1}{I} m_C, \end{aligned} \tag{4.22}$$

where $\omega = \bar{\omega} = \sqrt{g/\bar{z}_g}$. The two equations obtained are the ODEs coupled via m_C. The coupling term on the r.h.s. of (4.22) alters the centroidal angular momentum via $m_C = I\ddot{\phi}$, as explained. When compared to (4.18), it becomes apparent that the role of the centroidal moment m_C is the same as that of the ankle torque m_a: to induce an additional CoM acceleration in the horizontal direction.

The above model facilitates the design of control laws for increased balance stability of the LIP-on-foot model since the CoP can be manipulated with the rate of change of the centroidal angular momentum $\dot{l}_{cy} = I\ddot{\phi}$, in addition to the CoM acceleration. This becomes apparent from the CoP equation. We have

$$\begin{aligned} x_p &= x_g - \frac{\ddot{x}_g}{\omega^2} - \frac{\dot{l}_{cy}}{Mg} \\ &= x_g - \frac{f_{rx}}{f_{rz}} \bar{z}_g - \frac{m_C}{f_{rz}}. \end{aligned} \tag{4.23}$$

When the RW is nonaccelerating, i.e. stationary or spinning with constant angular velocity, then $\ddot{\phi} = 0$ and the relations are the same as with the LIP-on-cart model (cf. Fig. 4.4B). An accelerating RW, on the other hand, alters the direction of the reaction force $\boldsymbol{f}_r$ (cf. Fig. 4.4C). This means that the point on the ground where the moment of the reaction force is zero may be outside the BoS. This point cannot be referred to as the CoP (or ZMP) anymore since there will be a contradiction with the definition of the CoP or ZMP [158]. To alleviate the problem, new terms were introduced as follows. In [40], the point was referred to as the *zero rate of change of angular momentum* point, while in [118] the *zero spin center of pressure* was used. Another term has become commonly accepted, though: *centroidal moment pivot* (CMP) [120]. The CMP is defined by the following equation:

$$x_{cmp} = x_g - \frac{f_{rx}}{f_{rz}} \bar{z}_g. \tag{4.24}$$

Its relation to the CoP is obtained in a straightforward manner from the last two equations as

$$x_{cmp} = x_p + \frac{m_C}{f_{rz}}. \tag{4.25}$$

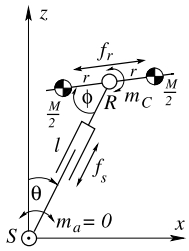

FIGURE 4.5 Model of a planar reaction mass pendulum. The two mass points slide under the action of force f_r, keeping thereby equal distance r from the center point R. Thus, the moment of inertia Mr^2 is controllable via f_r. Note that f_r and m_C are redundant control inputs with regard to the inertia moment $mr^2\ddot{\phi}$ that ensures the inertial coupling with passive coordinate θ.

Apparently, the CoP and the CMP will coincide whenever the centroidal angular momentum is conserved (this condition implies $m_C = 0$).

It would be appropriate to refer to the RWP model as the *linear RWP*. This model has been successfully implemented for gait generation and control of ASIMO [147].

Concluding this subsection, it is worth noting that RWs have been used for a long time as actuators in satellite attitude control systems. An RW can induce a desired variation in attitude via a controlled rate of change in the angular momentum. An RW should not be confused though with a "momentum wheel." The latter is used to store a constant bias momentum that ensures the satellite attitude stabilization against external disturbances and, hence, rotates only in one direction. In this sense, the terminology found in the robotics literature appears inconsistent; terms like "angular momentum pendulum," "flywheel pendulum," or "inertial wheel pendulum" have been used to denote the same model. Based on the above discussion, the term "reaction wheel pendulum" seems to be more appropriate.

4.3.4 Reaction Mass Pendulum Model

The linear RWP model can be further enhanced by resorting to a variable inertia moment $I = I(t)$. The variable centroidal inertia model matches the variable, posture-dependent centroidal dynamics of a humanoid robot to a greater extent. This can be demonstrated with the so-called *reaction mass pendulum* (RMP) model [67,68,130]. The RMP is an underactuated system comprising a pendulum with a massless telescopic leg and a "reaction mass" assembly at the tip of the pendulum. The mass assembly represents the total (constant) mass and the (varying) aggregate inertia of the humanoid in a concentrated form at the CoM.

A planar version of the RMP model is shown in Fig. 4.5. The mass assembly consists of two constant mass points with variable relative position r, symmetric w.r.t. the rotation joint R at the tip of the leg (the "hip" joint). Note that this joint is actuated via torque m_C. The inertia moment around R is adjustable by varying the mass distance r. The general form of the equation of motion is the same as (4.19). We have

$$\begin{bmatrix} M_p & \boldsymbol{M}_{pa} \\ \boldsymbol{M}_{pa}^T & \boldsymbol{M}_a \end{bmatrix} \begin{bmatrix} \ddot{q}_p \\ \ddot{\boldsymbol{q}}_a \end{bmatrix} + \begin{bmatrix} c_p \\ \boldsymbol{c}_a \end{bmatrix} + \begin{bmatrix} g_p \\ \boldsymbol{g}_a \end{bmatrix} = \begin{bmatrix} 0 \\ \mathcal{F}^a \end{bmatrix}, \tag{4.26}$$

where $q_p = \theta$, $\boldsymbol{q}_a = \begin{bmatrix} l & r & \phi \end{bmatrix}^T$ denote the generalized coordinates, $\mathcal{F}^a = \begin{bmatrix} f_s & f_r & m_C \end{bmatrix}^T$ stands for the generalized force, $M_p = M(l^2 + r^2)$, $\boldsymbol{M}_{pa} = \begin{bmatrix} 0 & 0 & Mr^2 \end{bmatrix}$, $\boldsymbol{M}_a = \text{diag}\begin{bmatrix} M & M & Mr^2 \end{bmatrix}$ are the inertia matrix components, $c_p = 2M((l\dot{l} + r\dot{r})\dot{\theta} + r\dot{r}\dot{\phi})$, $\boldsymbol{c}_a = \begin{bmatrix} Ml\dot{\theta}^2 & Mr(\dot{\theta} + \dot{\phi})^2 & 2Mr\dot{r}(\dot{\theta} + \dot{\phi}) \end{bmatrix}$ are the nonlinear velocity-dependent forces, and $g_p = -Mgl\cos\theta$, $\boldsymbol{g}_a = \begin{bmatrix} Mg\sin\theta & 0 & 0 \end{bmatrix}^T$ are the gravity-dependent forces.

As apparent from the coupling inertia matrix (row matrix $\boldsymbol{M}_{pa}$), there is one inertia coupling term that produces the coupling torque $mr^2\ddot{\phi}$. For a desired inertia coupling moment, a larger r would imply less effort, i.e. less RW torque m_C, or equivalently, less variation in angular acceleration $\ddot{\phi}$. This is the idea behind the "inertia shaping" approach discussed in [67,68,130].

4.3.5 Multilink Models on the Plane

Besides the simple IP-on-foot models discussed in Section 4.3.2, quite often multilink models on the plane (either sagittal or lateral) or in 3D are found to be useful. Such models are used to evaluate balance stability, as in the pioneering work [159,157]. They are also used in the field of biomechanics for evaluating balance stability of humans via single-leg models, e.g. the triple-IP-on-foot sagittal-plane model comprising foot, thigh (femur), shank (tibia), and trunk, as described in [52].[1]

In this work, examples can be found in Section 3.6.5 (lateral plane) and Section 7.6.3 (sagittal plane).

4.4 SIMPLE UNDERACTUATED MODELS IN 3D

When applied to a real robot, an extension of the above planar models to the third dimension is needed. With a 3D model, it becomes possible to account for the lateral acceleration of the CoM in the y-direction. Basically, there are two simple models, the 3D IP and the spherical IP that are supported on 3- and 2-DoF pivots, respectively. It is assumed that the mass is concentrated at the tip of the pendulum that determines the location of the CoM. Note also that these basic models are constant-length pendulums, s.t. the CoM motion is restricted on a spherical surface with radius equal to the pendulum length. The equation of motion of the 3D IP model, for example, can be represented in the form of Euler's equation of motion plus gravity term, i.e. as a set of three coupled nonlinear equations [134]. The equation of motion of the spherical IP is also nonlinear and coupled, in the x- and y-directions. Under the assumption of small deviations from the vertical, linearization and decoupling can be achieved [166].

4.4.1 3D Inverted Pendulum With Variable Length

The main goal is to make use of the 3D or spherical IP models to approximate the complex dynamics of a biped. In this case, a model with varying pendulum length would be appro-

[1] The dynamic equations are included in this work.

priate to account for arbitrary vertical displacements of the CoM. Note, however, that when the variations in length are left unconstrained, the equation of motion will be further complicated. The main problem in this regard is the abovementioned nonlinear coupling between the three components of the equation. As already noted, decoupling can be achieved under the assumption of small deviations from the vertical. In the case of a humanoid robot, though, this assumption is unrealistic. Fortunately, more suitable approaches do exist. One possibility is to restrict the CoM motion on piecewise linear surfaces that locally approximate the varying terrain height [171]. To this end, derive first the equation of motion of the 3D IP without the constraint. It is assumed that the pendulum forms a point contact at $\boldsymbol{r}_P$. The dynamic balance of moments can then be written as

$$\boldsymbol{r}_P \times \boldsymbol{f}_r = \boldsymbol{r}_C \times (\boldsymbol{f}_C + M\boldsymbol{a}_g) + \boldsymbol{m}_C. \tag{4.27}$$

Furthermore, since the balance of forces yields

$$\boldsymbol{f}_r = \boldsymbol{f}_C + M\boldsymbol{a}_g, \tag{4.28}$$

(4.27) can be rewritten as

$$(\boldsymbol{f}_C + M\boldsymbol{a}_g) \times (\boldsymbol{r}_C - \boldsymbol{r}_P) = \boldsymbol{m}_C. \tag{4.29}$$

Since point contact is assumed, the GRM and centroidal moment $\boldsymbol{m}_C$ are both zero.[2] Note also that $\boldsymbol{f}_C = M\ddot{\boldsymbol{r}}_C$. With these relations, the CoM acceleration components become

$$\begin{aligned}
\ddot{r}_{Cx} &= \frac{(r_{Cx} - r_{Px})(\ddot{r}_{Cz} + g)}{r_{Cz} - r_{Pz}}, \\
\ddot{r}_{Cy} &= \frac{(r_{Cy} - r_{Py})\ddot{r}_{Cx}}{r_{Cx} - r_{Px}}, \\
\ddot{r}_{Cx} &= \frac{(r_{Cz} - r_{Pz})\ddot{r}_{Cy}}{r_{Cy} - r_{Py}} - g.
\end{aligned} \tag{4.30}$$

It can be seen that these equations are coupled, nonlinear equations.

Next, constrain the CoM motion on the plane $r_{Cz} = a_p r_{Cx} + b_p$, $\forall r_{Cy}$. The CoM acceleration will then be constrained by $\ddot{r}_{Cz} = a_p \ddot{r}_{Cx}$. Insert these constraints into (4.30) to obtain the CoM acceleration in the sagittal and lateral planes as

$$\begin{aligned}
\ddot{r}_{Cx} - \omega^2 r_{Cx} &= -\omega^2 r_{Px}, \\
\ddot{r}_{Cy} - \omega^2 r_{Cy} &= -\omega^2 r_{Py},
\end{aligned} \tag{4.31}$$

respectively, where $\omega^2 \equiv g/(a_p r_{Px} + b_p - r_{Pz})$. Note that the form of these two equations is the same as that of the linearized IP-on-foot model in (4.11). Apparently, the above two equations are decoupled ODEs. Under the assumption of a constant CoP, explicit solutions in the form of (4.12) will be available.

[2] The case of plane contact that yields nonzero GRM and centroidal moment will be discussed shortly.

4.4.2 Spherical IP-on-Foot and Sphere-on-Plane Models

Consider now a spherical IP of variable length attached to a foot, i.e. a spherical IP-on-foot model. It should be noted at this point that since humanoid robots usually comprise 2-DoF ankle joints, the spherical IP model is more appropriate than the 3D IP one.

Furthermore, flat ground is assumed, s.t. the feet contacts are coplanar. Then, the projection of the CoM on the ground, i.e. the gCoM, plays an important role. This projection will be denoted as $\boldsymbol{r}_g = \begin{bmatrix} x_g & y_g \end{bmatrix}^T$. The net CoP, on the other hand, will be denoted as[3] $\boldsymbol{r}_p = \begin{bmatrix} x_p & y_p \end{bmatrix}^T$. As already noted, the CoP is constrained to lie within the convex hull of all contact points. It is convenient to approximate the convex hull by a convex polygon. The constraint, henceforth referred to as the *CoP-in-BoS* constraint, can then be formally expressed as

$$\boldsymbol{P}_s \boldsymbol{r}_p \preceq \boldsymbol{c}, \tag{4.32}$$

where $\boldsymbol{c} \in \Re^p$ is a set of constants, p denoting the number of polygon sides. The equation of the ith side[4] is given by $\boldsymbol{p}_{si} \boldsymbol{r}_p = c_i$, $i \in \{\overline{1, p}\}$, $\boldsymbol{p}_{si}$ denoting the ith row in $\boldsymbol{P}_s$.

The coupling problem pertinent to the equation of motion will be addressed as in Section 4.4.1, by restricting the CoM to move within a plane. In this case, the spherical IP model is referred to as the *3D LIP* [54]. The equation of motion is then determined by two ODEs that are decoupled in x and y, as in (4.31). The 3D LIP model can thus be regarded as an extension of the LIP-on-cart model (cf. Fig. 4.2C) in 3D.

Next, consider the extension of the planar IP-on-foot and the IP-on-cart models (shown in Fig. 4.2A and B, respectively) to 3D. The universal joint at the foot of the respective spherical IP (the ankle joint) is assumed actuated. The equation of motion of each of these models has the form of (4.10). Thus

$$\ddot{\boldsymbol{r}}_g = \omega^2 (\boldsymbol{r}_g - \boldsymbol{r}_p). \tag{4.33}$$

Here, $\omega = \omega_{IP} = \sqrt{g/l}$ for the constant-length ($l = \text{const}$) IP model, while $\omega = \bar{\omega} = \sqrt{g/\bar{z}_g}$ for the constant-height ($\bar{z}_g = \text{const}$) IP model. In the case of a variable-stroke model without the CoM vertical-motion constraint, use $\omega = \omega(t)$ as in (4.14). The equation of motion, expressed in terms of the CoP coordinates, assumes then the form of (4.15), i.e.

$$\boldsymbol{r}_p = \boldsymbol{r}_g - \frac{z_g}{\ddot{z}_g + g} \ddot{\boldsymbol{r}}_g. \tag{4.34}$$

Furthermore, the LIP-on-cart model in Fig. 4.2C can also be extended to 3D by replacing the cart with a sphere rolling on a horizontal plane of constant height $\bar{z}_g$ [23,22]. The tangential components of the GRM, $\boldsymbol{m}_t = \begin{bmatrix} m_x & m_y \end{bmatrix}^T$, are relevant. They can be obtained from the equation of motion as

$$\boldsymbol{m}_t = M g \mathbb{S}_2^{\times} \left(\frac{1}{\omega^2} \ddot{\boldsymbol{r}}_g - \boldsymbol{r}_g \right), \tag{4.35}$$

[3] A lower-case subscript is used to distinguish a 2D vector from a 3D one.
[4] Recall that the curly inequality sign denotes componentwise operation.

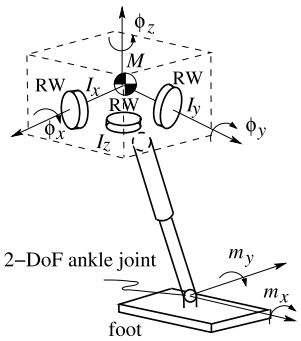

FIGURE 4.6 Model of a 3D reaction wheel pendulum with a telescopic massless leg. The spherical IP is connected to the foot via a 2-DoF ankle joint. The three RWs are mounted on three orthogonal axes. RW accelerations/torques produce a controlled variation of centroidal angular momentum. This results in a variation of the three reaction moments at the stance foot. The tangential reaction moments m_x and m_y induce displacements of the CoP. The vertical reaction moment m_z is used to compensate the gyroscopic moment [64].

where

$$\mathbb{S}_2^{\times} \equiv \begin{bmatrix} 0 & 1 \\ -1 & 0 \end{bmatrix}.$$

The subscript t signifies that the respective vector quantity is composed of tangential (i.e. x- and y-) components. The CoP is then determined as

$$\boldsymbol{r}_p = -\frac{1}{Mg}\mathbb{S}_2^{\times}\boldsymbol{m}_t. \tag{4.36}$$

4.4.3 The 3D Reaction Wheel Pendulum Model

An interesting question is whether the linear RWP model can be extended to a 3D one, in a similar way as the LIP was extended to the 3D LIP. It can be expected that a 3D linear RWP model will match humanoid gait dynamics to a greater extent and contribute to a further increase in balance stability w.r.t. the sagittal (pitch), frontal (roll), and transverse plane (yaw) dynamic components.

3D pendulum models with actuation have been introduced near the end of the 2000s as a means of teaching the foundations of nonlinear dynamics and control [134]. As shown in [20], with the help of the nonlinear control theory, it is possible to stabilize the IP to its equilibrium manifold. These models have been embodied recently in the form of self-balancing cubes [36,83,76]. The cubes comprise an assembly with three RWs mounted on mutually orthogonal axes, thus resembling the arrangement used in the three-axis attitude stabilization of spacecraft. In its essence, this system represents a 3D RWP.

The idea can be applied in humanoid robotics according to the conceptual representation in Fig. 4.6. The figure depicts the model of a 3D RWP supported by a telescopic massless leg. The spherical IP is connected to the foot via an actuated universal joint. The three RWs are mounted on three orthogonal axes. The RW accelerations/torques produce a controlled

variation in the centroidal angular momentum, in accordance with the Euler equation for rigid-body rotation, i.e.

$$\boldsymbol{I}\dot{\boldsymbol{\omega}} + \boldsymbol{\omega} \times \boldsymbol{I}\boldsymbol{\omega} = \boldsymbol{m}_{RW}. \tag{4.37}$$

Here $\boldsymbol{\omega}$ is the angular velocity in the inertia frame, $\boldsymbol{m}_{RW} = \dot{\boldsymbol{l}}_C = \boldsymbol{I}\ddot{\boldsymbol{\phi}}$, and $\boldsymbol{I}$ denotes the diagonal inertia matrix of the RW assembly. The RW moments are controlled to induce desirable GRMs at the stance foot. The moment about the vertical is undesirable; it leads to torsional slip at the foot. Thus, it is assumed that $\omega_z = 0$ and that the vertical RW moment is controlled to eliminate the gyroscopic moment, so $m_{RWz} = -(I_x - I_y)\omega_x\omega_y$. This also implies that $\dot{\omega}_z = 0$ [64].

The CoP equations can be obtained from (4.34) by adding a component for the rate of change of the angular momentum [71,120]. We have

$$\begin{aligned}\boldsymbol{r}_p &= \boldsymbol{r}_g - \frac{1}{\ddot{z}_g + g}(z_g\ddot{\boldsymbol{r}}_g - \frac{1}{M}\mathbb{S}_2^{\times}\dot{\boldsymbol{l}}_t) \\ &= \boldsymbol{r}_g - \frac{1}{f_{rz}}(z_g\boldsymbol{f}_t - \mathbb{S}_2^{\times}\boldsymbol{m}_t),\end{aligned} \tag{4.38}$$

where M denotes the total mass of the RW assembly. The equations have the same structure as the CoP equation of the planar RWP (4.23). Furthermore, the CMP can be obtained in analogy with (4.24) and (4.25) as (see also [120])

$$\boldsymbol{r}_{cmp} = \boldsymbol{r}_g - \frac{z_g}{f_{rz}}\boldsymbol{f}_t \tag{4.39}$$

and

$$\boldsymbol{r}_{cmp} = \boldsymbol{r}_p + \frac{1}{f_{rz}}\mathbb{S}_2^{\times}\boldsymbol{m}_t, \tag{4.40}$$

respectively, where $\boldsymbol{r}_{cmp} = \begin{bmatrix} x_{cmp} & y_{cmp} \end{bmatrix}^T$. On flat ground, z_{cmp} is assumed zero, similarly to the assumption that $z_p = 0$ (cf. (4.34)).

The above 3D RWP model can be further enhanced to match the humanoid robot dynamics to a higher degree. For example, a variable, posture-dependent inertia tensor can be introduced to mimic the variable inertia of the humanoid, e.g. as with the "Eulerian ZMP resolution" method [152].

4.4.4 The 3D Reaction Mass Pendulum Model

It is straightforward to extend the planar RMP model discussed in Section 4.3.4 to three dimensions with the help of a 3D reaction mass assembly. The assembly comprises three pairs of point masses sliding along three nonplanar linear tracks that intersect at the CoM. The distances between each pair of point masses are controlled independently. Thereby, the centroidal inertia can be "shaped" in a desirable way. This results in improved balance capabilities w.r.t. a desired angular momentum equilibrium, as shown in [67,68,130]. An implementation of the 3D RMP model for compass-type biped walking is discussed in [141].

4.4.5 Multilink Models in 3D

Multilink models in 3D have been introduced at an early stage in biped robot modeling. The dynamic model of such a robot was derived in [145] from the time derivatives of the linear and angular momenta of the robot. This approach will also be employed in this chapter. At this point, it is instructive to introduce the ZMP formula for the 3D multilink model suggested in [145] (see also [54], p. 97). To avoid complexity, each link of the robot is represented as a point mass. Then, the two components of the ZMP are

$$r_{Pt} = \frac{\sum_{i=1}^{n} M_i \left[(\ddot{r}_{Czi} + g) r_{Cti} - (r_{Czi} - r_{Pz}) \ddot{r}_{Cti} \right]}{\sum_{i=1}^{n} M_i (\ddot{r}_{Czi} + g)}, \quad t \in \{x, y\}, \tag{4.41}$$

where $\boldsymbol{r}_P = \begin{bmatrix} r_{Px} & r_{Py} & r_{Pz} \end{bmatrix}^T$ denotes the ZMP, M_i stands for the mass of the ith link, and

$$\boldsymbol{r}_{Ci} = \begin{bmatrix} r_{Cxi} & r_{Cyi} & r_{Czi} \end{bmatrix}^T$$

denotes its CoM position. The total number of links is n.

4.5 DYNAMIC MODELS OF A FIXED-BASE MANIPULATOR

Dynamic models of a fixed-base serial-link manipulator are helpful in understanding the limb dynamics of a humanoid robot. The focus here will be on modeling kinematically redundant manipulators and redundancy resolution with dynamic models (inverse dynamics). The models will be formulated in terms of joint-space and end-link (spatial) coordinates. Thereby, it is important to distinguish the cases of completely free (unconstrained) and constrained motion dynamics.

4.5.1 Dynamic Model in Joint-Space Coordinates

Consider first the completely free motion of a fixed-base manipulator. The kinetic energy, expressed in joint-space coordinates, is written as

$$T(\boldsymbol{\theta}) = \frac{1}{2} \dot{\boldsymbol{\theta}}^T \boldsymbol{M}_\theta(\boldsymbol{\theta}) \dot{\boldsymbol{\theta}}, \tag{4.42}$$

$\boldsymbol{M}_\theta(\boldsymbol{\theta}) \in \Re^{n \times n}$ denoting the joint-space manipulator inertia matrix. As known from introductory texts, this matrix can be expressed as

$$\boldsymbol{M}_\theta = \sum_{i=1}^{n} \left\{ M_i \boldsymbol{J}_{vi}^T \boldsymbol{J}_{vi} + \boldsymbol{J}_{\omega i}^T \boldsymbol{I}_i \boldsymbol{J}_{\omega i} \right\}. \tag{4.43}$$

Here M_i, $\boldsymbol{I}_i \in \Re^{3 \times 3}$ are the ith link's mass and inertia tensor and $\boldsymbol{J}_{vi}(\boldsymbol{\theta}) \in \Re^{3 \times n}$ (defined in (2.118)) and $\boldsymbol{J}_{\omega i}$ are the Jacobians for the ith link's CoM velocity and angular velocity,

respectively. The latter is written as

$$\boldsymbol{J}_{\omega i}(\boldsymbol{\theta}) = \begin{bmatrix} \boldsymbol{e}_1 & \boldsymbol{e}_2 & \cdots & \boldsymbol{e}_i & \boldsymbol{0} & \cdots & \boldsymbol{0} \end{bmatrix} \in \Re^{3\times n}, \tag{4.44}$$

$\boldsymbol{e}_j = \boldsymbol{R}_j {}^j\boldsymbol{e}_j$, ${}^j\boldsymbol{e}_j = [0\ 0\ 1]^T$. The link inertia tensor $\boldsymbol{M}_\theta$ is positive definite and, hence, its inverse can always be calculated. The respective Lagrangian form of manipulator dynamics is

$$\boldsymbol{M}_\theta(\boldsymbol{\theta})\ddot{\boldsymbol{\theta}} + \boldsymbol{c}_\theta(\boldsymbol{\theta}, \dot{\boldsymbol{\theta}}) + \boldsymbol{g}_\theta(\boldsymbol{\theta}) = \boldsymbol{\tau}. \tag{4.45}$$

Here $\boldsymbol{\tau} \in \Re^n$ is the joint torque, $\boldsymbol{g}_\theta(\boldsymbol{\theta}) \in \Re^n$ is the gravity torque, and $\boldsymbol{c}_\theta(\boldsymbol{\theta}, \dot{\boldsymbol{\theta}})$ denotes the nonlinear velocity-dependent torque. The latter can be expressed as

$$\boldsymbol{c}_\theta(\boldsymbol{\theta}, \dot{\boldsymbol{\theta}}) = \boldsymbol{C}_\theta(\boldsymbol{\theta}, \dot{\boldsymbol{\theta}})\dot{\boldsymbol{\theta}} = \dot{\boldsymbol{M}}_\theta(\boldsymbol{\theta})\dot{\boldsymbol{\theta}} - \frac{1}{2}\left(\frac{\partial}{\partial \boldsymbol{\theta}}\dot{\boldsymbol{\theta}}^T \boldsymbol{M}_\theta(\boldsymbol{\theta})\dot{\boldsymbol{\theta}}\right)^T, \tag{4.46}$$

where

$$\boldsymbol{C}_\theta(\boldsymbol{\theta}, \dot{\boldsymbol{\theta}}) = \frac{1}{2}\dot{\boldsymbol{M}}_\theta(\boldsymbol{\theta}) + \boldsymbol{S}^\times(\boldsymbol{\theta}, \dot{\boldsymbol{\theta}})$$

and

$$\boldsymbol{S}^\times(\boldsymbol{\theta}, \dot{\boldsymbol{\theta}})\dot{\boldsymbol{\theta}} = \frac{1}{2}\left[\dot{\boldsymbol{M}}_\theta(\boldsymbol{\theta})\dot{\boldsymbol{\theta}} - \left(\frac{\partial}{\partial \boldsymbol{\theta}}\dot{\boldsymbol{\theta}}^T \boldsymbol{M}_\theta(\boldsymbol{\theta})\dot{\boldsymbol{\theta}}\right)^T\right];$$

$\boldsymbol{S}^\times(\boldsymbol{\theta}, \dot{\boldsymbol{\theta}})$ is a skew-symmetric matrix that determines the passivity property of the equation of motion. This property plays an important role in control design [5,139]. Furthermore, note that since the end link does not contact any object, the only acting external force is the gravity. The equation of motion is an ODE. With an ODE solver, it is straightforward to find the solution to the *forward dynamics* problem: given the joint torque, find the joint acceleration, velocity, and positions. Given the current state, $(\boldsymbol{\theta}, \dot{\boldsymbol{\theta}})$, the joint acceleration is obtained as

$$\ddot{\boldsymbol{\theta}} = \boldsymbol{M}_\theta^{-1}(\boldsymbol{\theta})\left(\boldsymbol{\tau} - \boldsymbol{c}_\theta(\boldsymbol{\theta}, \dot{\boldsymbol{\theta}}) - \boldsymbol{g}_\theta(\boldsymbol{\theta})\right) \tag{4.47}$$

and is integrated twice to obtain the new state. The forward dynamics problem is used in simulation.

Furthermore, the following *inverse dynamics* problem needs to be solved in the case of dynamic control: given the state of the manipulator, $(\boldsymbol{\theta}, \dot{\boldsymbol{\theta}})$, and the desired acceleration, $\ddot{\boldsymbol{\theta}}$, find the joint torque. Note that in many cases, the motion task is specified in terms of end-link spatial coordinates. The inverse dynamics solution can then be obtained via the second-order inverse kinematics solution, (2.18) for a nonredundant manipulator, or (2.39) for a redundant one. The latter case is more interesting since there is an infinite number of solutions. Inserting (2.39) into (4.45) yields

$$\begin{aligned} \boldsymbol{\tau} &= \boldsymbol{\tau}_{lin} + \boldsymbol{\tau}_n + \boldsymbol{\tau}_{nl}, \\ \boldsymbol{\tau}_{lin} &= \boldsymbol{M}_\theta \boldsymbol{J}^{\#}\dot{\mathcal{V}}, \\ \boldsymbol{\tau}_n &= \boldsymbol{M}_\theta\left(\boldsymbol{E} - \boldsymbol{J}^{\#}\boldsymbol{J}\right)\ddot{\boldsymbol{\theta}}_a, \\ \boldsymbol{\tau}_{nl} &= \boldsymbol{c}_\theta + \boldsymbol{g}_\theta - \boldsymbol{M}_\theta \boldsymbol{J}^{\#}\dot{\boldsymbol{J}}\dot{\boldsymbol{\theta}}. \end{aligned} \tag{4.48}$$

The linear component $\boldsymbol{\tau}_{lin}$ results from the desired end-link acceleration, $\dot{\mathcal{V}}$; the null space component $\boldsymbol{\tau}_n$ represents an infinite number of joint torque vectors resulting from the self-motion acceleration vector parameter $\ddot{\boldsymbol{\theta}}_a$. Finally, $\boldsymbol{\tau}_{nl}$ is a nonlinear, state-dependent torque component. The behavior of the manipulator depends very much on the choice of the generalized inverse and the self-motion acceleration. To determine a specific joint torque, an additional task should be imposed, as discussed in Section 2.7. In [51], an attempt was made to use the null-space torque to locally minimize the deviation from the mid-range torque, i.e. $\|\boldsymbol{\tau} - \boldsymbol{\tau}^{mid}\|^2$, where $\boldsymbol{\tau}^{mid} = 0.5(\boldsymbol{\tau}^{max} + \boldsymbol{\tau}^{min})$. Substituting $\boldsymbol{\tau}$ from (4.48), the minimization yields the following self-motion acceleration:

$$\ddot{\boldsymbol{\theta}}_a = \left(\boldsymbol{W}^{1/2}\boldsymbol{M}_\theta(\boldsymbol{E} - \boldsymbol{J}^+\boldsymbol{J})\right)^+ \boldsymbol{W}^{1/2}\hat{\boldsymbol{\tau}}^{mid}. \tag{4.49}$$

The "hat" notation accounts for the linear and nonlinear torque components. The weight matrix $\boldsymbol{W} = \boldsymbol{W}^{1/2}\boldsymbol{W}^{1/2}$ scales the torque range of the individual joints.

Unfortunately, the above local torque minimization approach is plagued by a major problem: the solution lacks integrability. As a consequence, there is no control over the self-motion velocity. This quite often results in undesirable velocity build-up. Respective analysis has been provided by several authors [74,73,105]; see also the analysis in Section 2.11.3. Nevertheless, the problem is still actual, as apparent from more recent results in [112,14,127,18,170].

4.5.2 Dynamic Model in Spatial Coordinates

Humanoid robots interact with the environment mainly via their end links (feet and hands). Therefore, end-link motion/force control tasks are specified in spatial coordinates. When designing a controller, it would be reasonable to involve dynamic models expressed in terms of (end-link) spatial coordinates, rather than generalized (joint) coordinates. Indeed, a number of such controllers for fixed-base manipulators have been developed throughout the years. They are known as the "task space" [8], workspace/Cartesian space [50], or "operational space" [60] controllers. More recently, it has been shown that this type of controllers can be redesigned for use with floating-base humanoid robots. This section introduces basic relations pertinent to dynamic models in spatial coordinates for fixed-base manipulators. The application of such models to humanoid robots will be discussed in Section 4.13.3.

Consider first the completely free motion case. The derivation of a dynamic model in spatial coordinates is straightforward when the manipulator is a nonredundant one. Then, under the assumption that the inverse kinematic map exists, spatial coordinates can play the role of generalized coordinates. Making use of the inverse kinematics relation for the velocities, $\dot{\boldsymbol{\theta}} = \boldsymbol{J}(\boldsymbol{\theta})^{-1}\mathcal{V}$, kinetic energy (4.42) is expressed in spatial coordinates as [8,50]

$$T(\boldsymbol{\theta}) = \frac{1}{2}\mathcal{V}^T\mathbb{M}_e(\boldsymbol{\theta})\mathcal{V}. \tag{4.50}$$

Here $\mathbb{M}_e(\boldsymbol{\theta})$ is the manipulator inertia matrix represented in the end-link spatial coordinates. Its inverse equals the *end-effector mobility tensor* [49,50]

$$\mathbb{M}_e^{-1}(\boldsymbol{\theta}) = \boldsymbol{J}(\boldsymbol{\theta})\boldsymbol{M}_\theta^{-1}(\boldsymbol{\theta})\boldsymbol{J}^T(\boldsymbol{\theta}).$$

The term $\mathbb{M}_e(\boldsymbol{\theta})$ is also known as the "operational space inertia matrix" [19].

Furthermore, (4.45) is transformed into spatial coordinates through the following four steps. First premultiply by $\boldsymbol{J}\boldsymbol{M}_\theta^{-1}$ and then make use of the second-order kinematic relation $\boldsymbol{J}(\boldsymbol{\theta})\ddot{\boldsymbol{\theta}} = \dot{\mathcal{V}} - \dot{\boldsymbol{J}}(\boldsymbol{\theta})\dot{\boldsymbol{\theta}}$. The resultant equation is

$$\dot{\mathcal{V}} - \dot{\boldsymbol{J}}\dot{\boldsymbol{\theta}} = \boldsymbol{J}\boldsymbol{M}_\theta^{-1}\boldsymbol{\tau} - \boldsymbol{J}\boldsymbol{M}_\theta^{-1}(\boldsymbol{c}_\theta + \boldsymbol{g}_\theta). \tag{4.51}$$

Then, substitute the static force relation $\boldsymbol{\tau} = \boldsymbol{J}^T\mathcal{F}^m$ and solve the resulting equation for spatial force $\mathcal{F}^m$. The final result is

$$\begin{aligned}\mathcal{F}^m &= \mathbb{M}_e(\dot{\mathcal{V}} - \dot{\boldsymbol{J}}\dot{\boldsymbol{\theta}}) + \mathbb{M}_e\boldsymbol{J}\boldsymbol{M}_\theta^{-1}(\boldsymbol{c}_\theta + \boldsymbol{g}_\theta)\\ &= \mathbb{M}_e(\boldsymbol{\theta})\dot{\mathcal{V}} + \mathcal{C}_e(\boldsymbol{\theta}, \dot{\boldsymbol{\theta}}) + \mathcal{G}_e(\boldsymbol{\theta}),\end{aligned} \tag{4.52}$$

where $\mathcal{C}_e(\boldsymbol{\theta}, \dot{\boldsymbol{\theta}}) = \boldsymbol{J}^{-T}\boldsymbol{c} - \mathbb{M}_e\dot{\boldsymbol{J}}\dot{\boldsymbol{\theta}}$ denotes the nonlinear velocity-dependent force and $\mathcal{G}_e(\boldsymbol{\theta}) = \boldsymbol{J}^{-T}\boldsymbol{g}_\theta$ is the gravity force; these quantities are expressed as end-link wrenches. Furthermore, note that $\mathcal{F}^m = \boldsymbol{J}^{-T}\boldsymbol{\tau}$ is a quasistatic wrench stemming from the motion/force duality principle; it is not an external force. The m superscript is used to emphasize that this wrench should be related to mobility rather than to an external contact wrench.

Operational Space Method [60]

The dynamical model of a *kinematically redundant manipulator* could be transformed into end-link spatial coordinates with the same procedure as above. But the resultant equation would be an incomplete representation of the dynamics since the null-space joint torque does not appear in the equation. Indeed, for a redundant manipulator, the underlying coordinate transform should involve a generalized inverse of the Jacobian matrix. Since there is an infinite number of such inverses, the joint space dynamics cannot be uniquely represented in terms of spatial end-link coordinates. It is possible to choose a particular generalized inverse, but then subsequent analysis is needed to clarify the properties of the specific map. This approach was used in the operational space formulation [60], where the joint-to-spatial coordinates transform involves the inertia-weighted pseudoinverse of the Jacobian, i.e.

$$\begin{aligned}\boldsymbol{J}^{-M}(\boldsymbol{\theta}) &= \boldsymbol{M}_\theta^{-1}\boldsymbol{J}^T\left(\boldsymbol{J}\boldsymbol{M}_\theta^{-1}\boldsymbol{J}^T\right)^{-1}\\ &= \boldsymbol{M}_\theta^{-1}\boldsymbol{J}^T\mathbb{M}_e.\end{aligned} \tag{4.53}$$

Matrix $\boldsymbol{J}^{-MT}$ replaces $\boldsymbol{J}^{-T}$ in the nonlinear, gravity, and quasistatic wrench terms in (4.52). This particular inverse yields the so-called "dynamically consistent relationship" [61,33]: the end-link and the null-space dynamics become completely decoupled. Such decoupling of the dynamics is highly desirable from the viewpoint of controller design. A number of such controllers have been developed throughout the years, including the compliance [112] and impedance controllers [90,91,3]. The method has been applied to humanoid robots as well. Details will be given in Section 4.13.3.

To understand the dynamical decoupling property, assume a stationary manipulator configuration and zero gravity. Dynamical models (4.45) and (4.52) express then only linear motion/force relationships $\boldsymbol{M}_\theta\ddot{\boldsymbol{\theta}} = \boldsymbol{\tau}$ and $\mathbb{M}_e\dot{\mathcal{V}} = \mathcal{F}^m$, respectively. The kinetostatic relations,

on the other hand, are $\boldsymbol{J}\ddot{\boldsymbol{\theta}} = \dot{\mathcal{V}}$ and $\boldsymbol{\tau} = \boldsymbol{J}^T \mathcal{F}^m$. In the presence of kinematic redundancy, there is an infinite set of control joint torque vectors. The last relation is then rewritten as [60,61]

$$\boldsymbol{\tau}_f = \boldsymbol{J}^T \mathcal{F}^m + \left(\boldsymbol{E} - \boldsymbol{J}^T \boldsymbol{J}^{-WT}\right) \boldsymbol{\tau}_a. \tag{4.54}$$

Here $\boldsymbol{\tau}_a$ is an arbitrary joint torque that parametrizes (dual) null space $\mathcal{N}^*(\boldsymbol{J}) \equiv \mathcal{N}(\boldsymbol{J}^{-WT})$ (recall from Section 3.4.3 that $\left(\boldsymbol{E} - \boldsymbol{J}^T \boldsymbol{J}^{-WT}\right)$ denotes a projector onto this null space). The joint torque component obtained from the projection has no contribution to the resultant forces at the end link.

On the other hand, when the second-order inverse kinematic solution of a redundant manipulator, (2.39), is inserted into (4.45) (under the assumption of using a weighted pseudoinverse, a stationary configuration, and zero gravity), another infinite set of control joint torques can be derived [33], i.e.

$$\boldsymbol{\tau}_m = \boldsymbol{M}_\theta \boldsymbol{J}^{-W} \mathbb{M}_e^{-1} \mathcal{F}^m + \boldsymbol{M}_\theta \left(\boldsymbol{E} - \boldsymbol{J}^{-W} \boldsymbol{J}\right) \ddot{\boldsymbol{\theta}}_a. \tag{4.55}$$

Here $\ddot{\boldsymbol{\theta}}_a$ is an arbitrary joint acceleration that parametrizes the null space $\mathcal{N}(\boldsymbol{J})$. Its projection yields a joint acceleration that could be applied without affecting the resultant spatial acceleration of the end link. All $\ddot{\boldsymbol{\theta}}_a$-induced joint torques $\{\boldsymbol{\tau}_m\}$ produce the same end-link acceleration as the end-link force $\mathcal{F}^m$.

It is straightforward to show that the two joint torque sets (4.54) and (4.55) are compatible (or *dynamically consistent*), only when the inertia-weighted pseudoinverse of the Jacobian is used in the equations, i.e. require $\boldsymbol{W} = \boldsymbol{M}_\theta$. This leads to a *complete dynamical decoupling* between the particular components responsible for the motion/force control task and the null space components. It was shown in [33] that the following four conditions will then be satisfied:

$$\mathcal{F}_n = \boldsymbol{M}_\theta \mathcal{M}_n, \quad \mathcal{F}_r = \boldsymbol{M}_\theta \mathcal{M}_r \tag{4.56}$$

and

$$\mathcal{F}_n \perp \mathcal{M}_r, \quad \mathcal{F}_r \perp \mathcal{M}_n, \tag{4.57}$$

where $\mathcal{M}$ and $\mathcal{F} \equiv \mathcal{M}^*$ denote the joint motion (generalized velocity/acceleration) and dual (generalized momentum/joint torque) domains, respectively. Subscripts "r" and "n" stand for components from the row and null subspaces of the underlying transform, i.e. the Jacobian matrix.

The property of complete dynamical decoupling plays an important role in motion/force and impedance control design, since the task and null space control components can be designed independently.

Constrained Dynamics in Spatial Coordinates

Consider now a motion/force control scenario wherein the end link is in contact with the environment and moves along the contact surface. A closed loop is formed via the contact

joint, giving rise to the kinetostatic conditions introduced in Chapter 2. The first-order differential motion relation is of the same form as (2.95). Accordingly, the manipulator Jacobian decomposes into sub-Jacobians for the constrained and unconstrained directions: $\boldsymbol{J}_c(\boldsymbol{\theta}) \in \Re^{c\times n}$ and $\boldsymbol{J}_m(\boldsymbol{\theta}) \in \Re^{\eta\times n}$, respectively, c and η ($c+\eta=6$) denoting the number of constrained and unconstrained directions at the contact joint. The equation of motion is written as

$$\boldsymbol{M}_\theta(\boldsymbol{\theta})\ddot{\boldsymbol{\theta}} + \boldsymbol{c}_\theta(\boldsymbol{\theta},\dot{\boldsymbol{\theta}}) + \boldsymbol{g}_\theta(\boldsymbol{\theta}) = \boldsymbol{\tau} + \boldsymbol{J}_c^T(\boldsymbol{\theta})\overline{\mathcal{F}}^c, \tag{4.58}$$

$\overline{\mathcal{F}}^c$ denoting the contact wrench components (reactions). Furthermore, the Jacobian decomposition specifically structures the dynamical terms that are represented in spatial coordinates. Consequently, the operational space inertia matrix and the nonlinear velocity and gravity terms assume the form [28]

$$\mathbb{M}_e(\boldsymbol{\theta}) = \begin{bmatrix} \boldsymbol{J}_c\boldsymbol{M}_\theta^{-1}\boldsymbol{J}_c^T & \boldsymbol{J}_c\boldsymbol{M}_\theta^{-1}\boldsymbol{J}_m^T \\ \boldsymbol{J}_m\boldsymbol{M}_\theta^{-1}\boldsymbol{J}_c^T & \boldsymbol{J}_m\boldsymbol{M}_\theta^{-1}\boldsymbol{J}_m^T \end{bmatrix}^{-1} = \begin{bmatrix} \boldsymbol{M}_c & \boldsymbol{M}_{cm} \\ \boldsymbol{M}_{cm}^T & \boldsymbol{M}_m \end{bmatrix}, \tag{4.59}$$

$$\mathcal{C}_e(\boldsymbol{\theta},\dot{\boldsymbol{\theta}}) = \mathbb{M}_e \begin{bmatrix} \boldsymbol{J}_c\boldsymbol{M}_\theta^{-1}\boldsymbol{c}_\theta - \dot{\boldsymbol{J}}_c\dot{\boldsymbol{\theta}} \\ \boldsymbol{J}_m\boldsymbol{M}_\theta^{-1}\boldsymbol{c}_\theta - \dot{\boldsymbol{J}}_m\dot{\boldsymbol{\theta}} \end{bmatrix} = \begin{bmatrix} \mathcal{C}_c \\ \mathcal{C}_m \end{bmatrix}, \tag{4.60}$$

$$\mathcal{G}_e(\boldsymbol{\theta}) = \mathbb{M}_e \begin{bmatrix} \boldsymbol{J}_c \\ \boldsymbol{J}_m \end{bmatrix} \boldsymbol{M}_\theta^{-1}\boldsymbol{g}_\theta = \begin{bmatrix} \mathcal{G}_c \\ \mathcal{G}_m \end{bmatrix},$$

respectively. With the above notations, the equation of motion can be represented in spatial coordinates as

$$\begin{bmatrix} \boldsymbol{M}_c & \boldsymbol{M}_{cm} \\ \boldsymbol{M}_{cm}^T & \boldsymbol{M}_m \end{bmatrix} \begin{bmatrix} \boldsymbol{0} \\ \dot{\overline{\mathcal{V}}}^m \end{bmatrix} + \begin{bmatrix} \mathcal{C}_c \\ \mathcal{C}_m \end{bmatrix} + \begin{bmatrix} \mathcal{G}_c \\ \mathcal{G}_m \end{bmatrix} = \begin{bmatrix} \overline{\mathcal{F}}^c \\ \overline{\mathcal{F}}^m \end{bmatrix}, \tag{4.61}$$

where $\overline{\mathcal{V}}^m = \boldsymbol{J}_m\dot{\boldsymbol{\theta}} \in \Re^\eta$ is the velocity along the unconstrained motion directions at the contact joint. The dual quantity $\overline{\mathcal{F}}^m$ denotes the quasistatic force (along the unconstrained directions). Note that the acceleration $\dot{\overline{\mathcal{V}}}^m$ does not produce any reaction force. Likewise, the reaction force $\overline{\mathcal{F}}^c$ does not generate any acceleration along the unconstrained motion directions. This results in dynamic decoupling. Consequently, the end-effector motion and force are controllable in an independent manner, via $\overline{\mathcal{F}}^m$ and $\overline{\mathcal{F}}^c$, respectively.

Complete Dynamic Decoupling via the KD-JSD Method [116]

The kinematically decoupled joint-space decomposition (KD-JSD) method (cf. Section 2.7.5) can be applied to achieve complete dynamic decoupling, as with the operational space formulation. The minimal parametrization property of the method yields an important advantage when the dynamics are expressed in end-link coordinates, though.

The infinite set of static joint torques (4.54) can be represented with the help of the KD-JSD notation as

$$\boldsymbol{\tau}_f = \boldsymbol{J}^T\mathcal{F} + \boldsymbol{W}\boldsymbol{Z}^T\overline{\boldsymbol{\tau}}_a, \tag{4.62}$$

where $\overline{\boldsymbol{\tau}}_a$ is an arbitrary r-vector that parametrizes the dual null space $\mathcal{N}^*(\boldsymbol{J}) \equiv \mathcal{F}_n$ in a minimal way. The weighting matrix $\boldsymbol{W}(\boldsymbol{\theta}) \in \Re^{n\times n}$, the full row-rank matrix $\boldsymbol{Z}(\boldsymbol{\theta}) \in \Re^{r\times n}$, and the

"asymmetrically" weighted generalized inverse $\boldsymbol{Z}_W^{\#}(\boldsymbol{\theta})$ have been defined in Section 2.7.5. It can be shown that for a given nonminimal-parametrization vector $\boldsymbol{\tau}_a \in \Re^n$, there is a $\overline{\boldsymbol{\tau}}_a \in \Re^r$ s.t. the null space components (the second terms on the r.h.s.) in (4.54) and (4.62) are equal.

On the other hand, there is another infinite set of joint torques that result from the set of possible joint accelerations. The latter are obtained from the KD-JSD second-order inverse kinematic solution (derived via differentiation of (2.48) w.r.t. time) and inserted into (4.45). Under the assumption of a stationary configuration and zero gravity, the acceleration-induced joint torques are expressed as

$$\boldsymbol{\tau}_m = \boldsymbol{M}_\theta \begin{bmatrix} \boldsymbol{J}^{-W}(\boldsymbol{\theta}) & \boldsymbol{Z}_W^{\#}(\boldsymbol{\theta}) \end{bmatrix} \begin{bmatrix} \dot{\mathcal{V}} \\ \dot{\boldsymbol{b}} \end{bmatrix}. \tag{4.63}$$

Arbitrary r-vector $\dot{\boldsymbol{b}}$ parametrizes in a minimal way the null space $\mathcal{N}(\boldsymbol{J}) \equiv \mathcal{M}_n$. This null space comprises joint accelerations that could be applied without affecting the resultant spatial accelerations of the end link, as already discussed.

Under the joint-space decomposition scheme, the linear motion/force relations in joint space can be expressed as

$$\begin{bmatrix} \mathcal{F} \\ \overline{\boldsymbol{\tau}}_a \end{bmatrix} = \begin{bmatrix} \mathbb{M}_e(\boldsymbol{\theta}) & \boldsymbol{H}_{er}(\boldsymbol{\theta}) \\ \boldsymbol{H}_{er}^T(\boldsymbol{\theta}) & \boldsymbol{M}_r(\boldsymbol{\theta}) \end{bmatrix} \begin{bmatrix} \dot{\mathcal{V}} \\ \dot{\boldsymbol{b}} \end{bmatrix}, \tag{4.64}$$

where

$$\mathbb{M}_e = \boldsymbol{J}^{-WT} \boldsymbol{M}_\theta \boldsymbol{J}^{-W},$$

$$\boldsymbol{H}_{er} = \boldsymbol{J}^{-WT} \boldsymbol{M}_\theta \boldsymbol{Z}_W^{\#},$$

$$\boldsymbol{M}_r = \boldsymbol{Z}_W^{\#T} \boldsymbol{M}_\theta \boldsymbol{Z}_W^{\#}.$$

A dynamically consistent relationship for joint torques, (4.62) and (4.63) (i.e. complete dynamical decoupling), can be ensured only when the weighting matrix equals the joint-space inertia, i.e. $\boldsymbol{W}(\boldsymbol{\theta}) = \boldsymbol{M}_\theta(\boldsymbol{\theta})$. Then, $\boldsymbol{H}_{er} = \boldsymbol{0}$ since $\boldsymbol{J}\boldsymbol{Z}_W^{\#} = \boldsymbol{0}$. Hence, the inertia matrix in (4.64) assumes the block-diagonal form diag$\begin{bmatrix} \mathbb{M}_e & \boldsymbol{M}_r \end{bmatrix}$. This feature facilitates the design of control laws, as will be explained in Section 4.5.3.

4.5.3 Null-Space Dynamics With Dynamically Decoupled Hierarchical Structure

The complete dynamic decoupling approach discussed in Section 4.5.2 provides a basis to develop asymptotically stable null-space dynamic control. To this end, the approach is first reformulated for the general case of r prioritized tasks, in terms of differential kinematics [29], i.e.

$$\mathcal{V}_k = \bar{\boldsymbol{J}}_k \dot{\boldsymbol{\theta}}, \tag{4.65}$$

where $\mathcal{V}_k \in \Re^{m_k}$ and $\bar{\boldsymbol{J}}_k \in \Re^{m_k \times n}$, $k \in \{\overline{2, r}\}$ are the additional-task velocities and (null-space) restricted Jacobians, respectively. Recall that the Jacobians have to be determined in a way s.t.

the kinematic decoupling for all additional tasks is ensured (cf. Section 2.7.5). The kinematic decoupling also yields dynamic decoupling, as already discussed in Section 4.5.2.

The dynamic decoupling can be ensured when the restricted Jacobians are determined in the following form [29]:

$$\bar{\boldsymbol{J}}_k = \left(\boldsymbol{Z}_k \boldsymbol{M}_\theta \boldsymbol{Z}_k^T\right)^{-1} \boldsymbol{Z}_k \boldsymbol{M}_\theta. \tag{4.66}$$

Here $\boldsymbol{Z}_k$ represents a full row-rank null-space basis derived from matrix $\boldsymbol{J}_{C_{k-1}}$ appearing in the recursive scheme (2.52), s.t. $\boldsymbol{J}_{C_{k-1}} \boldsymbol{Z}_k^T = \boldsymbol{0}$. Apparently, the link inertia matrix, $\boldsymbol{M}_\theta$, plays the role of a weighting matrix in the above expression. With this notation, the inverse kinematics solution is expressed as

$$\dot{\boldsymbol{\theta}} = \boldsymbol{J}^{-M_\theta} \mathcal{V} + \sum_{k=2}^{r} \boldsymbol{Z}_k^T \mathcal{V}_k. \tag{4.67}$$

The $\boldsymbol{Z}_k$ null-space bases can be determined via singular-value decomposition (SVD) of the $\boldsymbol{J}_{C_{k-1}}$ matrices. Note also that the following relations hold:

$$\begin{aligned} \bar{\boldsymbol{J}}_k^T \boldsymbol{Z}_k \boldsymbol{J}_k^T &= \boldsymbol{N}^*(\boldsymbol{J}_{C_{k-1}}) \boldsymbol{J}_k^T, \\ \boldsymbol{N}^*(\boldsymbol{J}_{C_{k-1}}) &\equiv \boldsymbol{E} - \boldsymbol{J}_{C_{k-1}}^T \boldsymbol{J}_{C_{k-1}}^{-M\,T}. \end{aligned} \tag{4.68}$$

Furthermore, in accordance with (2.32), the null-space projector can be decomposed as $\boldsymbol{N}^*(\boldsymbol{J}_{C_{k-1}}) = \boldsymbol{V}_{k-1} \boldsymbol{V}_{k-1}^T$. Then,

$$\begin{aligned} \boldsymbol{Z}_k &= \boldsymbol{J}_k \boldsymbol{V}_{k-1} \left(\boldsymbol{V}_{k-1}^T \boldsymbol{M}_\theta \boldsymbol{V}_{k-1}\right)^{-1} \boldsymbol{V}_{k-1}^T, \; k = 2, 3, ..., (r-1), \\ \boldsymbol{Z}_r &= \boldsymbol{V}_{r-1}. \end{aligned} \tag{4.69}$$

As discussed in [29], when implemented appropriately in a controller, the above decomposition can ensure asymptotic stability without involving external force measurement, guaranteeing thereby successive convergence in accordance with the order of priority.

4.6 SPATIAL MOMENTUM OF A MANIPULATOR FLOATING FREELY IN ZERO GRAVITY

The complete dynamic model of a humanoid robot accounts for the presence of a floating base and external forces, such as gravity and contact (reaction) forces. Floating-base dynamic models comprise a specific component that distinguishes them from the fixed-base dynamic models discussed in Section 4.5. For the in-depth understanding of floating-base dynamic models, it will prove useful to focus first on the dynamics of a free-floating robot in zero gravity. In the absence of external forces, these dynamics refer solely to the motion of the robot. The properties of motion dynamics play an important role as an inherent part of the

complete dynamics. Note also that the study of pure free-floating, i.e. contactless, underactuated system models, is justifiable from a practical viewpoint as well. Indeed, there are humanoid robots that are able to attain a flight phase wherein the feet loose contact with the ground, e.g. during running or jumping [21,148,149,147,26]. To arrive at an appropriate posture for landing, the motion of the limbs needs to be controlled accordingly in mid-air. With an appropriate landing posture control, excessive reactions upon touchdown can be avoided. Balance stability in the postimpact phase is then also easier to achieve. Free-floating robot models are especially helpful in understanding the important role of angular momentum.

4.6.1 Brief Historical Background

Free-floating system models appeared first in the field of space robotics during the 1980s. In the pioneering work [154], the nonholonomic nature of a free-floating space robot was revealed. Attention was drawn to the disturbance of the spatial position of the base that is induced by the motion of the manipulator. Also, a related difficulty for the manipulator motion planning problem was highlighted. The use of kinematic redundancy for momentum compensation has been first investigated in [97,122]. In [97,94], velocity-based equations for simultaneous control of the end-link and base motions were established and a novel redundancy resolution approach with prioritization of tasks was developed to minimize or maximize the reactions at the base. Also, the so-called "manipulator inversion task" was introduced wherein the end link remains fixed in inertial space while the orientation of the floating base varies in a desirable way. This behavior is achieved via a specific null space: that of the coupling inertia matrix. Later it was shown that the same null space can also play an important role for balance control of a humanoid robot subjected to an external disturbance [102,101,168].

4.6.2 Spatial Momentum

Consider a free-floating serial-link chain in zero gravity comprising an n-joint manipulator arm mounted on a rigid-body satellite, as shown in Fig. 4.7A. The satellite represents the floating base of the system. It is assumed that the base is not actuated (there are no thrusters or RWs) while the manipulator joints are. Thus, the system is underactuated.

The linear momentum of the system is expressed uniquely as

$$\boldsymbol{p} = \sum_{i=0}^{n} M_i \dot{\boldsymbol{r}}_i = M \dot{\boldsymbol{r}}_C, \tag{4.70}$$

M_i and $\boldsymbol{r}_i$ denoting the mass and CoM position of Link i; M stands for the total mass and $\boldsymbol{r}_C$ is the position of the system CoM. The expression for the angular momentum depends on the point of reference. In the field of space robotics, expressions w.r.t. the origins of the inertial and the base-link frames as well as the system CoM are used. In the field of humanoid robotics, the latter two are exclusively employed. The simplest expression is obtained when

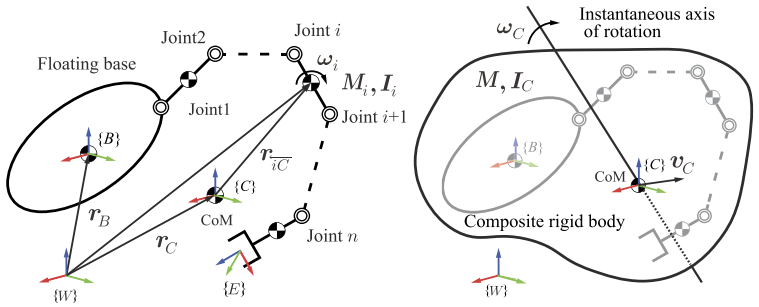

FIGURE 4.7 Model of a serial-link manipulator on a free-floating base. (A) Left: main coordinate frames and system parameters. (B) Right: representation as a composite rigid body (CRB) (all joints locked).

the angular momentum is represented w.r.t. the system CoM, i.e.

$$\boldsymbol{l}_C = \sum_{i=0}^{n} \boldsymbol{I}_i \boldsymbol{\omega}_i . \tag{4.71}$$

Here $\boldsymbol{I}_i$ and $\boldsymbol{\omega}_i$ denote the inertia tensor and angular velocity of Link i. Note that the base is designated as Link 0; related quantities, such as the base position, velocity, and inertia, will be denoted by subscript $(\circ)_B$. All quantities are expressed in the inertia frame, $\{W\}$. In the notation for angular momentum, the subscript signifies the reference point.

It is convenient to combine the above two momentum vectors into a single 6D vector that will represent the *spatial momentum* of the floating-base system w.r.t. its CoM, i.e.

$$\mathcal{L}_C \equiv \begin{bmatrix} \boldsymbol{p} \\ \boldsymbol{l}_C \end{bmatrix}. \tag{4.72}$$

The spatial momentum is an element of $se^*(3)$, as is the spatial force. Note that in the absence of external forces (e.g. gravity), the spatial momentum is conserved. In the presence of gravity, on the other hand, only the angular momentum is conserved. Note also that the angular momentum is nonintegrable and, hence, its conservation imposes a nonholonomic motion constraint.

4.6.3 Locked Joints: the Composite Rigid Body

When the manipulator joints are locked, the free-floating system behaves as a composite rigid body (CRB). Recall that the notation of a CRB as a composite system of links characterized by its CoM was introduced in Section 3.6. The CRB is characterized also by an inertia tensor defined as

$$\boldsymbol{I}_C(\boldsymbol{q}) \equiv \sum_{i=0}^{n} \left(\boldsymbol{I}_i + M_i [\boldsymbol{r}^{\times}_{\underleftarrow{iC}}][\boldsymbol{r}^{\times}_{\underleftarrow{Ci}}] \right) \in \Re^{3\times 3}. \tag{4.73}$$

Hereby, $\boldsymbol{r}_{\underleftarrow{iC}} = \boldsymbol{r}_i - \boldsymbol{r}_C$ and $\boldsymbol{q} = (\mathcal{X}_B, \boldsymbol{\theta})$ denotes the generalized coordinates of the floating-base

system, $\mathcal{X}_B$ standing for the 6D position of the floating base. At this point it is instructive to note that the states of the manipulator joints and the floating base are derived from the joint angle encoder and the inertial measurement sensor (IMU) readings, respectively. Sensor fusion techniques may increase the accuracy of the latter [126].

Furthermore, as shown in Fig. 4.7B, the CRB coordinate frame $\{C\}$ is conveniently attached to the system CoM. Since the CRB is not a real body, the coordinate axes are chosen to be parallel to those of the base-link frame $\{B\}$. With this choice, the spatial velocity of the CRB can be expressed by $\mathcal{V}_M$ (defined in Section 2.11.4), with components CoM velocity $\boldsymbol{v}_C = \dot{\boldsymbol{r}}_C$ and the angular velocity of the base link $\boldsymbol{\omega}_B$. As an alternative expression, the so-called *system spatial velocity* $\mathcal{V}_C = \begin{bmatrix}\boldsymbol{v}_C^T & \boldsymbol{\omega}_C^T\end{bmatrix}^T$ will be introduced here. Angular velocity $\boldsymbol{\omega}_C$ is referred to as the *system angular velocity*[5]; its meaning will be clarified in Section 4.6.4.

The relation between the spatial momentum and the system spatial velocity can be expressed as

$$\mathcal{L}_C = \mathbb{M}_C \mathcal{V}_C. \tag{4.74}$$

Matrix

$$\mathbb{M}_C(\boldsymbol{q}) \equiv \begin{bmatrix} M\boldsymbol{E} & \boldsymbol{0} \\ \boldsymbol{0} & \boldsymbol{I}_C(\boldsymbol{q}) \end{bmatrix} \in \Re^{6\times 6} \tag{4.75}$$

has the structure of a rigid-body *spatial inertia tensor* [32] (or a *locked inertia tensor* [86,109]). It plays an important role in floating-base system modeling, including humanoid robots. Note that the subscript indicates dependence on the reference point. In this case, the reference point is the system CoM (or centroid), thus $\mathbb{M}_C(\boldsymbol{q})$ is referred to as the *centroidal CRB inertia* [67]; $\mathcal{L}_C$, on the other hand, has been called a *centroidal spatial momentum* [107]. Other representations of the spatial inertia tensor, e.g. w.r.t. the origin of the floating-base or the inertia frame, will be given in what follows. The angular momentum derived from (4.74) is

$$\boldsymbol{l}_C = \boldsymbol{I}_C(\boldsymbol{q})\boldsymbol{\omega}_c. \tag{4.76}$$

The quantities $\boldsymbol{I}_C(\boldsymbol{q})$ and $\boldsymbol{l}_C$ are referred to as the *centroidal* inertia tensor and the *centroidal* angular momentum, respectively; $\boldsymbol{l}_C$ is also called a *spin* [119,120] or an *intrinsic* [32,152] angular momentum.

The preferable reference point for the spatial momentum and the respective spatial inertia tensor may differ in each application field. In the field of humanoid robots, the CoM may be the preferred choice (e.g. as in [55]). In the field of space robotics, on the other hand, the origin of the floating base frame is usually used. In this case, the spatial momentum is expressed as

$$\mathcal{L}_B = \mathbb{T}_{\overleftarrow{BC}}^T \mathcal{L}_C \tag{4.77}$$

or

$$\mathcal{L}_B \equiv \begin{bmatrix}\boldsymbol{p}\\ \boldsymbol{l}_B\end{bmatrix} = \begin{bmatrix}\boldsymbol{E} & \boldsymbol{0}\\ -[\boldsymbol{r}^\times_{\overleftarrow{BC}}] & \boldsymbol{E}\end{bmatrix}\begin{bmatrix}\boldsymbol{p}\\ \boldsymbol{l}_C\end{bmatrix} = \begin{bmatrix}\boldsymbol{p}\\ \boldsymbol{l}_C\end{bmatrix} - \begin{bmatrix}\boldsymbol{0}\\ [\boldsymbol{r}^\times_{\overleftarrow{BC}}]\boldsymbol{p}\end{bmatrix}.$$

[5] The system angular/spatial velocity $\boldsymbol{\omega}_C/\mathcal{V}_C$ have been named the *average* angular/spatial velocity in [107].

Note that since spatial momentum is an element of $se^*(3)$, in (4.77) the transformation rule for wrenches (cf. (3.4)) was used. Note also that the transformation is valid in general, i.e. not only for the locked-joint case. Furthermore, by inserting (4.74) into (4.77) and using $\mathcal{V}_C = \mathbb{T}_{\overleftarrow{CB}}\mathcal{V}_B$ (cf. (2.4)), one obtains

$$\widetilde{\mathcal{L}}_B = \mathbb{M}_B \mathcal{V}_B.$$

Here $\mathcal{V}_B = \begin{bmatrix} \boldsymbol{v}_B^T & \boldsymbol{\omega}_B^T \end{bmatrix}^T$ denotes the spatial velocity of the base. The overtilde notation signifies that the above expression for the spatial momentum in the locked-joint case may differ from that in the unlocked-joint one. The matrix

$$\mathbb{M}_B \equiv \mathbb{T}_{\overleftarrow{BC}}^T \mathbb{M}_C \mathbb{T}_{\overleftarrow{CB}} \tag{4.78}$$

represents the spatial inertia tensor. Relation (4.78) provides a useful formula for transforming spatial inertia tensors. The above tensor can be expanded as

$$\mathbb{M}_B(\boldsymbol{q}) = \begin{bmatrix} M\boldsymbol{E} & -M[\boldsymbol{r}^\times_{\overleftarrow{CB}}] \\ -M[\boldsymbol{r}^\times_{\overleftarrow{CB}}]^T & \boldsymbol{I}_B \end{bmatrix}, \tag{4.79}$$

where

$$\begin{aligned} \boldsymbol{I}_B(\boldsymbol{q}) &= \boldsymbol{I}_C(\boldsymbol{q}) + M[\boldsymbol{r}^\times_{\overleftarrow{CB}}][\boldsymbol{r}^\times_{\overleftarrow{BC}}] \\ &= \boldsymbol{I}_0 + \sum_{i=1}^{n} \left(\boldsymbol{I}_i + M_i[\boldsymbol{r}^\times_{\overleftarrow{iB}}][\boldsymbol{r}^\times_{\overleftarrow{Bi}}] \right). \end{aligned} \tag{4.80}$$

Here $\boldsymbol{I}_0$ denotes the inertia tensor of the base link.

Furthermore, the spatial momentum can be expressed w.r.t. the inertial frame, if needed, as

$$\mathcal{L}_W = \mathbb{T}_{\overleftarrow{WC}}^T \mathcal{L}_C. \tag{4.81}$$

The expanded form is given as

$$\mathcal{L}_W \equiv \begin{bmatrix} \boldsymbol{p} \\ \boldsymbol{l}_W \end{bmatrix} = \begin{bmatrix} \boldsymbol{E} & \boldsymbol{0} \\ -[\boldsymbol{r}^\times_{\overleftarrow{WC}}] & \boldsymbol{E} \end{bmatrix} \begin{bmatrix} \boldsymbol{p} \\ \boldsymbol{l}_C \end{bmatrix} = \begin{bmatrix} \boldsymbol{p} \\ \boldsymbol{l}_C \end{bmatrix} - \begin{bmatrix} \boldsymbol{0} \\ [\boldsymbol{r}^\times_{\overleftarrow{WC}}]\boldsymbol{p} \end{bmatrix}.$$

The CRB angular momentum can then be written as

$$\boldsymbol{l}_W = \boldsymbol{I}_C \boldsymbol{\omega}_c + [\boldsymbol{r}^\times_{\overleftarrow{CW}}]\boldsymbol{p} = \sum_{i=0}^{n} \left(\boldsymbol{I}_i \boldsymbol{\omega}_i + M_i[\boldsymbol{r}^\times_{\overleftarrow{iW}}]\dot{\boldsymbol{r}}_i \right). \tag{4.82}$$

4.6.4 Joints Unlocked: Multibody Notation

It will be shown in what follows that, when the joints are unlocked, the representation of spatial momentum depends on the particular choice of the quasivelocity. Recall that, so

far, two kinds of quasivelocity were used: the base quasivelocity $\dot{\boldsymbol{q}}_B = (\mathcal{V}_B, \dot{\boldsymbol{\theta}})$ and the mixed quasivelocity $\dot{\boldsymbol{q}}_M = (\mathcal{V}_M, \dot{\boldsymbol{\theta}})$. The system spatial velocity $\mathcal{V}_C$ gives rise of a third type of quasivelocity: the *centroidal quasivelocity* $\dot{\boldsymbol{q}}_C = (\mathcal{V}_C, \dot{\boldsymbol{\theta}})$.

To clarify the dependence on the quasivelocity formulation, note first that the (linear) momentum can be represented as

$$\begin{aligned}\boldsymbol{p}(\boldsymbol{q}, \dot{\boldsymbol{q}}_B) &= M\boldsymbol{v}_B + \sum_{i=1}^{n} M_i \left(-[\boldsymbol{r}^{\times}_{\overleftarrow{iB}}]\boldsymbol{\omega}_B + \boldsymbol{J}_{vi}(\boldsymbol{\theta})\dot{\boldsymbol{\theta}}\right) \\ &= M\left(\boldsymbol{v}_B - [\boldsymbol{r}^{\times}_{\overleftarrow{CB}}]\boldsymbol{\omega}_B + \boldsymbol{J}_{\overleftarrow{CB}}(\boldsymbol{\theta})\dot{\boldsymbol{\theta}}\right),\end{aligned} \tag{4.83}$$

$\boldsymbol{J}_{\overleftarrow{CB}}(\boldsymbol{\theta})$ denoting the CoM Jacobian of the robot.[6] Since $\boldsymbol{p} = \boldsymbol{p}(\boldsymbol{q}, \dot{\boldsymbol{q}}_B) = M\boldsymbol{v}_C$, it follows that

$$\boldsymbol{v}_C = \boldsymbol{v}_B - [\boldsymbol{r}^{\times}_{\overleftarrow{CB}}]\boldsymbol{\omega}_B + \boldsymbol{J}_{\overleftarrow{CB}}\dot{\boldsymbol{\theta}}. \tag{4.84}$$

On the other hand, the *system angular momentum* (SAM) w.r.t. the CoM can be represented as a sum, i.e.

$$\boldsymbol{l}_C(\boldsymbol{q}, \dot{\boldsymbol{q}}_\omega) = \boldsymbol{I}_C(\boldsymbol{q})\boldsymbol{\omega}_B + \boldsymbol{H}_C(\boldsymbol{q})\dot{\boldsymbol{\theta}}, \tag{4.85}$$

where $\dot{\boldsymbol{q}}_\omega = (\boldsymbol{\omega}_B, \dot{\boldsymbol{\theta}})$ and

$$\boldsymbol{H}_C(\boldsymbol{q}) = \sum_{i=1}^{n} \left(\boldsymbol{I}_i \boldsymbol{J}_{\omega i}(\boldsymbol{\theta}) + M_i[\boldsymbol{r}^{\times}_{\overleftarrow{iC}}]\boldsymbol{J}_{vi}(\boldsymbol{\theta})\right), \tag{4.86}$$

$\boldsymbol{J}_{\omega i}(\boldsymbol{\theta})$ being defined in (4.44). Here and henceforth, $\boldsymbol{H}_{(\circ)}$ will be used to denote a map that is composed of mass/inertia-Jacobian products. This type of map represents the *mechanical connection* [86,109] in coordinate form; $\boldsymbol{H}_{(\circ)}$ is referred to as the *coupling inertia* matrix [96].

Furthermore, since the CRB (locked) inertia tensor $\boldsymbol{I}_C(\boldsymbol{q})$ is p.d., its inverse exists. Premultiply (4.85) by $\boldsymbol{I}_C^{-1}$ to obtain

$$\boldsymbol{I}_C^{-1}\boldsymbol{l}_C(\boldsymbol{q}, \dot{\boldsymbol{q}}_\omega) = \boldsymbol{\omega}_B + \boldsymbol{J}_\omega(\boldsymbol{\theta})\dot{\boldsymbol{\theta}}, \tag{4.87}$$

where $\boldsymbol{J}_\omega \equiv \boldsymbol{I}_C^{-1}\boldsymbol{H}_C$. The compact form representation can be written as

$$\boldsymbol{\omega}_C \equiv \hat{\boldsymbol{J}}_\omega(\boldsymbol{\theta})\dot{\boldsymbol{q}}_\omega, \tag{4.88}$$

where $\hat{\boldsymbol{J}}_\omega \equiv \begin{bmatrix}\boldsymbol{E} & \boldsymbol{J}_\omega\end{bmatrix}$. The angular velocity $\boldsymbol{\omega}_C$ is the sum of the angular velocities of all bodies that constitute the system; it is the *system angular velocity* that was introduced in Section 4.6.3. Note that when the joints are locked, $\boldsymbol{\omega}_C = \boldsymbol{\omega}_B = \boldsymbol{\omega}_i$, $i \in \{\overline{1, n}\}$.

The simplest expression of the *system spatial momentum* (SSM) w.r.t. the CoM (i.e. the centroidal SSM) is obtained by employing the centroidal quasivelocity. Then,

$$\mathcal{L}_C(\boldsymbol{q}, \dot{\boldsymbol{q}}_C) = \mathcal{L}_C(\boldsymbol{q}, \mathcal{V}_C) = \mathbb{M}_C\mathcal{V}_C. \tag{4.89}$$

[6] Jacobians $\boldsymbol{J}_{\overleftarrow{CB}}(\boldsymbol{\theta})$ and $\boldsymbol{J}_{vi}(\boldsymbol{\theta})$ have been defined in (2.118).

Apparently, there is no dependency on the joint rates whatsoever. In other words, in this representation, the SSM equals the *CRB spatial momentum* (CRB-SM); we can write: $\mathcal{L}_C(\boldsymbol{q}, \mathcal{V}_C) = \widetilde{\mathcal{L}}_C(\boldsymbol{q}, \mathcal{V}_C)$.

When expressed in terms of the mixed quasivelocity, the SSM assumes the form

$$\begin{aligned}\mathcal{L}_C(\boldsymbol{q}, \dot{\boldsymbol{q}}_M) &= \widetilde{\mathcal{L}}_C(\boldsymbol{q}, \mathcal{V}_M) + \mathcal{L}_{CM}(\boldsymbol{q}, \dot{\boldsymbol{\theta}}) \\ &= \mathbb{M}_C \mathcal{V}_M + \boldsymbol{H}_{CM}\dot{\boldsymbol{\theta}} \\ &= \begin{bmatrix} M\boldsymbol{E} & \boldsymbol{0} \\ \boldsymbol{0} & \boldsymbol{I}_C \end{bmatrix} \begin{bmatrix} \boldsymbol{v}_C \\ \boldsymbol{\omega}_B \end{bmatrix} + \begin{bmatrix} \boldsymbol{0} \\ \boldsymbol{I}_C \boldsymbol{J}_\omega \end{bmatrix} \dot{\boldsymbol{\theta}} \\ &= \boldsymbol{\mathcal{A}}_C(\boldsymbol{q}) \dot{\boldsymbol{q}}_M .\end{aligned} \tag{4.90}$$

There are two components: a CRB-SM one, $\widetilde{\mathcal{L}}_C(\boldsymbol{q}, \mathcal{V}_M)$, and a joint velocity-dependent one, $\mathcal{L}_{CM}$. The latter is referred to as the *coupling spatial momentum (CSM)* [96].

The SSM can also be expressed with the base quasivelocity, as follows:

$$\begin{aligned}\mathcal{L}_C(\boldsymbol{q}, \dot{\boldsymbol{q}}_B) &= \widetilde{\mathcal{L}}_C(\boldsymbol{q}, \mathcal{V}_B) + \mathcal{L}_{CB}(\boldsymbol{q}, \dot{\boldsymbol{\theta}}) \\ &= \mathbb{M}_{CB} \mathcal{V}_B + \boldsymbol{H}_{CB}\dot{\boldsymbol{\theta}} \\ &= \begin{bmatrix} M\boldsymbol{E} & -M[\boldsymbol{r}^{\times}_{\overleftarrow{CB}}] \\ \boldsymbol{0} & \boldsymbol{I}_C \end{bmatrix} \begin{bmatrix} \boldsymbol{v}_B \\ \boldsymbol{\omega}_B \end{bmatrix} + \begin{bmatrix} M\boldsymbol{J}_{\overleftarrow{CB}} \\ \boldsymbol{I}_C \boldsymbol{J}_\omega \end{bmatrix} \dot{\boldsymbol{\theta}} \\ &= \boldsymbol{\mathcal{A}}_{\overleftarrow{CB}}(\boldsymbol{q}) \dot{\boldsymbol{q}}_B .\end{aligned} \tag{4.91}$$

In this representation, there are also two components: CRB-SM $\widetilde{\mathcal{L}}_C(\boldsymbol{q}, \mathcal{V}_B)$ and CSM $\mathcal{L}_{CB}$. The map from the base quasivelocity to the centroidal SSM, $\boldsymbol{\mathcal{A}}_{\overleftarrow{CB}}$, has been named "centroidal momentum matrix" [106,107].

The last equation can be transformed with (4.77) to represent the SSM w.r.t. the base centroid. One arrives then at

$$\begin{aligned}\mathcal{L}_B(\boldsymbol{q}, \dot{\boldsymbol{q}}_B) &= \widetilde{\mathcal{L}}_B(\boldsymbol{q}, \mathcal{V}_B) + \mathcal{L}_{BB}(\boldsymbol{q}, \dot{\boldsymbol{\theta}}) \\ &= \mathbb{M}_B \mathcal{V}_B + \boldsymbol{H}_{BB}\dot{\boldsymbol{\theta}} \\ &= \begin{bmatrix} M\boldsymbol{E} & -M[\boldsymbol{r}^{\times}_{\overleftarrow{CB}}] \\ -M[\boldsymbol{r}^{\times}_{\overleftarrow{CB}}]^T & \boldsymbol{I}_B \end{bmatrix} \begin{bmatrix} \boldsymbol{v}_B \\ \boldsymbol{\omega}_B \end{bmatrix} + \mathbb{T}^T_{\overleftarrow{BC}} \begin{bmatrix} M\boldsymbol{J}_{\overleftarrow{CB}} \\ \boldsymbol{I}_C \boldsymbol{J}_\omega \end{bmatrix} \dot{\boldsymbol{\theta}} \\ &= \boldsymbol{\mathcal{A}}_B \dot{\boldsymbol{q}}_B .\end{aligned} \tag{4.92}$$

Hereby, the parallel-axis inertia transform (4.80) was used. The two components of the SSM in (4.92) are CRB-SM $\widetilde{\mathcal{L}}_B(\boldsymbol{q}, \mathcal{V}_B)$ and CSM $\mathcal{L}_{BB}$.

The following remarks are due. First, note that the locked inertia tensors $\mathbb{M}_C$ and $\mathbb{M}_B$, appearing in (4.89)/(4.90) and (4.92), respectively, are symmetric and positive definite. Thus, they comprise the property of a rigid-body inertia tensor. On the other hand, note that $\mathbb{M}_{CB}$ in (4.91) is p.d. (since $[\boldsymbol{r}^{\times}_{\overleftarrow{CB}}]\boldsymbol{\omega}_B = -\boldsymbol{v}_B$) but not symmetric. Furthermore, the representation in terms of the mixed quasivelocity, (4.90), provides for inertial decoupling between the linear and angular CRB momentum components and the independence of the former from the joint rates. This representation yields important advantages from the viewpoint of humanoid robot balance control design (cf. Chapter 5):

1. the block-diagonal form of the spatial (locked) inertia tensor is quite desirable for control decoupling,
2. the CoM velocity plays an essential role in balance control, and
3. the angular velocity of the base relates directly to orientation control of the base link (and, hence, of the upper body).

4.6.5 Instantaneous Motion of a Free-Floating Manipulator

From the definitions of the centroidal and mixed quasivelocities and the system angular velocity in (4.87), the following relation can be established:

$$\dot{\boldsymbol{q}}_C = \boldsymbol{T}_{\overleftarrow{CM}}(\boldsymbol{q})\dot{\boldsymbol{q}}_M. \tag{4.93}$$

The matrix

$$\boldsymbol{T}_{\overleftarrow{CM}}(\boldsymbol{q}) = \begin{bmatrix} \boldsymbol{E} & \boldsymbol{0} & \boldsymbol{0} \\ \boldsymbol{0} & \boldsymbol{E} & \boldsymbol{J}_\omega(\boldsymbol{q}) \\ \boldsymbol{0} & \boldsymbol{0} & \boldsymbol{E} \end{bmatrix} \tag{4.94}$$

plays the role of a coordinate transform for the quasivelocities. Note that the common rule for coordinate transforms, $\boldsymbol{T}^{-1}_{\overleftarrow{CM}} = \boldsymbol{T}_{\overleftarrow{MC}}$, applies. From (4.93), the following relation for the spatial velocities can be obtained:

$$\mathcal{V}_C = \mathcal{V}_M + \begin{bmatrix} \boldsymbol{0} \\ \boldsymbol{J}_\omega \end{bmatrix} \dot{\boldsymbol{\theta}}. \tag{4.95}$$

The following is an important observation: given the system spatial velocity $\mathcal{V}_C$,[7] *the joint rates will determine the angular velocity of the base link in a unique way*. This is the formulation of the instantaneous-motion forward kinematic problem w.r.t. the floating base of a free-floating system. On the other hand, the determination of the joint rates that ensure the desired rotational state of the floating base can be recognized as the respective inverse problem. The solution to the inverse problem will be presented in Section 4.7. Apparently, the forward and inverse kinematic problems of the free-floating system are expressed in the same form as the instantaneous-motion kinematic problems discussed in Chapter 2.

Furthermore, from the SSM expressions (4.89) and (4.90) one obtains

$$\mathcal{V}_C = \mathbb{M}_C^{-1}\mathcal{L}_C(\boldsymbol{q}, \dot{\boldsymbol{q}}_M) = \mathcal{V}_M + \mathbb{M}_C^{-1}\boldsymbol{H}_{CM}\dot{\boldsymbol{\theta}}. \tag{4.96}$$

Comparing this result with (4.95), we arrive at the identity

$$\mathbb{M}_C^{-1}\boldsymbol{H}_{CM} \equiv \begin{bmatrix} \boldsymbol{0}^T & \boldsymbol{J}_\omega^T \end{bmatrix}^T, \tag{4.97}$$

which holds for any $\mathcal{V}_C$, $\mathcal{V}_M$ and $\dot{\boldsymbol{\theta}}$.

[7] Note that in zero gravity and absence of other external forces, the system spatial velocity $\mathcal{V}_C$ is constant (as is $\boldsymbol{\omega}_C$).

Next, consider the relation between the centroidal and base quasivelocities. Combine (4.84) with (4.87) to obtain

$$\mathcal{V}_C = \mathbb{T}_{\overleftarrow{CB}}\mathcal{V}_B + \boldsymbol{J}_\theta(\boldsymbol{\theta})\dot{\boldsymbol{\theta}} \tag{4.98}$$

$$= \boldsymbol{J}_q(\boldsymbol{q})\dot{\boldsymbol{q}}_B, \tag{4.99}$$

where

$$\boldsymbol{J}_q(\boldsymbol{q}) \equiv \begin{bmatrix}\mathbb{T}_{\overleftarrow{CB}} & \boldsymbol{J}_\theta(\boldsymbol{\theta})\end{bmatrix} \in \Re^{6\times(n+6)}$$

and

$$\boldsymbol{J}_\theta(\boldsymbol{\theta}) \equiv \begin{bmatrix}\boldsymbol{J}^T_{\overleftarrow{CB}}(\boldsymbol{\theta}) & \boldsymbol{J}^T_\omega(\boldsymbol{\theta})\end{bmatrix}^T \in \Re^{6\times n}.$$

Spatial velocity relation (4.98) can be rewritten as

$$\mathcal{V}_B + \mathbb{T}_{\overleftarrow{BC}}\boldsymbol{J}_\theta\dot{\boldsymbol{\theta}} = \mathbb{T}_{\overleftarrow{BC}}\mathcal{V}_C. \tag{4.100}$$

Then, the following relation between quasivelocities $\dot{\boldsymbol{q}}_B$ and $\dot{\boldsymbol{q}}_C$ can be obtained:

$$\dot{\boldsymbol{q}}_C = \boldsymbol{T}_{\overleftarrow{CB}}(\boldsymbol{q})\dot{\boldsymbol{q}}_B. \tag{4.101}$$

The coordinate transform is

$$\boldsymbol{T}_{\overleftarrow{CB}} = \begin{bmatrix}\boldsymbol{E} & -[\boldsymbol{r}^\times_{\overleftarrow{CB}}] & \boldsymbol{J}_{\overleftarrow{CB}}(\boldsymbol{\theta}) \\ \boldsymbol{0} & \boldsymbol{E} & \boldsymbol{J}_\omega(\boldsymbol{q}) \\ \boldsymbol{0} & \boldsymbol{0} & \boldsymbol{E}\end{bmatrix}. \tag{4.102}$$

On the other hand, from (4.91) we have

$$\mathcal{V}_B + \mathbb{M}^{-1}_{CB}\boldsymbol{H}_{CB}\dot{\boldsymbol{\theta}} = \mathbb{M}^{-1}_{CB}\mathcal{L}_C(\boldsymbol{q}, \dot{\boldsymbol{q}}_B). \tag{4.103}$$

Comparing the last equation with (4.100), the following identity can be established:

$$\mathbb{M}^{-1}_{CB}\boldsymbol{H}_{CB} \equiv \mathbb{T}_{\overleftarrow{BC}}\boldsymbol{J}_\theta, \tag{4.104}$$

and thus

$$\mathbb{M}^{-1}_{CB}\mathcal{L}_C(\boldsymbol{q}, \dot{\boldsymbol{q}}_B) \equiv \mathbb{T}_{\overleftarrow{BC}}\mathcal{V}_C. \tag{4.105}$$

These identities hold for any $\mathcal{V}_C$, $\mathcal{V}_B$ and $\dot{\boldsymbol{\theta}}$.

Finally, a rule for transforming quasivelocity $\dot{\boldsymbol{q}}_B$ to quasivelocity $\dot{\boldsymbol{q}}_M$ will be obtained. To this end, make use of (2.121):

$$\dot{\boldsymbol{q}}_M = \boldsymbol{T}_{\overleftarrow{MB}}(\boldsymbol{q})\dot{\boldsymbol{q}}_B. \tag{4.106}$$

The coordinate transform is written as (see also [47])

$$\boldsymbol{T}_{\overleftarrow{MB}}(\boldsymbol{q}) = \begin{bmatrix} \boldsymbol{E} & -[\boldsymbol{r}^{\times}_{\overleftarrow{CB}}] & \boldsymbol{J}_{\overleftarrow{CB}}(\boldsymbol{\theta}) \\ \boldsymbol{0} & \boldsymbol{E} & \boldsymbol{0} \\ \boldsymbol{0} & \boldsymbol{0} & \boldsymbol{E} \end{bmatrix}. \tag{4.107}$$

The following relation for the spatial velocities can then be obtained:

$$\mathcal{V}_B + \mathbb{T}_{\overleftarrow{BM}} \begin{bmatrix} \boldsymbol{J}_{\overleftarrow{CB}} \\ \boldsymbol{0} \end{bmatrix} \dot{\boldsymbol{\theta}} = \mathbb{T}_{\overleftarrow{BM}} \mathcal{V}_M. \tag{4.108}$$

4.7 MOMENTUM-BASED REDUNDANCY RESOLUTION

4.7.1 The Momentum Equilibrium Principle

It is assumed that a completely unconstrained space robot comprising a kinematically redundant arm ($n > 6$) is floating freely in zero gravity. The SSM can be represented as a sum, i.e.

$$\text{SSM} = \text{CRB-SM} + \text{CSM}.$$

This relation is valid for all SSM expressions in the form of a sum, i.e. $\mathcal{L}_C(\boldsymbol{q}, \dot{\boldsymbol{q}}_M)$, $\mathcal{L}_C(\boldsymbol{q}, \dot{\boldsymbol{q}}_B)$, and $\mathcal{L}_B(\boldsymbol{q}, \dot{\boldsymbol{q}}_B)$. The above relation, henceforth referred to as the *momentum equilibrium principle*, plays a fundamental role in momentum-based redundancy resolution. It is worth noting that the momentum equilibrium principle results from the dynamic equilibrium of the wrenches in the spatial dynamics component of the equation of motion, that is observed when no external forces act on the floating-base system (cf. Section 4.8).

Furthermore, note that the instantaneous motion in the joints, expressed by the joint velocity vector $\dot{\boldsymbol{\theta}}$, is explicitly present in the CSM term of the above relation. The joint velocity can be used as a control input in motion and balance control tasks. It should be noted that although any instantaneous motion in the joints induces a variation in the CSM, it does alter the SSM. Indeed, in the case of a free-floating space robot, the SSM is conserved during the unconstrained manipulator motion since the environmental forces (i.e. the solar pressure, the air drag when operating in low orbit, etc.) acting on the system can be ignored; they only matter in a relatively long term. It should be also noted that, since the system is underdetermined, there is a set of joint velocities that do not alter the CRB-SM at all. This type of instantaneous motion plays an important role, as will be shown in what follows.

Furthermore, the angular momentum component of spatial momentum deserves special attention. This component plays a more important role than the linear one, as revealed in a number of studies in the field of free-floating space robotics [97,98,94,93].[8] In the field of humanoid robotics, the CRB rotational motion plays likewise an important role (e.g. in balance control). When redundancy resolution is based on angular momentum only, the dimension of the system can be decreased. This approach helps to avoid overconstrained states and to

[8] The floating-base mounted communication antenna should always be pointing with high accuracy in the direction of the remote control center.

decrease the computational cost. It should also be noted that the special case of *angular momentum conservation* is quite essential in relation to such humanoid robot tasks as jumping or running. The representation of the spatial momentum in terms of mixed quasivelocity is quite useful in angular momentum–based analysis, motion generation, and control.

4.7.2 Spatial Momentum–Based Redundancy Resolution

Without loss of generality, the following derivations will be based on the base link–centered SSM representation in terms of the base quasivelocity, $\mathcal{L}_B(\boldsymbol{q}, \dot{\boldsymbol{q}}_B)$. The momentum equation (4.92) can be solved for the manipulator joint rates that can then be used as input variables in velocity–based motion control schemes. Since the equation is linear in the velocities, its solution type depends on the number of manipulator joints n. The system is assumed underdetermined and thus, there is an infinite number of solutions for the joint velocities. The general solution can be represented as a sum of two orthogonal components, very much like in the case of a kinematically redundant limb (cf. Section 2.7, (2.34)), i.e.

$$\dot{\boldsymbol{\theta}} = \boldsymbol{H}_{BB}^{+}(\mathcal{L}_B - \mathbb{M}_B\mathcal{V}_B) + \boldsymbol{N}(\boldsymbol{H}_{BB})\dot{\boldsymbol{\theta}}_a. \tag{4.109}$$

Here $\boldsymbol{H}_{BB}^{+}$ and $\boldsymbol{N}(\boldsymbol{H}_{BB})$ denote the (right) pseudoinverse of the coupling inertia matrix and a projector onto its null space, respectively.

Coupling Spatial Momentum Conservation: the Reaction Null Space

The CSM is conserved at zero ($\mathcal{L}_{BB} \equiv \boldsymbol{H}_{BB}(\boldsymbol{q})\dot{\boldsymbol{\theta}} = \boldsymbol{0}$) when the SSM equals the CRB-SM, i.e. $\mathcal{L}_B = \widetilde{\mathcal{L}}_B = \mathbb{M}_B\mathcal{V}_B$. Vector $\dot{\boldsymbol{\theta}}_a$ in (4.109) is a joint velocity vector that parametrizes the following infinite set of joint velocities:

$$\{\dot{\boldsymbol{\theta}}_{csm}(\boldsymbol{q}, \dot{\boldsymbol{\theta}}_a) \in \mathcal{N}(\boldsymbol{H}_{BB}(\boldsymbol{q})) : \dot{\boldsymbol{\theta}} = \boldsymbol{N}(\boldsymbol{H}_{BB}(\boldsymbol{q})\dot{\boldsymbol{\theta}}_a, \forall\dot{\boldsymbol{\theta}}_a\}. \tag{4.110}$$

Joint velocities derived from the set $\{\dot{\boldsymbol{\theta}}_{csm}(\boldsymbol{q}, \dot{\boldsymbol{\theta}}_a)\}$ are solutions to the homogeneous equation $\boldsymbol{H}_{BB}(\boldsymbol{q})\dot{\boldsymbol{\theta}} = \boldsymbol{0}$. Thus, they can be characterized as *CSM conserving*.

The above set is orthogonal to the particular solution component (the pseudoinverse term in (4.109)). This implies that whatever the CSM conserving joint velocity, it will not affect the state of the CRB. Notice that the set is defined in a similar way as the set of self-motion velocities (2.29) of a fixed-base kinematically redundant manipulator; $\mathcal{N}(\boldsymbol{H}_{BB}(\boldsymbol{q}))$ determines a subspace at $\boldsymbol{q}$ that is tangent to a manifold in the joint space (similar to the self-motion manifold mentioned in Section 2.7.1). Locally, the dimension of this manifold, henceforth referred to as the *CSM conserving manifold*, equals the rank of the null-space projector. At a nonsingular manipulator configuration s.t. the coupling inertia matrix is full row-rank, $\text{rank}\boldsymbol{N}(\boldsymbol{H}_{BB}) = n - 6$. With a 7-DOF manipulator, for example, the manifold will be just 1D. In this case, the set of CSM conserving joint velocities can be represented in the form of an autonomous dynamical system, i.e.

$$\dot{\boldsymbol{\theta}} = b\boldsymbol{n}_{BB}(\boldsymbol{q}). \tag{4.111}$$

Scalar b is an arbitrary parameter having the dimension of joint rate. The null space vector $\boldsymbol{n}_{BB}(\boldsymbol{q}) \in \mathcal{N}(\boldsymbol{H}_{BB}(\boldsymbol{q}))$ determines the *CSM conserving vector field* in the joint space. Its integral curves constitute the CSM conserving manifold. The projection of an integral curve onto the

workspace of the manipulator (via forward kinematics) will be referred to as a *CSM conserving path*.

From the above discussion it becomes apparent that the role of the coupling inertia matrix of a free-floating system is similar to that of the Jacobian of a fixed-base manipulator, in the sense that $\boldsymbol{H}_{BB}$ induces a local, orthogonal decomposition formalism on the CSM conserving manifold. Thereby, the null space of the coupling inertia matrix, $\mathcal{N}(\boldsymbol{H}_{BB})$, represents the tangent subspace at $\boldsymbol{q}$. The respective map is defined via the null-space projector $\boldsymbol{N}(\boldsymbol{H}_{BB}) = \boldsymbol{E} - \boldsymbol{H}_{BB}^{+}\boldsymbol{H}_{BB}$. The orthogonal complement of this map, $\boldsymbol{H}_{BB}^{+}\boldsymbol{H}_{BB}$, determines the normal component at the manifold. It will be shown below (cf. Section 4.8.1) that when an instantaneous motion originates from within the CSM conserving set, no force/moment will be impressed upon the base link. Thus, the term "*reactionless motion*" can be used as an alternative to the "CSM conserving motion." The set (4.110) (i.e. the null space of the coupling inertia matrix) is referred to as the (spatial momentum) *Reaction Null Space* (RNS) [96,95]. It follows then that the RNS is the tangent subspace to the CSM conserving manifold at $\boldsymbol{q}$.

The decomposition formalism outlined above is the essence of the *RNS method*. This method plays an important role in motion analysis, generation, and control of floating-base systems, including humanoid robots [100]. Readers interested in the theoretical aspect of the decomposition formalism for generic underactuated systems are referred to [86,109].

System Spatial-Momentum Conservation

According to the spatial velocity relation (4.99), there is an infinite number of base-link and coupling spatial velocity combinations for a given (constant) system spatial velocity, i.e.

$$\dot{\boldsymbol{q}}_B(\dot{\boldsymbol{q}}_a) = \boldsymbol{J}_q^{+}(\boldsymbol{q})\mathcal{V}_C + \boldsymbol{N}(\boldsymbol{J}_q)\dot{\boldsymbol{q}}_a. \tag{4.112}$$

Here $\dot{\boldsymbol{q}}_a$ parametrizes the null space $\mathcal{N}(\boldsymbol{J}_q)$ in a nonminimal way. This null space comprises instantaneous motion components that preserve the system spatial velocity and thus the spatial momentum of the system, i.e.

$$\{\dot{\boldsymbol{q}}_{sm} \in \mathcal{N}(\boldsymbol{J}_q) : \dot{\boldsymbol{q}}_B = \boldsymbol{N}(\boldsymbol{J}_q)\dot{\boldsymbol{q}}_a,\ \forall \dot{\boldsymbol{q}}_a\};$$

$\mathcal{N}(\boldsymbol{J}_q)$ will be henceforth referred to as the *SSM conserving null space*.

When the SSM is conserved, as usually assumed in the field of free-floating space robotics, the system spatial velocity will be constant: $\mathcal{V}_C = \mathcal{V}_{\text{const}}$. In the general case of instantaneous joint motion that does not originate from within the (spatial momentum) RNS, the base twist will be altered via the CSM component, as apparent from (4.103), i.e.

$$\mathcal{V}_B = \mathcal{V}_{\text{const}} - \mathbb{M}_B^{-1}\boldsymbol{H}_{BB}\dot{\boldsymbol{\theta}}. \tag{4.113}$$

In the special case of reactionless motion, $\boldsymbol{H}_{BB}\dot{\boldsymbol{\theta}} = \boldsymbol{0},\ \forall\dot{\boldsymbol{\theta}} \Rightarrow \mathcal{V}_B = \mathcal{V}_{\text{const}}$.

4.7.3 Angular Momentum–Based Redundancy Resolution

The redundancy resolution approach outlined above can be recast in terms of angular momentum only, thus decreasing the dimension of the linear system from six to three. The representation of the centroidal SSM in terms of the mixed quasivelocity is quite suitable for

this purpose, as already clarified. The SAM relation, given in (4.85), is an underdetermined linear system of three equations in n unknowns. As already noted, this relation can be rewritten in terms of angular velocity (cf. (4.87)). The general solution of (4.87) can be written as

$$\dot{\boldsymbol{\theta}} = \boldsymbol{J}_{\omega}^{+}(\boldsymbol{\theta})\Delta\boldsymbol{\omega} + \boldsymbol{N}(\boldsymbol{J}_{\omega}(\boldsymbol{\theta}))\dot{\boldsymbol{\theta}}_a. \tag{4.114}$$

The particular solution component (the pseudoinverse term) can be used to control the *relative angular velocity* $\Delta\boldsymbol{\omega} = \boldsymbol{\omega}_C - \boldsymbol{\omega}_B$, i.e. the system angular velocity, $\boldsymbol{\omega}_C$, w.r.t. a given base angular velocity $\boldsymbol{\omega}_B$. The homogeneous solution component, on the other hand, is useful to reconfigure the limbs in a desirable way, by employing $\dot{\boldsymbol{\theta}}_a$ as a control input. Thereby, the relative angular velocity will be unaffected. Since the two components are orthogonal, they provide the base for decoupled control of these two control objectives.

Coupling Angular Momentum Conservation

The homogeneous component in (4.114) is obtained by setting the relative angular velocity at zero, i.e. $\boldsymbol{\omega}_C = \boldsymbol{\omega}_B$. This condition implies that the coupling angular momentum (CAM) will be conserved, e.g. at zero, so $\boldsymbol{H}_C\dot{\boldsymbol{\theta}} = \boldsymbol{0}$. The set of joint velocities satisfying this condition is obtained as

$$\{\dot{\boldsymbol{\theta}}_{cam}(\boldsymbol{\theta}, \dot{\boldsymbol{\theta}}_a) \in \mathcal{N}(\boldsymbol{J}_{\omega}(\boldsymbol{\theta})) : \dot{\boldsymbol{\theta}} = \boldsymbol{N}(\boldsymbol{J}_{\omega}(\boldsymbol{\theta}))\dot{\boldsymbol{\theta}}_a,\ \forall\dot{\boldsymbol{\theta}}_a\}.$$

Any joint velocity from within the set $\{\dot{\boldsymbol{\theta}}_{cam}\}$ will be referred to as a *CAM conserving* joint velocity; $\{\dot{\boldsymbol{\theta}}_{cam}(\boldsymbol{\theta}, \dot{\boldsymbol{\theta}}_a)\}$ determines the tangent subspace of a manifold (the CAM conserving manifold) at $\boldsymbol{\theta}$. Since $\mathcal{N}(\boldsymbol{J}_{\omega}) = \mathcal{N}(\boldsymbol{H}_C)$ and $\text{rank}\boldsymbol{N}(\boldsymbol{H}_C) = n - 3 > \text{rank}\boldsymbol{N}(\boldsymbol{H}_{BB}) = n - 6$, it can be concluded that the tangent bundle of the CAM conserving manifold is a *superset* of that of the CSM conserving manifold. In analogy to the spatial momentum RNS, the tangent subspace of the CAM conserving manifold at $\boldsymbol{\theta}$ can be referred to as the *angular momentum RNS*. Noting that angular momentum plays an important role in motion generation and control of free-floating space robots and humanoid robots alike (e.g. in satellite-base orientation and balance control, respectively), the angular momentum RNS will be henceforth simply referred to as the RNS.

System Angular Momentum Conservation

According to the angular velocity relation (4.88), there is an infinite number of base-link and coupling angular velocity combinations for a given system angular velocity, i.e.

$$\dot{\boldsymbol{q}}_{\omega} = \hat{\boldsymbol{J}}_{\omega}^{+}(\boldsymbol{\theta})\boldsymbol{\omega}_C + \boldsymbol{N}(\hat{\boldsymbol{J}}_{\omega})\dot{\boldsymbol{q}}_{\omega a}; \tag{4.115}$$

$\dot{\boldsymbol{q}}_{\omega a} = \begin{bmatrix}\boldsymbol{\omega}_{Ba}^T & \dot{\boldsymbol{\theta}}_a^T\end{bmatrix}^T$ parametrizes the null space $\mathcal{N}(\hat{\boldsymbol{J}}_{\omega})$ in a nonminimal way. This null space comprises instantaneous motion components that do not alter the system angular velocity and thus conserve the SAM ($\boldsymbol{l}_C = \boldsymbol{I}_C\boldsymbol{\omega}_C = \text{const.}$), so we have

$$\{\dot{\boldsymbol{q}}_{\bar{\omega}} \in \mathcal{N}(\hat{\boldsymbol{J}}_{\omega}) : \dot{\boldsymbol{q}}_{\omega} = \boldsymbol{N}(\hat{\boldsymbol{J}}_{\omega}(\boldsymbol{\theta}))\dot{\boldsymbol{q}}_{\omega a},\ \forall\dot{\boldsymbol{q}}_{\omega a}\}. \tag{4.116}$$

The null space $\mathcal{N}(\hat{\boldsymbol{J}}_{\omega})$ will be henceforth referred to as the *SAM conserving null space*. Base-link/joint velocity combinations from within this null space are used when a humanoid robot is airborne.

Example: a Dual-Task Scenario With a Free-Floating Space Manipulator

It is straightforward to apply the RNS method to a dual-task scenario wherein the instantaneous motion of each end link (base and end effector) of the free-floating manipulator is to be controlled [94]. Denote by $\boldsymbol{J}_E(\boldsymbol{q}) \in \Re^{6\times n}$ the *fixed-base* manipulator end-effector Jacobian expressed w.r.t. the inertial frame. The spatial velocity of the end effector results from the instantaneous motion of the base and the manipulator joints; hence

$$\mathcal{V}_E = \mathbb{T}_{\overleftarrow{EB}}\mathcal{V}_B + \boldsymbol{J}_E\dot{\boldsymbol{\theta}}. \tag{4.117}$$

Furthermore, assume zero initial momentum, s.t. $\mathcal{V}_{\text{const}} = \boldsymbol{0}$. Then, the momentum conservation (4.113) can be used as a constraint to eliminate $\mathcal{V}_B$ from the last equation. One arrives at

$$\mathcal{V}_E = \hat{\boldsymbol{J}}_E(\boldsymbol{q})\dot{\boldsymbol{\theta}}. \tag{4.118}$$

The matrix $\hat{\boldsymbol{J}}_E = \boldsymbol{J}_E - \mathbb{T}_{\overleftarrow{EB}}\mathbb{M}_B^{-1}\boldsymbol{H}_{BB}$ is called the "generalized Jacobian" [153]. The terminology stems from the fact that the last equation can be used not only for floating-base systems in zero gravity, but also for fixed-base systems. Indeed, when the CRB inertia approaches infinity, e.g. as a result of using a very heavy or fixed base, the $\mathbb{M}_B^{-1}$ term becomes infinitesimally small. Hence, the generalized Jacobian approaches that of the fixed-base manipulator, i.e. $\hat{\boldsymbol{J}}_E \to \boldsymbol{J}_E$. Note also that, using (4.104), the generalized Jacobian can be represented as

$$\hat{\boldsymbol{J}}_E = \boldsymbol{J}_E - \mathbb{T}_{\overleftarrow{EC}}\boldsymbol{J}_\theta. \tag{4.119}$$

When the manipulator is kinematically redundant, the generalized Jacobian comprises a nontrivial null space, so $\mathcal{N}(\hat{\boldsymbol{J}}_E) \neq \emptyset$. The redundancy can be resolved in accordance with the approaches introduced in Chapter 2. For instance, a task prioritization can be introduced. The end-effector task can be solved within the RNS, i.e. as a lower-priority task, or vice versa. Thereby, the self-motion obtained from the null space of the generalized Jacobian yields the so-called "manipulator inversion task," wherein the end effector is fixed in inertial space but the base is not [94,93]. Furthermore, when the degree of redundancy is sufficiently large ($n > 12$), it becomes possible to immobilize both end links s.t. only the intermittent links will be in motion. The motion of the free-floating manipulator resembles then the self-motion of a kinematically redundant fixed-base manipulator. To achieve this, the joint velocity should be derived from within the intersection of the two null spaces, i.e. $\mathcal{N}(\hat{\boldsymbol{J}}_E) \cap \mathcal{N}(\boldsymbol{H}_{BB})$.

To avoid the frequent appearance of an overconstrained state, it would be useful to introduce task priorities with regard to the translational and rotational motion subtasks of the satellite base. From a practical viewpoint, the latter subtask should have a higher priority, as already mentioned. The translational motion constraint can be, in fact, fully relaxed. In other words, the angular momentum RNS should be employed instead of the spatial momentum RNS. This is the so-called "selective RNS" approach [99].

4.7.4 Motion of a Free-Floating Humanoid Robot in Zero Gravity

Motion analysis of a free-floating humanoid robot in zero gravity is helpful for better understanding the role of the spatial momentum components introduced in the previous

sections. It is also helpful for designing control methods for humanoid robots [132]. As an example, consider the implementation of the RNS-based redundancy resolution method in the following multitask scenario. The robot is required to track the motion of a translating and rotating box with its hands (first motion task), aiming at a precontact posture with zero relative twists. To ensure sufficient time for the tracking, the rotation of the base link of the robot has to be synchronized with that of the box, otherwise the box could leave the workspace before the robot attains the correct posture for grasping. Base reorientation control is achieved via cyclic (circular) motion in the feet, without a phase difference (this is the second motion task). Note, however, that if the motion of the box is arbitrary, the tracking could result in an overconstrained system and/or self-collision. To avoid this, the motion of the box is constrained within the sagittal plane. It is then sufficient to reorient the base link in the pitch direction only (this is the third motion control task). The result of the simulation is shown in Video 4.7-1 [45].

Note that if a phase difference is introduced in the feet motion, significant shaking in the yaw direction will be observed. The problem can be alleviated with the help of a yaw compensation control. This can be achieved with inertial coupling induced by the arm motion, as shown in Video 4.7-2 [44]. Apparently, to compensate the deviation of the base in the yaw direction, the arms have to move significantly since their inertia is much lower than that of the CRB yaw inertia. Such motion is practically infeasible, though, because of the high probability of self-collision. A possible solution to the problem is shown in Video 4.7-3 [43]. The goal is achieved in two phases. During the first phase, only base pitch control is invoked whereby the hand position/orientation control is relaxed. In this way, the ill-conditioning leading to a significant arm motion can be avoided. After achieving the desired base pitch orientation, the hand control is invoked to attain a suitable grasp posture (this is the second phase). Thereby, the feet move slightly to compensate the base-link deviation induced by the approaching motion of the hands. This example demonstrates how important motion generation is in preventing the frequent occurrence of an overconstrained system.

It is worth noting that the method of floating-base reorientation control of a space-borne manipulator via end-link cyclic motion was introduced in the pioneering work [154]. Note also that this approach is used by an astronaut when reorienting his/her body via limb motion [143,142]. A simulation for body-roll reorientation via cyclic arm motion is shown in Video 4.7-4 [42]. Such reorientation can also be achieved with cyclic motion in the feet, as shown in Video 4.7-5 [103]. In this relation, it is interesting to observe that while walking in zero gravity, the orientation of the body in the pitch direction changes gradually, as shown in Video 4.7-6 [82]. This effect stems from the inertial coupling, as in the rest of the above examples. The following important conclusion can then be made: angular momentum control in the pitch direction is essential during normal gait on flat terrain (see also [161]).

4.8 EQUATION OF MOTION OF A FREE-FLOATING MANIPULATOR IN ZERO GRAVITY

The equation of motion of a free-floating manipulator in zero gravity will be derived in terms of the base, the mixed, and the centroidal quasivelocity.

4.8.1 Representation in Terms of Base Quasivelocity

The kinetic energy of the system can be written as

$$T = \frac{1}{2}\dot{\boldsymbol{q}}_B^T \boldsymbol{M}_B(\boldsymbol{q})\dot{\boldsymbol{q}}_B, \tag{4.120}$$

where

$$\boldsymbol{M}_B(\boldsymbol{q}) = \begin{bmatrix} \mathbb{M}_B & \boldsymbol{H}_{BB} \\ \boldsymbol{H}_{BB}^T & \boldsymbol{M}_{\theta B} \end{bmatrix}, \tag{4.121}$$

$\boldsymbol{M}_{\theta B}(\boldsymbol{\theta})$ denoting the joint-space inertia matrix of the *fixed-base* manipulator (cf. (4.43)). The equation of motion, obtained from the Lagrangian

$$\frac{\partial}{\partial t}\left(\frac{\partial T}{\partial \dot{\boldsymbol{q}}_B}\right) - \frac{\partial T}{\partial \boldsymbol{q}} = \mathcal{Q},$$

can be written as

$$\boldsymbol{M}_B(\boldsymbol{q})\ddot{\boldsymbol{q}}_B + \boldsymbol{c}_B(\boldsymbol{q}, \dot{\boldsymbol{q}}_B) = \mathcal{Q}. \tag{4.122}$$

The nonlinear velocity-dependent force term $\boldsymbol{c}_B(\boldsymbol{q}, \dot{\boldsymbol{q}}_B)$ can be expressed in the form of (4.46), $\mathcal{Q} = \boldsymbol{S}^T\boldsymbol{\tau} = \begin{bmatrix}\boldsymbol{0}^T & \boldsymbol{\tau}^T\end{bmatrix}^T \in \Re^{6+n}$ denotes the *generalized force*, $\boldsymbol{S} = \begin{bmatrix}\boldsymbol{0}_{n\times 6} & \boldsymbol{E}_n\end{bmatrix}$ is the underactuation filtering matrix (cf. (2.102)), and $\boldsymbol{\tau} \in \Re^n$ denotes the joint torque of the manipulator. Note that since the system is underactuated, the generalized force does not depend on the specific type of quasivelocity. Thus, there is no subscript attached to $\mathcal{Q}$.

Furthermore, for the purpose of analysis and control, the following expanded-form representations of the equation of motion are found to be useful:

$$\begin{bmatrix} \mathbb{M}_B & \boldsymbol{H}_{BB} \\ \boldsymbol{H}_{BB}^T & \boldsymbol{M}_{\theta B} \end{bmatrix}\begin{bmatrix} \dot{\mathcal{V}}_B \\ \ddot{\boldsymbol{\theta}} \end{bmatrix} + \begin{bmatrix} \mathcal{C}_B \\ \boldsymbol{c}_{\theta B} \end{bmatrix} = \begin{bmatrix} \boldsymbol{0} \\ \boldsymbol{\tau} \end{bmatrix} \tag{4.123}$$

and

$$\begin{bmatrix} M\boldsymbol{E} & -M[\boldsymbol{r}^{\times}_{\overleftarrow{CB}}] & M\boldsymbol{J}_{\overleftarrow{CB}} \\ -M[\boldsymbol{r}^{\times}_{\overleftarrow{CB}}]^T & \boldsymbol{I}_B & \boldsymbol{H}_B \\ M\boldsymbol{J}_{\overleftarrow{CB}}^T & \boldsymbol{H}_B^T & \boldsymbol{M}_{\theta B} \end{bmatrix}\begin{bmatrix} \dot{\boldsymbol{v}}_B \\ \dot{\boldsymbol{\omega}}_B \\ \ddot{\boldsymbol{\theta}} \end{bmatrix} + \begin{bmatrix} \boldsymbol{c}_{fB} \\ \boldsymbol{c}_{mB} \\ \boldsymbol{c}_{\theta B} \end{bmatrix} = \begin{bmatrix} \boldsymbol{0} \\ \boldsymbol{0} \\ \boldsymbol{\tau} \end{bmatrix}; \tag{4.124}$$

$\mathcal{C}_B = \begin{bmatrix}\boldsymbol{c}_{fB}^T & \boldsymbol{c}_{mB}^T\end{bmatrix}^T$ is a nonlinear velocity-dependent wrench stemming from the spatial dynamics component. We have

$$\begin{aligned} \mathcal{C}_B &= \dot{\mathbb{M}}_B\mathcal{V}_B + \dot{\boldsymbol{H}}_{BB}\dot{\boldsymbol{\theta}} + \mathcal{C}'_B \\ &= \overbrace{\begin{bmatrix} M\left(-[\dot{\boldsymbol{r}}^{\times}_{\overleftarrow{CB}}]^T\boldsymbol{\omega}_B + \dot{\boldsymbol{J}}_{\overleftarrow{BC}}\dot{\boldsymbol{\theta}}\right) \\ \dot{\boldsymbol{I}}_B\boldsymbol{\omega}_B + \dot{\boldsymbol{H}}_{BB}\dot{\boldsymbol{\theta}} - M[\dot{\boldsymbol{r}}^{\times}_{\overleftarrow{CB}}]^T\boldsymbol{v}_B \end{bmatrix}}^{} + \overbrace{\begin{bmatrix} \boldsymbol{0} \\ M[\dot{\boldsymbol{r}}^{\times}_{\overleftarrow{CB}}]^T\boldsymbol{v}_C \end{bmatrix}}^{}. \end{aligned} \tag{4.125}$$

Note that $\mathcal{C}'_B$ is a derivative of the moment of momentum. The $\boldsymbol{c}_{\theta B}$-term, on the other hand, denotes the nonlinear velocity-dependent joint torque of the fixed-base manipulator (cf. (4.46)).

In the Case of Momentum Conservation (no External Forces)

In the above derivation of the equation of motion it was assumed that no external forces act on the system. In this case, spatial momentum is conserved with $\mathcal{V}_C = \text{const}$. In the special case of momentum conservation at zero (i.e. $\boldsymbol{v}_C = \boldsymbol{0}$), $\mathcal{C}'_B$ in (4.125) becomes zero.

Furthermore, from analytical mechanics it is known that conserved quantities in the equation of motion are related to *ignorable or cyclic coordinates* [65]. This implies that the dynamics of the system can be represented in *reduced* form. Indeed, by inserting velocity relation (4.113) into the expression for the kinetic energy, (4.120), one obtains

$$T = \frac{1}{2}\left(\dot{\boldsymbol{\theta}}^T \hat{\boldsymbol{M}}_{\theta B}\dot{\boldsymbol{\theta}} + \mathcal{V}_{\text{const}}^T \mathbb{M}_B \mathcal{V}_{\text{const}}\right). \tag{4.126}$$

The matrix

$$\hat{\boldsymbol{M}}_{\theta B} = \boldsymbol{M}_{\theta B} - \boldsymbol{H}_{BB}^T \mathbb{M}_B^{-1} \boldsymbol{H}_{BB} \tag{4.127}$$

is referred to as the *generalized inertia tensor* [163]. In this case, the equation of motion obtained from the Lagrangian

$$\frac{\partial}{\partial t}\left(\frac{\partial T}{\partial \dot{\boldsymbol{\theta}}}\right) - \frac{\partial T}{\partial \boldsymbol{\theta}} = \boldsymbol{\tau}$$

assumes the form

$$\hat{\boldsymbol{M}}_{\theta B}\ddot{\boldsymbol{\theta}} + \hat{\boldsymbol{c}}_{\theta B} = \boldsymbol{\tau}. \tag{4.128}$$

The term

$$\hat{\boldsymbol{c}}_{\theta B} = \boldsymbol{c}_{\theta B} - \boldsymbol{H}_{BB}^T \mathbb{M}_B^{-1} \mathcal{C}_B$$

denotes the nonlinear velocity-dependent joint torque in the reduced-form representation. The above equation stands for the system dynamics mapped onto joint space. The dimension of the system has thus been reduced from $n+6$ to n. This form of the equation of motion of the floating-base system is similar to that of a fixed-base manipulator. An important observation is that *the joint torque does not alter the spatial momentum of the system whatsoever*.

The reduced-form representation (4.128) exhibits explicitly how the fixed-base manipulator dynamics are generalized to that of a free-floating base system; with a heavy base s.t. $\mathbb{M}_B \to \infty$, the terms containing $\mathbb{M}_B^{-1}$ become infinitesimally small and, hence, $\hat{\boldsymbol{M}}_{\theta B} \to \boldsymbol{M}_{\theta B}$, $\hat{\boldsymbol{c}}_{\theta B} \to \boldsymbol{c}_{\theta B}$. This was also the case with the generalized Jacobian appearing in (4.118). Readers interested in a rigorous theoretical foundation with regard to the reduced-form dynamics in relation to conserved quantities are referred to [86,109].

In the Presence of External Forces

As clarified in Chapter 3, the sum of all external wrenches can be mapped at a specific link of interest. For clarity and without loss of generality, in what follows it will be assumed

that the net external wrench acts at Link $n \equiv E$, i.e. at the end effector. Then, the equation of motion (4.123) can be written as

$$\begin{bmatrix} \mathbb{M}_B & \boldsymbol{H}_{BB} \\ \boldsymbol{H}_{BB}^T & \boldsymbol{M}_{\theta B} \end{bmatrix} \begin{bmatrix} \dot{\mathcal{V}}_B \\ \ddot{\boldsymbol{\theta}} \end{bmatrix} + \begin{bmatrix} \mathcal{C}_B \\ \boldsymbol{c}_{\theta B} \end{bmatrix} = \begin{bmatrix} \boldsymbol{0} \\ \boldsymbol{\tau} \end{bmatrix} + \begin{bmatrix} \mathbb{T}_{\overleftarrow{BE}}^T \\ \boldsymbol{J}_E^T \end{bmatrix} \mathcal{F}_E. \tag{4.129}$$

From the upper part of the above equation and the expression for SSM $\mathcal{L}_B$ in (4.92), the following relation is derived:

$$\frac{d}{dt}\mathcal{L}_B(\boldsymbol{q}, \dot{\boldsymbol{q}}_B) = \mathbb{M}_B \dot{\mathcal{V}}_B + \dot{\mathbb{M}}_B \mathcal{V}_B + \mathcal{C}'_B + \boldsymbol{H}_{BB}\ddot{\boldsymbol{\theta}} + \dot{\boldsymbol{H}}_{BB}\dot{\boldsymbol{\theta}} = \mathcal{F}_B, \tag{4.130}$$

where $\mathcal{C}'_B$ is defined in (4.125) and $\mathcal{F}_B = \mathbb{T}_{\overleftarrow{BE}}^T \mathcal{F}_E$. This equation reveals the following important points:

- the spatial dynamics are derived as the time differential of the SSM;
- the rate of change of the SSM depends on the external wrench only.

The manipulator joint motion/torque does not alter the rate of change of the SSM whatsoever; joint motion induces a zero dynamic force component, i.e.

$$\frac{d}{dt}\mathcal{L}_{BB} = \boldsymbol{H}_{BB}\ddot{\boldsymbol{\theta}} + \dot{\boldsymbol{H}}_{BB}\dot{\boldsymbol{\theta}} = \boldsymbol{0}. \tag{4.131}$$

Thus, when subjected to an *nonimpulsive* external force,[9] the free-floating manipulator will behave as a rigid body, as if the joints were locked, so we have

$$\frac{d}{dt}\widetilde{\mathcal{L}}_B = \mathbb{M}_B \dot{\mathcal{V}}_B + \dot{\mathbb{M}}_B \mathcal{V}_B + \mathcal{C}'_B = \mathcal{F}_B. \tag{4.132}$$

This relation also implies that $\mathcal{F}_B = \mathcal{F}_C$ holds, $\mathcal{F}_C = \begin{bmatrix} \boldsymbol{f}_C^T & \boldsymbol{m}_C^T \end{bmatrix}^T = \mathbb{T}_{\overleftarrow{CE}}^T \mathcal{F}_E$ denoting the external wrench mapped at the system CoM. It can then be reconfirmed that instantaneous motion derived from the tangent bundle of the CSM conserving manifold (cf. (4.110)) does not disturb the dynamic force balance at the CRB. This is the reason why the tangent bundle was named the (spatial momentum) RNS in Section 4.7 (cf. also [96,95,100]).

Finally, note that in the presence of an external force, the reduced form of the equation of motion, (4.128), becomes

$$\hat{\boldsymbol{M}}_{\theta B}\ddot{\boldsymbol{\theta}} + \hat{\boldsymbol{c}}_{\theta B} = \boldsymbol{\tau} + \hat{\boldsymbol{J}}_E^T \mathcal{F}_E, \tag{4.133}$$

where $\hat{\boldsymbol{J}}_E$ stands for the generalized Jacobian (cf. (4.119)). Apparently, the equation of motion of a floating-base underactuated system can be expressed as that of a fixed-base manipulator (cf. (4.58)).

[9] The case of an impulsive external force will be discussed in Section 7.8.

4.8.2 Representation in Terms of Mixed Quasivelocity

The representation of spatial momentum in terms of the mixed quasivelocity is expected to yield simpler expressions in the equation of motion because of the decoupling of the linear CoM motion component. The equation of motion, expressed in terms of the base quasivelocity (4.122), can be transformed with the help of the quasivelocity relation (4.106) and the transform (4.107) as

$$\boldsymbol{M}_M(\boldsymbol{q})\ddot{\boldsymbol{q}}_M + \boldsymbol{c}_M(\boldsymbol{q}, \dot{\boldsymbol{q}}_M) = \mathcal{Q}, \tag{4.134}$$

where

$$\boldsymbol{M}_M(\boldsymbol{q}) \equiv \boldsymbol{T}^T_{\overleftarrow{MB}} \boldsymbol{M}_B \boldsymbol{T}_{\overleftarrow{BM}}, \tag{4.135}$$

$$\boldsymbol{c}_M(\boldsymbol{q}, \dot{\boldsymbol{q}}_M) \equiv \boldsymbol{T}^T_{\overleftarrow{MB}} \left(\boldsymbol{c}_B(\boldsymbol{q}, \dot{\boldsymbol{q}}_B) + \boldsymbol{M}_B \dot{\boldsymbol{T}}_{\overleftarrow{BM}} \dot{\boldsymbol{q}}_B \right). \tag{4.136}$$

The expanded-form representations of (4.134) are

$$\begin{bmatrix} \mathbb{M}_C & \boldsymbol{H}_{CM} \\ \boldsymbol{H}^T_{CM} & \boldsymbol{M}_{\theta M} \end{bmatrix} \begin{bmatrix} \dot{\mathcal{V}}_M \\ \ddot{\boldsymbol{\theta}} \end{bmatrix} + \begin{bmatrix} \mathcal{C}_M \\ \boldsymbol{c}_{\theta M} \end{bmatrix} = \begin{bmatrix} \boldsymbol{0} \\ \boldsymbol{\tau} \end{bmatrix} \tag{4.137}$$

and

$$\begin{bmatrix} M\boldsymbol{E} & \boldsymbol{0} & \boldsymbol{0} \\ \boldsymbol{0} & \boldsymbol{I}_C & \boldsymbol{H}_C \\ \boldsymbol{0} & \boldsymbol{H}^T_C & \boldsymbol{M}_{\theta M} \end{bmatrix} \begin{bmatrix} \dot{\boldsymbol{v}}_C \\ \dot{\boldsymbol{\omega}}_B \\ \ddot{\boldsymbol{\theta}} \end{bmatrix} + \begin{bmatrix} \boldsymbol{0} \\ \boldsymbol{c}_{mM} \\ \boldsymbol{c}_{\theta M} \end{bmatrix} = \begin{bmatrix} \boldsymbol{0} \\ \boldsymbol{0} \\ \boldsymbol{\tau} \end{bmatrix}, \tag{4.138}$$

where

$$\boldsymbol{M}_{\theta M}(\boldsymbol{q}) \equiv \boldsymbol{M}_{\theta B}(\boldsymbol{q}) - M \boldsymbol{J}^T_{\overleftarrow{CB}}(\boldsymbol{\theta}) \boldsymbol{J}_{\overleftarrow{CB}}(\boldsymbol{\theta}). \tag{4.139}$$

Apparently, $\mathcal{C}_M = \begin{bmatrix} \boldsymbol{0}^T & \boldsymbol{c}^T_{mM} \end{bmatrix}^T$, with the nonlinear velocity-dependent moment

$$\boldsymbol{c}_{mM}(\boldsymbol{q}, \dot{\boldsymbol{q}}_B) = \dot{\boldsymbol{I}}_C \omega_B + \dot{\boldsymbol{H}}_C \dot{\boldsymbol{\theta}}, \tag{4.140}$$

whereby

$$\dot{\boldsymbol{I}}_C(\boldsymbol{q}) = \sum_{i=1}^{n} \left([\boldsymbol{\omega}_i^\times] \boldsymbol{I}_i - \boldsymbol{I}_i [\boldsymbol{\omega}_i^\times] - M_i \left([\dot{\boldsymbol{r}}^\times_{\overleftarrow{Ci}}][\boldsymbol{r}^\times_{\overleftarrow{iC}}] + [\boldsymbol{r}^\times_{\overleftarrow{Ci}}][\dot{\boldsymbol{r}}^\times_{\overleftarrow{iC}}] \right) \right), \tag{4.141}$$

$$\dot{\boldsymbol{H}}_C(\boldsymbol{q}) = \sum_{i=1}^{n} \left(\left([\boldsymbol{\omega}_i^\times] \boldsymbol{I}_i - \boldsymbol{I}_i [\boldsymbol{\omega}_i^\times] \right) \boldsymbol{J}_{\boldsymbol{\omega}_i} + \boldsymbol{I}_i \dot{\boldsymbol{J}}_{\boldsymbol{\omega}_i} + M_i \left([\dot{\boldsymbol{r}}^\times_{\overleftarrow{Ci}}] \boldsymbol{J}_{vi} + [\boldsymbol{r}^\times_{\overleftarrow{Ci}}] \dot{\boldsymbol{J}}_{vi} \right) \right), \tag{4.142}$$

and

$$\dot{\boldsymbol{J}}_{vi} = \begin{bmatrix} [\dot{\boldsymbol{e}}_1^\times] \boldsymbol{r}_{\overleftarrow{i1}} + [\boldsymbol{e}_1^\times] \dot{\boldsymbol{r}}_{\overleftarrow{i1}} & [\dot{\boldsymbol{e}}_2^\times] \boldsymbol{r}_{\overleftarrow{i2}} + [\boldsymbol{e}_2^\times] \dot{\boldsymbol{r}}_{\overleftarrow{i2}} & \cdots & [\dot{\boldsymbol{e}}_j^\times] \boldsymbol{r}_{\overleftarrow{ij}} + [\boldsymbol{e}_j^\times] \dot{\boldsymbol{r}}_{\overleftarrow{ij}} & \boldsymbol{0} & \cdots & \boldsymbol{0} \end{bmatrix} \in \Re^{3 \times n},$$

$$\dot{\boldsymbol{J}}_{\omega i} = \begin{bmatrix} \dot{\boldsymbol{e}}_1 & \dot{\boldsymbol{e}}_2 & \cdots & \dot{\boldsymbol{e}}_i & \boldsymbol{0} & \cdots & \boldsymbol{0} \end{bmatrix} \in \Re^{3\times n},$$
$$\dot{\boldsymbol{e}}_i = [\boldsymbol{\omega}_i^{\times}]\boldsymbol{R}_i {}^i\boldsymbol{e}_i .$$

Here $\boldsymbol{e}_i = \boldsymbol{R}_i {}^i\boldsymbol{e}_i$, ${}^i\boldsymbol{e}_i = [0\ 0\ 1]^T$, and $\boldsymbol{r}_{\overleftarrow{ij}}$ is the distance vector from the jth joint axis to the ith link CoM ($1 \le j \le i$).

With this notation, the nonlinear velocity-dependent wrench in the spatial dynamics component can be represented in the following form:

$$\mathcal{C}_M = \dot{\mathbb{M}}_C \mathcal{V}_M + \dot{\boldsymbol{H}}_{CM}\dot{\boldsymbol{\theta}}. \tag{4.143}$$

Note also that the nonlinear velocity-dependent wrench (4.125) and the joint torque can be written as

$$\mathcal{C}_B = \begin{bmatrix} \boldsymbol{a} \\ \boldsymbol{c}_{mM} + [\boldsymbol{r}^{\times}_{\overleftarrow{CB}}]^T \boldsymbol{a} \end{bmatrix} \tag{4.144}$$

and

$$\boldsymbol{c}_{\theta M}(\boldsymbol{q}, \dot{\boldsymbol{q}}_M) = \boldsymbol{c}_{\theta B}(\boldsymbol{\theta}, \dot{\boldsymbol{\theta}}) - \dot{\boldsymbol{J}}^T_{\overleftarrow{CB}}\boldsymbol{a}, \tag{4.145}$$

respectively, where $\boldsymbol{a} \equiv M\left(-[\dot{\boldsymbol{r}}^{\times}_{\overleftarrow{CB}}]^T \boldsymbol{\omega}_B + \dot{\boldsymbol{J}}_{\overleftarrow{BC}}\dot{\boldsymbol{\theta}}\right)$.

External Wrench Applied

An external wrench alters the rate of change of the SSM, as follows:

$$\frac{d}{dt}\mathcal{L}_C(\boldsymbol{q}, \dot{\boldsymbol{q}}_M) = \mathbb{M}_C\dot{\mathcal{V}}_M + \dot{\mathbb{M}}_C\mathcal{V}_M + \boldsymbol{H}_{CM}\ddot{\boldsymbol{\theta}} + \dot{\boldsymbol{H}}_{CM}\dot{\boldsymbol{\theta}} = \mathcal{F}_M, \tag{4.146}$$

where $\mathcal{F}_M = \begin{bmatrix} \boldsymbol{f}_C^T & \boldsymbol{m}_B^T \end{bmatrix}^T = \mathbb{T}^T_{\overleftarrow{ME}}\mathcal{F}_E$ is the external wrench mapped in accordance with the mixed quasivelocity notation. Relations similar to those with the base quasivelocity notation in Section 4.8.1 exist. That is, the CSM rate of change is zero, i.e.

$$\frac{d}{dt}\mathcal{L}_{CM} = \boldsymbol{H}_{CM}\ddot{\boldsymbol{\theta}} + \dot{\boldsymbol{H}}_{CM}\dot{\boldsymbol{\theta}} = \boldsymbol{0}. \tag{4.147}$$

This implies that the system response w.r.t. an applied nonimpulsive wrench is that of a rigid body, i.e.

$$\frac{d}{dt}\tilde{\mathcal{L}}_C(\boldsymbol{q}, \dot{\boldsymbol{q}}_M) = \mathbb{M}_C\dot{\mathcal{V}}_M + \dot{\mathbb{M}}_C\mathcal{V}_M = \mathcal{F}_M. \tag{4.148}$$

Thus, $\mathcal{F}_M = \mathcal{F}_C$ holds.

4.8.3 Representation in Terms of Centroidal Quasivelocity

An expression for the spatial dynamics in terms of the centroidal spatial velocity will be derived first. In analogy to (4.132), the rate of change of the centroidal SSM is determined

by the external wrench acting on the system. Using the time differential of (4.89), the spatial dynamics can be expressed as

$$\frac{d}{dt}\mathcal{L}_C(\boldsymbol{q},\mathcal{V}_C)=\mathbb{M}_C\dot{\mathcal{V}}_C+\dot{\mathbb{M}}_C\mathcal{V}_C=\mathcal{F}_C. \tag{4.149}$$

Note that since the centroidal quasivelocity is employed, the SSM equals the CRB-SM, as in the locked-joints case; there is no contribution from the joint motion at all. It is then straightforward to conclude that the above expression is equivalent to that in (4.132) and (4.148).

The expanded form of the above equation can be written as

$$\begin{bmatrix} m\boldsymbol{E} & \boldsymbol{0} \\ \boldsymbol{0} & \boldsymbol{I}_C \end{bmatrix}\begin{bmatrix} \dot{\boldsymbol{v}}_C \\ \dot{\boldsymbol{\omega}}_C \end{bmatrix}+\begin{bmatrix} \boldsymbol{0} \\ \boldsymbol{c}_\omega \end{bmatrix}=\begin{bmatrix} \boldsymbol{f}_C \\ \boldsymbol{m}_C \end{bmatrix}. \tag{4.150}$$

Recall that when the joints are locked, $\boldsymbol{\omega}_C=\boldsymbol{\omega}_B$ and $\mathcal{V}_C=\mathcal{V}_M$. The structure of (4.150) resembles the Newton–Euler equation of motion of a free-floating rigid body. It should be noted, though, that the nonlinear moment $\boldsymbol{c}_\omega=\dot{\boldsymbol{I}}_C(\boldsymbol{q})\boldsymbol{\omega}_C$ comprises terms containing time and partial derivatives of the posture-dependent inertia matrix $\boldsymbol{I}_C(\boldsymbol{q})$ (cf. (4.141)). Such terms do not appear in the nonlinear-velocity term of the rigid-body Euler equation (i.e. in the gyroscopic torque $\boldsymbol{\omega}_C\times\bar{\boldsymbol{I}}_C\boldsymbol{\omega}_C$, $\bar{\boldsymbol{I}}_C=\text{const.}$).

The CRB motion induced by the impressed external wrench depends on the line of action of the force component. A special case deserves to be mentioned. Let the external wrench, acting at point E, represent a pure force, i.e. $\mathcal{F}_E=\begin{bmatrix}\boldsymbol{f}_E^T & \boldsymbol{0}^T\end{bmatrix}^T$. When the line of action of this force goes through the CRB centroid, the angular momentum will be conserved since the moment component of $\mathcal{F}_C=\mathbb{T}^T_{\overleftarrow{CE}}\mathcal{F}_E$ is identically zero; $\boldsymbol{m}_C=\boldsymbol{0}$. On the other hand, when the line of action is apart from the centroid, a change in the angular momentum will be induced (cf. Fig. 4.8), so

$$\frac{d}{dt}\boldsymbol{l}_C\equiv\boldsymbol{m}_C=-[\boldsymbol{r}^\times_{\overleftarrow{CE}}]\boldsymbol{f}_E\neq\boldsymbol{0}.$$

Assuming an external force of a unit magnitude, the magnitude of the rate of change of the angular momentum will be in proportion to the distance $\|\boldsymbol{r}_{\overleftarrow{CE}}\|$. This simple relation plays an important role in balance stability of humanoid robots (cf. Chapter 5).

Finally, to obtain the system dynamics expressed in terms of the centroidal quasivelocity, adjoin the decoupled CRB dynamics (4.149) to the reduced-form dynamics (4.133). We have

$$\begin{bmatrix} \mathbb{M}_C & \boldsymbol{0} \\ \boldsymbol{0} & \hat{\boldsymbol{M}}_{\theta B} \end{bmatrix}\begin{bmatrix} \dot{\mathcal{V}}_C \\ \ddot{\boldsymbol{\theta}} \end{bmatrix}+\begin{bmatrix} \mathcal{C}_C \\ \hat{\boldsymbol{c}}_{\theta B} \end{bmatrix}=\begin{bmatrix} \boldsymbol{0} \\ \boldsymbol{\tau} \end{bmatrix}+\begin{bmatrix} \mathbb{T}^T_{\overleftarrow{CE}} \\ \hat{\boldsymbol{J}}_E^T \end{bmatrix}\mathcal{F}_E, \tag{4.151}$$

$\mathcal{C}_C\equiv\dot{\mathbb{M}}_C\mathcal{V}_C$. This form of the equation of motion of a floating-base system was first revealed in [164]. With this notation, the three distinctive partial dynamic components (i.e. the linear and angular CRB and the joint-space dynamics) have been *completely* dynamically decoupled.

It should be noted that the above result can be confirmed by transforming the equation of motion expressed in terms of the base quasivelocity, (4.129), with a similar procedure as in Section 4.8.2, by making use of the quasivelocity relation and transform given in (4.101) and (4.102), respectively.

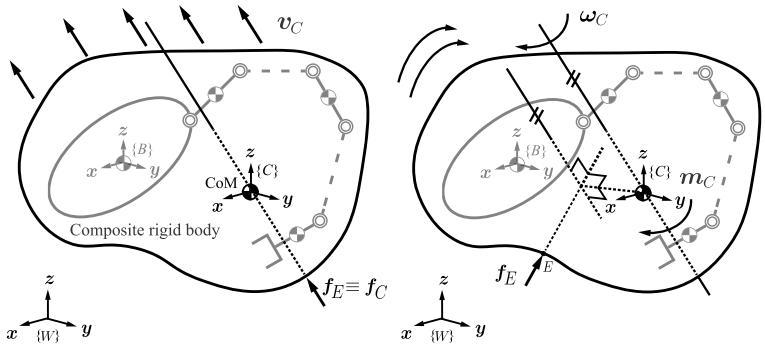

FIGURE 4.8 External wrench $f_E \neq 0$, $m_E = 0$ acting on the CRB. Left (A): The angular momentum is conserved when the line of action of f_E passes through the CRB centroid. Right (B): When the line of action of the external force does not pass through the CoM, the force induces an angular momentum with rate of change in proportion to the distance between C and E.

4.9 REACTION NULL SPACE–BASED INVERSE DYNAMICS

The spatial dynamics equation, (e.g. (4.130)), can be resolved for the manipulator joint acceleration. The solution can be used to derive control inputs in dynamic control schemes, e.g. resolved acceleration control [72] or computed torque control [24]. Since the case of a nonredundant manipulator has a unique solution, it will be more interesting to focus on the redundant manipulator case with an infinite number of solutions. The joint acceleration can be obtained as

$$\ddot{\boldsymbol{\theta}} = \boldsymbol{H}_{BB}^{+}\left(\mathcal{F}_B - \mathbb{M}_B\dot{\mathcal{V}}_B - \mathcal{C}_B\right) + \boldsymbol{N}(\boldsymbol{H}_{BB})\ddot{\boldsymbol{\theta}}_a. \tag{4.152}$$

The homogeneous solution component $\boldsymbol{N}(\boldsymbol{H}_{BB})\ddot{\boldsymbol{\theta}}_a$ determines the following infinite set of joint accelerations:

$$\{\ddot{\boldsymbol{\theta}}_{rl} \in \mathcal{N}(\boldsymbol{H}_{BB}) : \ddot{\boldsymbol{\theta}} = \boldsymbol{N}(\boldsymbol{H}_{BB})\ddot{\boldsymbol{\theta}}_a,\ \forall\ddot{\boldsymbol{\theta}}_a\}.$$

Apparently, joint accelerations $\{\ddot{\boldsymbol{\theta}}_{rl}\}$ belong to the (spatial momentum) RNS. They can be characterized as *reactionless* since they do not alter the force balance at the base whatsoever. On the other hand, the particular solution component (the pseudoinverse term) yields joint acceleration that ensures optimal inertial coupling in terms of the coupling kinetic energy minimization (cf. (4.120)). Such minimization is a highly desirable feature from a control viewpoint. For instance, a reactionless motion control objective [94] would be based on two control components: (i) reactionless-motion generation, via the null-space term (a feedforward control component) and (ii) base deviation[10] compensation via the pseudoinverse term (a feedback control component). Coupling energy minimization will thereby ensure better performance with regard to the error compensation dynamics.

[10] Stemming e.g. from modeling errors.

The inverse dynamics solution can be derived in a straightforward manner by inserting the joint acceleration (4.152) into the lower part of the equation of motion, (4.129). We have

$$\begin{aligned}\boldsymbol{\tau} &= \boldsymbol{H}_{BB}^{T}\dot{\mathcal{V}}_B + \boldsymbol{M}_{\theta B}\,\ddot{\boldsymbol{\theta}} + \boldsymbol{c}_{\theta B} \\ &= \hat{\boldsymbol{M}}_{\theta B}\dot{\mathcal{V}}_B + \overline{\boldsymbol{M}}_{\theta B}\,\ddot{\boldsymbol{\theta}}_a + \hat{\boldsymbol{c}}_{\theta B}.\end{aligned} \tag{4.153}$$

The "hat" notation stems from the reduced-form representation of the equation of motion introduced in Section 4.8.1. This notation is typical for underactuated system inverse dynamics; it will also appear in the humanoid robot inverse dynamics notation, to be introduced in what follows. The overbar notation, on the other hand, denotes a *restricted matrix* [92] stemming from the constrained least-squares redundancy resolution (cf. (2.49)); $\overline{\boldsymbol{M}}_{\theta B} \equiv \boldsymbol{M}_{\theta B}\boldsymbol{N}(\boldsymbol{H}_{BB})$ will be referred to as the *RNS-restricted joint-space inertia matrix*. According to the abovementioned control scenario, $\ddot{\boldsymbol{\theta}}_a$ and $\dot{\mathcal{V}}_B$ could be used in the feedforward and error compensation (feedback) control components, respectively.

4.10 SPATIAL MOMENTUM OF A HUMANOID ROBOT

From the discussion on simple dynamic models in Section 4.3 it became apparent that the two components of the spatial momentum, determined by the CoM motion and a centroidal moment, play an important role in balance control. Furthermore, in Section 4.8 it was shown that the spatial dynamics of a manipulator floating freely in zero gravity are determined by the rate of change of the spatial momentum resulting from the external forces (cf. (4.130)); the joint-space partial dynamics have no contribution at all. This is true for floating-base systems in general (i.e. under gravity), humanoid robots included.

Most of the early studies on gait generation and balance control of humanoid robots were based on IP models; they focused almost exclusively on the linear component of the spatial momentum determined by the CoM motion (cf. (4.70)). The role of the angular momentum component was also discussed at an early stage [128,129]. Nevertheless, follow-up research began appearing much later [89,41,119,81]. It has been clarified that the impressed moment on the foot can be controlled in two ways: (1) via the rate of change of the *moment of momentum*, by accelerating the CoM horizontally, as in the so-called "angular momentum pendulum model" (AMPM) approach [62], and (2) via the centroidal angular momentum, as in the RWP approach.

Besides in gait generation and balance control, spatial momentum also plays an important role in whole-body motion control. The focus in this area has been especially on the spatial momentum represented w.r.t. the CRB centroid in terms of the base quasivelocity, (4.91), as in the so-called "resolved momentum control" method [56,135,57]. This representation also appears in other studies on balance control [40,69,107,160].

The following properties of the spatial momentum and its two components, linear and angular momentum, and the respective rates of change are derived from the free-floating space robot models in the previous sections; these properties play an important role in humanoid robotics as well.

- The reference point for angular momentum is essential; the base and CRB CoMs are of particular interest as points of reference.
- The spatial momentum of the system (the SSM) is expressed as the sum of CRB (the CRB-SM) and coupling spatial momentum (the CSM), i.e.

$$\text{SSM} = \text{CRB-SM} + \text{CSM}.$$

  This relation is referred to as the *momentum equilibrium principle*. Momentum equilibrium stems from the dynamic equilibrium of wrenches in the spatial dynamics component of the equation of motion, in the absence of external forces (e.g. as in (4.123)).
- The expression of spatial momentum depends on the chosen type of quasivelocity:
  - The representation in terms of the centroidal quasivelocity, $\mathcal{V}_C$, is the simplest one; it is independent from the motion in the joints and yields inertial decoupling between all dynamic components, i.e. *complete* inertial decoupling.
  - The representation with the base quasivelocity, $\mathcal{V}_B$, yields inertial coupling between all dynamic components. This coupling determines the *coupling spatial momentum conserving* manifold in joint space. The tangent subspace to this manifold at $\boldsymbol{q}$ is called the *spatial momentum Reaction Null Space*.
  - The representation with the mixed quasivelocity, $\mathcal{V}_M$, yields inertial decoupling between the CoM dynamics on one side and the angular momentum and joint-space partial dynamics on the other. The latter two components are inertially coupled; the coupling determines the *coupling angular momentum conserving* manifold in joint space. The tangent subspace to this manifold at $\boldsymbol{q}$ is called the *angular momentum Reaction Null Space*.
- The angular component of the spatial momentum is conserved:
  - in the absence of external forces;
  - when the CRB centroid lies on the line of action of the external force (as with the IP models in Fig. 4.2).

Using the appropriate representation of the angular momentum is important in balance control design, as will be shown in Chapter 5.

Furthermore, note that with the exception of the flight phase during running and jumping, a humanoid robot is always in contact with the environment. The posture is then typically characterized as single/double stance, or multicontact. In the latter case, multiple interdependent closed loops are formed via the hand contacts, in addition to those at the feet. In this situation, the momentum control objectives have to be determined as constraint-consistent. This can be done in a straightforward manner, by employing the constraint-consistent generalized velocity/accelerations, as described in Section 2.11. To this end, note that it would be sufficient to restrict the spatial momentum matrix, $\boldsymbol{\mathcal{A}}_{(\circ)}$, by the null space of the appropriate constraint Jacobian. Two expressions of the *constrained-consistent centroidal spatial momentum* can then be obtained, as follows:

$$\overline{\mathcal{L}}_C(\boldsymbol{q}, \dot{\boldsymbol{q}}_{(\circ)}) = \overline{\boldsymbol{\mathcal{A}}}_{(\circ)}(\boldsymbol{q})\dot{\boldsymbol{q}}_u. \tag{4.154}$$

This notation covers expressions in terms of the base ($\dot{\boldsymbol{q}}_{(\circ)} = \dot{\boldsymbol{q}}_B$) and the mixed ($\dot{\boldsymbol{q}}_{(\circ)} = \dot{\boldsymbol{q}}_M$) quasivelocity, whereby $\overline{\boldsymbol{\mathcal{A}}}_{\underleftarrow{CB}}(\boldsymbol{q}) = \boldsymbol{\mathcal{A}}_{\underleftarrow{CB}}\boldsymbol{N}(\boldsymbol{J}_{cB})$ and $\overline{\boldsymbol{\mathcal{A}}}_C(\boldsymbol{q}) = \boldsymbol{\mathcal{A}}_C\boldsymbol{N}(\boldsymbol{J}_{cM})$, respectively; $\overline{\boldsymbol{\mathcal{A}}}_{(\circ)}$ is

referred to as a *restricted centroidal momentum matrix*, $\dot{\boldsymbol{q}}_u$ is an arbitrary quasivelocity vector of the unconstrained system. Note that the spatial momentum $\mathcal{L}_B(\boldsymbol{q}, \dot{\boldsymbol{q}}_B)$ can be restricted in a similar way. Note also that the expression of centroidal spatial momentum in terms of the centroidal quasivelocity, $\mathcal{L}_C(\boldsymbol{q}, \mathcal{V}_C)$, does not have to be restricted because of the complete dynamic decoupling property.

4.11 EQUATION OF MOTION OF A HUMANOID ROBOT

A humanoid robot is modeled as an underactuated multibody system on a floating base. The Lagrangian form of the equation of motion of the robot is of the same form as that of a free-floating space robot, as described in Section 4.8. The main difference is the presence of the gravity field. Other external wrenches include determinate reactions at the contact joints as well as indeterminate disturbance wrenches. Both continuous and impact-type reaction/disturbance wrenches have to be taken in consideration. The Lagrangian form of the equation of motion will be used as a base for the dynamic modeling.

From the discussion in Section 4.8 it is apparent that the representations of the equation of motion depend upon the particular choice for the quasivelocity. The classical representation is in terms of the base quasivelocity [35]. From the viewpoint of a whole-body balance control, more convenient is the mixed quasivelocity, though. The simplest expression is obtained with the centroidal quasivelocity. These notations will be introduced below. First, consider the classical representation

$$\begin{bmatrix} \mathbb{M}_B & \boldsymbol{H}_{BB} \\ \boldsymbol{H}_{BB}^T & \boldsymbol{M}_{\theta B} \end{bmatrix} \begin{bmatrix} \dot{\mathcal{V}}_B \\ \ddot{\boldsymbol{\theta}} \end{bmatrix} + \begin{bmatrix} \mathcal{C}_B \\ \boldsymbol{c}_{\theta B} \end{bmatrix} + \begin{bmatrix} \mathcal{G}_B \\ \boldsymbol{g}_\theta \end{bmatrix} = \begin{bmatrix} \boldsymbol{0} \\ \boldsymbol{\tau} \end{bmatrix} + \begin{bmatrix} \mathbb{C}_{cB} \\ \mathcal{J}_{cB}^T \end{bmatrix} \overline{\mathcal{F}}^c. \tag{4.155}$$

The upper and lower parts express the spatial and joint-space partial dynamics, respectively; $\overline{\mathcal{F}}^c \in CWC$, and $\mathcal{G}_B$ and $\boldsymbol{g}_\theta$ stand for the reactions stemming from the contact joints and the gravity wrench acting on the base link and the gravity joint torque vector. Their expressions are given in (3.55), (3.59), and (3.60), respectively. In the following derivations it will be assumed that the contact joints are formed by one or more end links (feet/hands). In practice, other links, such as fingers and intermittent links, may establish contacts as well. Such contacts can be easily incorporated without altering the qualitative properties of the model described herein. The reactions are mapped, first at the base link via the contact map of the robot (cf. (2.74)) and second to the joint torque via the transpose of the joint-space constraint Jacobian, $\mathcal{J}_{cB}^T \in \Re^{n \times c}$ (cf. (2.75)).

Equation of motion (4.155) together with the motion constraint (2.104)–(2.105) and the contact wrench cones will be referred to as the *complete model*. With this model, the spatial and joint-space partial dynamics are made apparent. The two parts play important and distinctive roles in analysis and controller design.

Some models make use of a more detailed representation of the equation of motion. The following expanded-form representation renders the spatial rotational and translational dy-

namic motion components explicitly visible (cf. also (4.124)):

$$\begin{bmatrix} \boldsymbol{M}\boldsymbol{E} & -M[\boldsymbol{r}^{\times}_{\overleftarrow{CB}}] & \boldsymbol{M}\boldsymbol{J}_{\overleftarrow{CB}} \\ -M[\boldsymbol{r}^{\times}_{\overleftarrow{CB}}]^T & \boldsymbol{I}_B & \boldsymbol{H}_B \\ \boldsymbol{M}\boldsymbol{J}^T_{\overleftarrow{CB}} & \boldsymbol{H}^T_B & \boldsymbol{M}_{\theta B} \end{bmatrix} \begin{bmatrix} \dot{\boldsymbol{v}}_B \\ \dot{\boldsymbol{\omega}}_B \\ \ddot{\boldsymbol{\theta}} \end{bmatrix} + \begin{bmatrix} \boldsymbol{c}_{fB} \\ \boldsymbol{c}_{mB} \\ \boldsymbol{c}_{\theta B} \end{bmatrix} + \begin{bmatrix} \boldsymbol{g}_f \\ \boldsymbol{g}_m \\ \boldsymbol{g}_\theta \end{bmatrix} = \begin{bmatrix} \boldsymbol{0} \\ \boldsymbol{0} \\ \boldsymbol{\tau} \end{bmatrix} + \begin{bmatrix} \mathbb{C}_{cB_f} \\ \mathbb{C}_{cB_m} \\ \boldsymbol{\mathcal{J}}_{cB}{}^T \end{bmatrix} \overline{\mathcal{F}}^c. \tag{4.156}$$

This equation appeared first in [35]. The meaning of the nonlinear velocity-dependent and gravity terms is apparent from (4.125) and (3.59), respectively. The force and moment component maps, $\mathbb{C}_{cB_f}$, $\mathbb{C}_{cB_m} \in \Re^{3\times c}$, are defined in (2.120).

The above representations of the equation of motion can be rewritten in terms of the *mixed quasivelocity* in accordance with the procedure described in Section 4.8.2. The compact and expanded-form representations are

$$\begin{bmatrix} \mathbb{M}_C & \boldsymbol{H}_{CM} \\ \boldsymbol{H}^T_{CM} & \boldsymbol{M}_{\theta M} \end{bmatrix} \begin{bmatrix} \dot{\mathcal{V}}_M \\ \ddot{\boldsymbol{\theta}} \end{bmatrix} + \begin{bmatrix} \mathcal{C}_M \\ \boldsymbol{c}_{\theta M} \end{bmatrix} + \begin{bmatrix} \mathcal{G}_C \\ \boldsymbol{0} \end{bmatrix} = \begin{bmatrix} \boldsymbol{0} \\ \boldsymbol{\tau} \end{bmatrix} + \begin{bmatrix} \mathbb{C}_{cC} \\ \boldsymbol{\mathcal{J}}^T_{cM} \end{bmatrix} \overline{\mathcal{F}}^c \tag{4.157}$$

and

$$\begin{bmatrix} \boldsymbol{M}\boldsymbol{E} & \boldsymbol{0} & \boldsymbol{0} \\ \boldsymbol{0} & \boldsymbol{I}_C & \boldsymbol{H}_C \\ \boldsymbol{0} & \boldsymbol{H}^T_C & \boldsymbol{M}_{\theta M} \end{bmatrix} \begin{bmatrix} \dot{\boldsymbol{v}}_C \\ \dot{\boldsymbol{\omega}}_B \\ \ddot{\boldsymbol{\theta}} \end{bmatrix} + \begin{bmatrix} \boldsymbol{0} \\ \boldsymbol{c}_{mM} \\ \boldsymbol{c}_{\theta M} \end{bmatrix} + \begin{bmatrix} \boldsymbol{g}_f \\ \boldsymbol{0} \\ \boldsymbol{0} \end{bmatrix} = \begin{bmatrix} \boldsymbol{0} \\ \boldsymbol{0} \\ \boldsymbol{\tau} \end{bmatrix} + \begin{bmatrix} \mathbb{C}_{cC_f} \\ \mathbb{C}_{cC_m} \\ \boldsymbol{\mathcal{J}}^T_{cM}(\boldsymbol{q}) \end{bmatrix} \overline{\mathcal{F}}^c, \tag{4.158}$$

respectively. The link inertia tensor, $\boldsymbol{M}_{\theta M}$, the nonlinear velocity-dependent moment, $\boldsymbol{c}_{mM}$, and the nonlinear velocity-dependent joint torque, $\boldsymbol{c}_{\theta M}$, are defined in (4.139), (4.140), and (4.145), respectively. The constraint Jacobian and contact map components are defined in (2.126) and (2.127), respectively. The decoupling of the linear spatial dynamics component (i.e. the CoM partial dynamics in the upper row of (4.158)) from the rest is apparent. The decoupling yields an advantage in balance controller design. This topic will be discussed in Chapter 5.

The simplest expression of the equation of motion is obtained with the *centroidal quasivelocity*, i.e.

$$\begin{bmatrix} \mathbb{M}_C & \boldsymbol{0} \\ \boldsymbol{0} & \hat{\boldsymbol{M}}_{\theta B} \end{bmatrix} \begin{bmatrix} \dot{\mathcal{V}}_C \\ \ddot{\boldsymbol{\theta}} \end{bmatrix} + \begin{bmatrix} \mathcal{C}_C \\ \hat{\boldsymbol{c}}_{\theta B} \end{bmatrix} + \begin{bmatrix} \mathcal{G}_C \\ \boldsymbol{0} \end{bmatrix} = \begin{bmatrix} \boldsymbol{0} \\ \boldsymbol{\tau} \end{bmatrix} + \begin{bmatrix} \mathbb{C}_{cC} \\ \boldsymbol{\mathcal{J}}^T_{cC} \end{bmatrix} \overline{\mathcal{F}}^c. \tag{4.159}$$

The expanded-form representation is

$$\begin{bmatrix} \boldsymbol{M}\boldsymbol{E} & \boldsymbol{0} & \boldsymbol{0} \\ \boldsymbol{0} & \boldsymbol{I}_C & \boldsymbol{0} \\ \boldsymbol{0} & \boldsymbol{0} & \hat{\boldsymbol{M}}_{\theta B} \end{bmatrix} \begin{bmatrix} \dot{\boldsymbol{v}}_C \\ \dot{\boldsymbol{\omega}}_C \\ \ddot{\boldsymbol{\theta}} \end{bmatrix} + \begin{bmatrix} \boldsymbol{0} \\ \boldsymbol{c}_{\omega} \\ \hat{\boldsymbol{c}}_{\theta B} \end{bmatrix} + \begin{bmatrix} \boldsymbol{g}_f \\ \boldsymbol{0} \\ \boldsymbol{0} \end{bmatrix} = \begin{bmatrix} \boldsymbol{0} \\ \boldsymbol{0} \\ \boldsymbol{\tau} \end{bmatrix} + \begin{bmatrix} \mathbb{C}_{cC_f} \\ \mathbb{C}_{cC_m} \\ \boldsymbol{\mathcal{J}}^T_{cC} \end{bmatrix} \overline{\mathcal{F}}^c. \tag{4.160}$$

The link inertia matrix, $\hat{\boldsymbol{M}}_{\theta B}$, and the nonlinear velocity-dependent joint torque, $\hat{\boldsymbol{c}}_{\theta B}$, are defined in (4.127) and (4.128), respectively, whereas $\boldsymbol{c}_{\omega} = \dot{\boldsymbol{I}}_C \boldsymbol{\omega}$. The Jacobian

$$\boldsymbol{\mathcal{J}}_{cC} = \boldsymbol{\mathcal{J}}_{cB} - \mathbb{C}_{cC} \boldsymbol{J}_{\theta} \tag{4.161}$$

is referred to as the *generalized joint-space constraint Jacobian*. It is defined in analogy to the generalized Jacobian (4.119). Apparently, all three partial dynamic components in the above equation are inertially decoupled.

When using a standard solver (e.g. a quadratic programming solver) for the inverse dynamics, the following compact-form representation of the equation of motion is quite often preferred:

$$\boldsymbol{M}_{(\circ)}(\boldsymbol{q})\ddot{\boldsymbol{q}}_{(\circ)} + \boldsymbol{c}_{(\circ)}(\boldsymbol{q}, \dot{\boldsymbol{q}}_{(\circ)}) + \boldsymbol{g}_{(\circ)}(\boldsymbol{q}) = \mathcal{Q} - \mathcal{Q}_{c(\circ)}(\boldsymbol{q}). \tag{4.162}$$

The $(\circ)$ subscript is replaced with B, M, and C for the notations in terms of the base, mixed, and centroidal quasivelocities, respectively. The inertia, nonlinear velocity-dependent and the gravity force components are apparent from the respective expanded-form representations. The generalized force $\mathcal{Q}$ is defined in (4.122). The terms $\mathcal{Q}_{c(\circ)}(\boldsymbol{q}) \equiv \boldsymbol{J}_{c(\circ)}^T(\boldsymbol{q})\boldsymbol{\lambda}$ stand for the *generalized constraint force*, $\boldsymbol{\lambda} = -\overline{\mathcal{F}}^c$ denoting Lagrange's multiplier vector. Jacobians $\boldsymbol{J}_{cB}$ and $\boldsymbol{J}_{cM}$ were defined in (2.96) and (2.129), respectively. The Jacobian

$$\boldsymbol{J}_{cC} = \begin{bmatrix} \mathbb{C}_{cC}^T & \mathcal{J}_{cC} \end{bmatrix}.$$

Apparently, the expression of the generalized constraint force depends on the respective quasivelocity. From the principle of virtual work it follows that one type of a generalized constraint force can be transformed into another, via the transpose of the quasivelocity transform, e.g. $\mathcal{Q}_{cC} = \boldsymbol{T}_{\underleftarrow{CB}}^T \mathcal{Q}_{cB}$, $\boldsymbol{T}_{\underleftarrow{CB}}$ being defined in (4.102).

It should be noted that Lagrange's multiplier vector is frequently used in constrained optimization problems. In optimization frameworks that focus on extrema, the sign of the vector would be irrelevant. When used in the field of robotics, though, the vector is quite often endowed with a physical meaning. The sign is then of utmost importance, e.g. to honor the requirement that the normal reaction force at a unilateral contact must be positive (cf. Section 2.9.3). This can be ensured by taking the sign to be opposite to that of the constraint force, as above.

4.12 CONSTRAINT-FORCE ELIMINATION METHODS

Constraint-force elimination is a well-known approach within the field of constrained multibody system studies. The generalized constraint force is considered unknown and eliminated from the equation of motion [9,151,32,66,84]. The method can be directly applied in the field of humanoid robotics. The following derivations are valid for any type of quasivelocity. For simplicity, but with some abuse in the notation, the quasivelocity-related subscripts will be omitted. In what follows, holonomic (cf. Section 2.11.1), hard constraints will be assumed, s.t. $\boldsymbol{J}_c(\boldsymbol{q})\dot{\boldsymbol{q}} = \boldsymbol{0}$ (cf. (2.96)) holds. Also, the initial state is assumed to be consistent with the constraints $\boldsymbol{q}_0 \in \boldsymbol{\gamma}(\boldsymbol{q}_0)$ and $\dot{\boldsymbol{q}}_0 \in \mathcal{N}\left(\boldsymbol{J}_c(\boldsymbol{q}_0)\right)$. Combining the compact-form representation of the equation of motion, (4.162), with the time differential of the constraint equation yields

$$\begin{bmatrix} \boldsymbol{M} & \boldsymbol{J}_c^T \\ \boldsymbol{J}_c & \boldsymbol{0} \end{bmatrix} \begin{bmatrix} \ddot{\boldsymbol{q}} \\ \boldsymbol{\lambda} \end{bmatrix} = \begin{bmatrix} \mathcal{Q}_u \\ -\dot{\boldsymbol{J}}_c\dot{\boldsymbol{q}} \end{bmatrix}. \tag{4.163}$$

The generalized force appearing on the r.h.s. is defined as $\mathcal{Q}_u \equiv \mathcal{Q} - (\boldsymbol{c} + \boldsymbol{g})$. In the analysis, all terms of this force are assumed known; the generalized input force is determined by the controller, while the other two terms are state-dependent. The subscript "u" is used to denote the dynamics of the *unconstrained system* ($\boldsymbol{\lambda} = \boldsymbol{0}$). We have

$$\boldsymbol{M}\ddot{\boldsymbol{q}}_u = \mathcal{Q}_u. \tag{4.164}$$

Note that any initial state is admissible for the unconstrained system. The generalized acceleration $\ddot{\boldsymbol{q}}_u$ is obtained in a straightforward way from the last equation since the inverse of the inertia matrix exists at all system postures. The quantities $\ddot{\boldsymbol{q}}_u$ and $\mathcal{Q}_u$ play an important role in the following analysis. They will be referred to in short as the *unconstrained* generalized acceleration and generalized force, respectively.

The compact form of the complete model, (4.163), represents a set of differential-algebraic equations (DAEs). The forces of constraint, collected in $\boldsymbol{\lambda}$, are algebraic variables, i.e. no time derivatives of these variables appear in the equation. As already mentioned, it is customary to eliminate these forces from the equation of motion. As a result, one arrives at a set of ODEs which are easier to solve with conventional solvers. Since (4.163) was constructed by combining the equation of motion with the second-order motion constraint relation (2.105), it can be anticipated that the latter will be useful to eliminate the unknown Lagrange multiplier, $\boldsymbol{\lambda}$. There are different ways to eliminate the forces of constraint in a constraint multibody system formulation [151,66]. The following methods have been adopted in the field of humanoid robotics.

4.12.1 Gauss' Principle of Least Constraint

Gauss [37] was surprised to find out that ... *"The motion of a system of mass particles, whatever their relative displacements and the constraints they obey, takes place at every instant in maximum accordance with the free motion of the system, or under least constraint, whereby the measure of constraint (that the whole system is subjected to) is considered as the sum of products of mass and the square of the deviation of each mass particle from its free motion."*.[11]

The principle is formulated as a quadratic minimization problem: Minimize

$$\mathcal{Z} = \frac{1}{2}\sum_j M_j \left(\ddot{\boldsymbol{r}}_j - \frac{\boldsymbol{f}_j}{M_j}\right)^T \left(\ddot{\boldsymbol{r}}_j - \frac{\boldsymbol{f}_j}{M_j}\right), \tag{4.165}$$

where $\mathcal{Z}$ is the *measure of the constraint* (Zwang in German), M, $\boldsymbol{r}$ denote the particle mass and position, and $\boldsymbol{f}$ is the force acting on the particle.

The principle has been applied to constrained multibody systems [70,59,151]. It was introduced in the field of robotics in the pioneering work [117]; see also [16,28]. In the case of a multibody system, the above measure of constraint assumes the form [151]

$$\mathcal{Z} = \frac{1}{2}\left(\ddot{\boldsymbol{q}}_u - \ddot{\boldsymbol{q}}\right)^T \boldsymbol{M}\left(\ddot{\boldsymbol{q}}_u - \ddot{\boldsymbol{q}}\right) = \frac{1}{2}\ddot{\boldsymbol{q}}_c^T \boldsymbol{M}\ddot{\boldsymbol{q}}_c. \tag{4.166}$$

[11] Translation by the author of this chapter.

Here $\ddot{\boldsymbol{q}}_u$ denotes the generalized acceleration of the unconstrained system, $\ddot{\boldsymbol{q}}$ stands for the constraint-consistent generalized acceleration, and the difference $\ddot{\boldsymbol{q}}_c = \ddot{\boldsymbol{q}}_u - \ddot{\boldsymbol{q}}$ is the constraint enforcing generalized acceleration (cf. Section 2.11.3). It is important to note that, at each time instant of the motion, the state $(\boldsymbol{q}, \dot{\boldsymbol{q}})$ and the generalized input force $\boldsymbol{\tau}$ are assumed to be known. Therefore, the generalized acceleration of the unconstrained system can be determined uniquely via (4.164). With this notation, the equation of motion can be rewritten as

$$\boldsymbol{M}\left(\ddot{\boldsymbol{q}}_u - \ddot{\boldsymbol{q}}\right) = \boldsymbol{J}_c^T \boldsymbol{\lambda} \tag{4.167}$$

or

$$\boldsymbol{M}\ddot{\boldsymbol{q}}_c = \mathcal{Q}_c. \tag{4.168}$$

From the last relation it is seen that $\mathcal{Q}_c$ (resp. $\boldsymbol{\lambda}$) determines $\boldsymbol{q}_c$ in a unique way:

$$\ddot{\boldsymbol{q}}_c = \boldsymbol{M}^{-1}\mathcal{Q}_c = \boldsymbol{M}^{-1}\boldsymbol{J}_c^T\boldsymbol{\lambda}. \tag{4.169}$$

To determine the unknown Lagrange multiplier (and hence the constraint enforcing acceleration), the (second-order) motion constraint has to be imposed on the equation of motion. To this end, solve (4.167) for the constraint-consistent generalized acceleration and substitute into (2.105) to obtain

$$\boldsymbol{\lambda} = \boldsymbol{M}_c(\dot{\boldsymbol{J}}_c\dot{\boldsymbol{q}} + \boldsymbol{J}_c\ddot{\boldsymbol{q}}_u), \tag{4.170}$$

where $\boldsymbol{M}_c \equiv (\boldsymbol{J}_c\boldsymbol{M}^{-1}\boldsymbol{J}_c^T)^{-1}$ is the system inertia matrix mapped along the constrained-motion directions. Then, inserting (4.170) into (4.169), the constraint enforcing generalized acceleration is obtained as

$$\ddot{\boldsymbol{q}}_c = \boldsymbol{J}_c^{-M}(\dot{\boldsymbol{J}}_c\dot{\boldsymbol{q}} + \boldsymbol{J}_c\ddot{\boldsymbol{q}}_u), \tag{4.171}$$

where

$$\boldsymbol{J}_c^{-M} = \boldsymbol{M}^{-1}\boldsymbol{J}_c^T\left(\boldsymbol{J}_c\boldsymbol{M}^{-1}\boldsymbol{J}_c^T\right)^{-1} = \boldsymbol{M}^{-1}\boldsymbol{J}_c^T\boldsymbol{M}_c \tag{4.172}$$

is the inertia-weighted (right) pseudoinverse. The generalized constraint force can also be derived, if needed, via (4.168). We have

$$\mathcal{Q}_c = \boldsymbol{J}_c^T\boldsymbol{T}_c^{-1}(\dot{\boldsymbol{J}}_c\dot{\boldsymbol{q}} + \boldsymbol{J}_c\ddot{\boldsymbol{q}}_u). \tag{4.173}$$

Note that $\boldsymbol{\lambda}$ (and hence $\mathcal{Q}_c$ and $\ddot{\boldsymbol{q}}_c$) comprises a linear and a nonlinear component. The former results from the generalized acceleration of the unconstrained system. The latter is state-dependent, whereby the velocity state is constraint-consistent, i.e. it is in accordance with (2.100).

Next, the constraint-consistent generalized acceleration is derived by substituting (4.170) into (4.167). We have

$$\ddot{\boldsymbol{q}} = -\boldsymbol{J}_c^{-M}\dot{\boldsymbol{J}}_c\dot{\boldsymbol{q}} + \ddot{\boldsymbol{q}}_m, \tag{4.174}$$

$$\ddot{\boldsymbol{q}}_m \equiv \left(\boldsymbol{E} - \boldsymbol{J}_c^{-M}\boldsymbol{J}_c\right)\ddot{\boldsymbol{q}}_u. \tag{4.175}$$

This is recognized as the general solution to the underdetermined second-order differential constraint, (2.105), comprising a particular and a homogeneous solution component (the first and second terms on the r.h.s., respectively). The particular solution component stands for the nonlinear, state-dependent acceleration. The homogeneous component, on the other hand, is determined uniquely via the projection of the unconstrained generalized acceleration $\ddot{\boldsymbol{q}}_u$ onto null space $\mathcal{N}(\boldsymbol{J}_c)$. The resultant unique acceleration, $\ddot{\boldsymbol{q}}_m$, will be called *constraint maintaining*: this acceleration does not impress any inertial force in the constrained directions. Note also that the unconstrained generalized acceleration $\ddot{\boldsymbol{q}}_u$ is decomposed respectively via (4.171) and (4.175).

With the above notation, the equation of motion (4.167) can be rewritten as

$$\begin{aligned}\boldsymbol{M}\ddot{\boldsymbol{q}} &= -\boldsymbol{J}_c^T\boldsymbol{M}_c\dot{\boldsymbol{J}}_c\dot{\boldsymbol{q}} + \boldsymbol{M}\left(\boldsymbol{E} - \boldsymbol{J}_c^{-M}\boldsymbol{J}_c\right)\ddot{\boldsymbol{q}}_u \\ &= -\boldsymbol{J}_c^T\boldsymbol{M}_c\dot{\boldsymbol{J}}_c\dot{\boldsymbol{q}} + \boldsymbol{M}\ddot{\boldsymbol{q}}_m.\end{aligned} \tag{4.176}$$

4.12.2 Direct Elimination

It is interesting to note that the results obtained with Gauss' principle of least constraint can be confirmed via direct elimination, as follows. First, solve (4.163) for $\boldsymbol{\lambda}$, i.e.

$$\boldsymbol{\lambda} = \boldsymbol{M}_c\left(\dot{\boldsymbol{J}}_c\dot{\boldsymbol{q}} + \boldsymbol{J}_c\boldsymbol{M}^{-1}\mathcal{Q}_u\right). \tag{4.177}$$

Then, substitute (4.177) back into the upper part of (4.163) to obtain

$$\boldsymbol{M}\ddot{\boldsymbol{q}} = \mathcal{Q}_u - \mathcal{Q}_c, \tag{4.178}$$

$$\mathcal{Q}_c = \boldsymbol{J}_c^T\boldsymbol{M}_c\left(\dot{\boldsymbol{J}}_c\dot{\boldsymbol{q}} + \boldsymbol{J}_c\boldsymbol{M}^{-1}\mathcal{Q}_u\right) \tag{4.179}$$

or

$$\boldsymbol{M}\ddot{\boldsymbol{q}} = -\boldsymbol{J}_c^T\boldsymbol{M}_c\dot{\boldsymbol{J}}_c\dot{\boldsymbol{q}} + \mathcal{Q}_m, \tag{4.180}$$

$$\mathcal{Q}_m = \left(\boldsymbol{E} - \boldsymbol{J}_c^T\boldsymbol{J}_c^{-MT}\right)\mathcal{Q}_u. \tag{4.181}$$

To show that this result is identical to the result obtained with Gauss' principle of least constraint, note first that since $\boldsymbol{M}^{-1}\mathcal{Q}_u = \ddot{\boldsymbol{q}}_u$, relations (4.177) and (4.179) are identical to (4.170) and (4.173), respectively. Note also that (4.178) can be directly obtained from the definition of the constraint enforcing generalized acceleration, i.e. $\ddot{\boldsymbol{q}}_c = \ddot{\boldsymbol{q}}_u - \ddot{\boldsymbol{q}}$. In addition, solving (4.180) for the generalized acceleration yields

$$\ddot{\boldsymbol{q}} = -\boldsymbol{J}_c^{-M}\dot{\boldsymbol{J}}_c\dot{\boldsymbol{q}} + \boldsymbol{M}^{-1}\mathcal{Q}_m. \tag{4.182}$$

The second term on the r.h.s. can be represented as

$$\boldsymbol{M}^{-1}\mathcal{Q}_m = \boldsymbol{M}^{-1}\left(\boldsymbol{E} - \boldsymbol{J}_c^T\boldsymbol{J}_c^{-MT}\right)\mathcal{Q}_u = \left(\boldsymbol{E} - \boldsymbol{J}_c^{-M}\boldsymbol{J}_c\right)\boldsymbol{M}^{-1}\mathcal{Q}_u = \left(\boldsymbol{E} - \boldsymbol{J}_c^{-M}\boldsymbol{J}_c\right)\ddot{\boldsymbol{q}}_u = \ddot{\boldsymbol{q}}_m. \tag{4.183}$$

The above relations were obtained with the help of the similarity transform (3.36), whereby the inertia matrix $\boldsymbol{M}$ was used as the weighing matrix. These relations imply that (4.182) and (4.174) are identical. Note also that the dynamical system (4.180) is driven by the force $\mathcal{Q}_m$ which is a projection of the unconstrained generalized force $\mathcal{Q}_u$ onto the (dual) null space $\mathcal{N}^*(\boldsymbol{J}_c)$; $\mathcal{Q}_m$ will be called a *constraint maintaining* generalized force, in analogy to $\ddot{\boldsymbol{q}}_m$. It is straightforward to confirm that, with the help of the above identity relations, the equation of motion derived under Gauss' principle, (4.168), is identical to (4.180).

The resultant equations in both approaches, Gauss' approach and the direct elimination one, are obtained in a specific form, expressed via the inertia-weighted pseudoinverse $\boldsymbol{J}_c^{-M}$ and its transpose, as in (4.174) and (4.182), respectively. Indeed, note that (4.182) and (4.174) likewise are generalized solutions to the motion constraint (2.105). Recall that (2.106) also represents a general solution to the same motion constraint. As already clarified, the role of its particular solution component is to account for the nonlinearity in the constraints, within the normal subspace at the constraint manifold (i.e. for centrifugal and centripetal forces). This is also the role of the particular solution components in (4.182) and (4.174). Recall further that the homogeneous component in (2.106) was specified in a particular way to ensure integrability.

The direct elimination approach was used in [115,133] to derive the equation of motion of a humanoid robot.

4.12.3 Maggi's Equations (Null-Space Projection Method)

Lagrange's multiplier vector can be eliminated by projecting the equation of motion onto the null space of the system constraint matrix, $\mathcal{N}(\boldsymbol{J}_c)$. In constrained multibody system analysis, the method is known as *Maggi's equations* [114,11,151,66]. The first step of the procedure is to complement the differential constraints (2.96) by a set of $r = n + 6 - c$ independent kinematic relations, i.e.

$$\begin{bmatrix} \boldsymbol{J}_c \\ \boldsymbol{A}_r \end{bmatrix} \dot{\boldsymbol{q}} = \begin{bmatrix} \boldsymbol{0} \\ \mathcal{V}_r \end{bmatrix}. \tag{4.184}$$

The newly introduced relations do not necessarily have to be integrable; $\mathcal{V}_r$ is therefore sometimes referred to as the *quasivelocity* or *virtual speeds* or *independent kinematic parameters* [11] (see also Section 2.11.1). Matrix $\boldsymbol{A}_r \in \Re^{r\times(n+6)}$ is composed in such a way that the *extended* matrix $\boldsymbol{A}_e \equiv \begin{bmatrix} \boldsymbol{J}_c^T & \boldsymbol{A}_r^T \end{bmatrix}^T \in \Re^{(n+6)\times(n+6)}$ is always invertible. The inverse is represented as

$$\boldsymbol{A}_e^{-1} = \begin{bmatrix} \boldsymbol{V}_c & \boldsymbol{V}_r \end{bmatrix} \tag{4.185}$$

so that

$$\begin{bmatrix} \boldsymbol{J}_c^T & \boldsymbol{A}_r^T \end{bmatrix}^T \begin{bmatrix} \boldsymbol{V}_c & \boldsymbol{V}_r \end{bmatrix} = \operatorname{diag}\begin{bmatrix} \boldsymbol{E}_c & \boldsymbol{E}_r \end{bmatrix}.$$

The constraint-consistent generalized velocity can then be expressed as

$$\dot{\boldsymbol{q}} = \boldsymbol{V}_r \mathcal{V}_r. \tag{4.186}$$

Since $\boldsymbol{J}_c \boldsymbol{V}_r = \boldsymbol{0}$, it follows that $\boldsymbol{V}_r \in \Re^{(n+6)\times r}$ spans the null space of $\boldsymbol{J}_c$.

It is interesting to observe that (4.184) has the same form as (2.46) and that matrix $\boldsymbol{A}_e$ plays the same role as the extended Jacobian used in kinematic redundancy resolution (cf. Section 2.7.5). Moreover, it can be concluded that if $\boldsymbol{V}_r$ is composed in analogy to matrix $\boldsymbol{Z}_W^{\#}$ of the KD-JSD method discussed in the same section, then the invertability of the extended matrix, $\boldsymbol{A}_e$, will be ensured. Furthermore, note that $\boldsymbol{V}_r\boldsymbol{V}_r^T$ is a null-space projector onto $\mathcal{N}^*(\boldsymbol{J}_c)$. This implies that $\boldsymbol{V}_r$ can be derived from the SVD of the system constraint Jacobian $\boldsymbol{J}_c$, in analogy to the null-space projector of a kinematically redundant manipulator (cf. Section 2.7.1).

The next step is to differentiate the generalized velocity (4.186) w.r.t. time. We have

$$\ddot{\boldsymbol{q}} = \boldsymbol{V}_r\dot{\mathcal{V}}_r + \dot{\boldsymbol{V}}_r\mathcal{V}_r. \tag{4.187}$$

Finally, substitute into the equation of motion and premultiply the result by $\boldsymbol{V}_r^T$. Then we have

$$\boldsymbol{V}_r^T\boldsymbol{M}\left(\boldsymbol{V}_r\dot{\mathcal{V}}_r + \dot{\boldsymbol{V}}_r\mathcal{V}_r\right) = \boldsymbol{V}_r^T\mathcal{Q}_u. \tag{4.188}$$

This equation represents the dynamics projected onto the null space of the system constraint matrix and expressed in terms of the quasivelocity. Apparently, the generalized constraint force $\mathcal{Q}_c = \boldsymbol{J}_c^T\boldsymbol{\lambda}$ has been annihilated (by $\boldsymbol{V}_r^T$). Note also that the dimension has been reduced from $n+6$ to r, to obtain an undetermined system with $n+6$ unknowns, as in (4.187). The general solution can be obtained via the pseudoinverse $\boldsymbol{V}_r^{+T} = \boldsymbol{V}_r$, i.e.

$$\boldsymbol{M}\left(\boldsymbol{V}_r\dot{\mathcal{V}}_r + \dot{\boldsymbol{V}}_r\mathcal{V}_r\right) = \boldsymbol{V}_r\boldsymbol{V}_r^T\mathcal{Q}_u + (\boldsymbol{E} - \boldsymbol{V}_r\boldsymbol{V}_r^T)\mathcal{Q}_a. \tag{4.189}$$

The generalized force $\mathcal{Q}_a$ parametrizes the null space $\mathcal{N}(\boldsymbol{V}_r^T)$. An appropriate way for the determination of this force will be introduced in short. Note that in the above derivation, the columns of $\boldsymbol{V}_r$ were assumed orthonormal (i.e. as derived from the SVD of $\boldsymbol{J}_c$). The following identities were used thereby:

$$\boldsymbol{V}_r^T\boldsymbol{V}_r = \boldsymbol{E}_r, \tag{4.190}$$

$$\boldsymbol{V}_r^{+T}\boldsymbol{V}_r^T = \boldsymbol{V}_r\boldsymbol{V}_r^T. \tag{4.191}$$

From (4.189) it can be confirmed that the null-space projector $\boldsymbol{V}_r\boldsymbol{V}_r^T$ maps the generalized forces. Thus, it is characterized as a projector onto the *dual* null space of $\boldsymbol{J}_c$, i.e. $\boldsymbol{N}^*(\boldsymbol{J}_c) \equiv \boldsymbol{V}_r\boldsymbol{V}_r^T$. There is an infinite number of representations of this projector, when parametrized by a generalized inverse. Consider the particular choice

$$\boldsymbol{N}^*(\boldsymbol{J}_c) = (\boldsymbol{E} - \boldsymbol{J}_c^T\boldsymbol{J}_c^{-MT}), \tag{4.192}$$

which also appears in the direct elimination/Gauss approach. Replacing $\boldsymbol{V}_r\boldsymbol{V}_r^T$ with $(\boldsymbol{E} - \boldsymbol{J}_c^T\boldsymbol{J}_c^{-MT})$ in (4.189) and using (4.187), the constraint-consistent generalized accelera-

tion can be derived as

$$\begin{aligned}\ddot{\boldsymbol{q}} &= \boldsymbol{M}^{-1}\boldsymbol{J}_c^T\boldsymbol{J}_c^{-MT}\mathcal{Q}_a + \boldsymbol{M}^{-1}(\boldsymbol{E}-\boldsymbol{J}_c^T\boldsymbol{J}_c^{-MT})\mathcal{Q}_u \\ &= \boldsymbol{J}_c^{-M}\boldsymbol{J}_c\boldsymbol{M}^{-1}\mathcal{Q}_a + \boldsymbol{M}^{-1}\mathcal{Q}_m.\end{aligned} \tag{4.193}$$

When the arbitrary force $\mathcal{Q}_a$ is set to satisfy the second-order differential constraint (2.105),

$$\begin{aligned}\boldsymbol{J}_c\boldsymbol{M}^{-1}\mathcal{Q}_a &= -\dot{\boldsymbol{J}}_c\dot{\boldsymbol{q}}, \\ \mathcal{Q}_a &= \boldsymbol{M}\ddot{\boldsymbol{q}},\end{aligned} \tag{4.194}$$

the constraint-consistent generalized acceleration (4.193) becomes identical to (4.182) from the direct elimination/Gauss approach. Under these conditions and from (4.193), the equation of motion can be written as

$$\boldsymbol{M}\ddot{\boldsymbol{q}} = -\boldsymbol{J}_c^T\boldsymbol{M}_c\dot{\boldsymbol{J}}_c\dot{\boldsymbol{q}} + \mathcal{Q}_m. \tag{4.195}$$

This is identical to (4.180) from the direct elimination/Gauss approach. Thus, the equivalence between the direct elimination/Gauss and the Maggi method has been confirmed.

The constraint force can be recovered, if needed. To this end, premultiply the equation of motion by $\boldsymbol{V}_c^T$. Then we have

$$\boldsymbol{\lambda} = \boldsymbol{V}_c^T(\boldsymbol{M}\ddot{\boldsymbol{q}} - \mathcal{Q}_u) = \boldsymbol{V}_c^T\boldsymbol{M}\ddot{\boldsymbol{q}}_c.$$

Hereby, the relations $\boldsymbol{J}_c\boldsymbol{V}_c = \boldsymbol{E}_c$, $\mathcal{Q}_u = \boldsymbol{M}\ddot{\boldsymbol{q}}_u$, and $\ddot{\boldsymbol{q}}_c = \ddot{\boldsymbol{q}}_u - \ddot{\boldsymbol{q}}$ were used. The generalized constraint force can also be confirmed, via $\mathcal{Q}_c = \boldsymbol{J}_c^T\boldsymbol{\lambda} = \boldsymbol{J}_c^T\boldsymbol{V}_c^T\boldsymbol{M}\ddot{\boldsymbol{q}}_c = \boldsymbol{M}\ddot{\boldsymbol{q}}_c$.

The projection of the dynamics onto the null space of the Jacobian of constrained fixed-base manipulators has been introduced in the field of robotics in [1]. The method has been later adopted for use with underactuated manipulators [78], humanoid robots [77,125,124], and a dual-arm robot [108]. In the case of humanoid robots, the motivation was to alleviate problems related to contact force sensing, e.g. the lack of sensors at certain contacts or the presence of noisy signals and/or time delays resulting from filtering [77]. Note also that when the constraints are eliminated, there is no need to include the contact joints into the model. In this way, the difficulty in handling the inequality constraints pertinent to the friction cone can be alleviated [124].

According to [1], the dynamics are projected onto $\mathcal{N}(\boldsymbol{J}_c)$ with null-space projector $\boldsymbol{N}(\boldsymbol{J}_c) = (\boldsymbol{E} - \boldsymbol{J}_c^+\boldsymbol{J}_c)$, i.e.

$$\boldsymbol{N}\boldsymbol{M}\ddot{\boldsymbol{q}} = \boldsymbol{N}\mathcal{Q}_u. \tag{4.196}$$

If a solution to the generalized acceleration could be found, it would be compatible with the constraints. However, since the projector is singular ($\text{rank}\boldsymbol{N} = r < n + 6$), the solution cannot be obtained directly. As shown in [1], the problem can be tackled by adding the motion constraint (2.115) to the above projected equation of motion. This is possible because the two equations are orthogonal. Therefore, the respective parts can be summed as follows:

$$\tilde{\boldsymbol{M}}\ddot{\boldsymbol{q}} = \boldsymbol{N}\mathcal{Q}_u + \dot{\boldsymbol{N}}\dot{\boldsymbol{q}}, \tag{4.197}$$

where

$$\tilde{\boldsymbol{M}} \equiv \{\boldsymbol{N}\boldsymbol{M} + \boldsymbol{M}(\boldsymbol{E} - \boldsymbol{N})\}. \tag{4.198}$$

The matrix $\tilde{\boldsymbol{M}}$ is called the *constrained joint-space inertia matrix* [1]. It can be represented as $\tilde{\boldsymbol{M}} = \boldsymbol{M} + \tilde{\boldsymbol{S}}$, $\tilde{\boldsymbol{S}} \equiv \boldsymbol{N}\boldsymbol{M} - (\boldsymbol{N}\boldsymbol{M})^T$. Since $\boldsymbol{M}$ is positive definite and $\tilde{\boldsymbol{S}}$ is skew-symmetric ($\tilde{\boldsymbol{S}} = -\tilde{\boldsymbol{S}}^T$), it follows that $\tilde{\boldsymbol{M}}$ is also positive definite. Hence, this matrix will be always invertible, irrespective of the particular set of constraints.

It is important to note that the constrained joint-space inertia matrix does not retain the properties of an inertia matrix; $\tilde{\boldsymbol{M}}$ is *asymmetric* and *nonunique*. This leads to problems pertinent to the specific choice of this matrix. Fortunately, there is a straightforward approach to avoid the appearance of $\tilde{\boldsymbol{M}}$ into the projected dynamics. Since the null-space projector $\boldsymbol{N}$ and its dual, $\boldsymbol{N}^*$, are isomorphic, they can be decomposed in the same way. Thus,

$$\boldsymbol{N} = \boldsymbol{V}_r \boldsymbol{V}_r^T \Rightarrow \boldsymbol{V}_r^T \boldsymbol{N} = \boldsymbol{V}_r^T. \tag{4.199}$$

Then, premultiply projected dynamics (4.196) by $\boldsymbol{V}_r^T$ to obtain

$$\boldsymbol{V}_r^T \boldsymbol{M}\ddot{\boldsymbol{q}} = \boldsymbol{V}_r^T \mathcal{Q}_u. \tag{4.200}$$

This equation is identical to (4.188) from Maggi's method. By following the rest of the steps of this method, one arrives at the equation of motion represented as in (4.195). Thus, the important conclusion can be made that the $\boldsymbol{N}$-based projection of the dynamics yields the same result as Gauss'/direct elimination/Maggi's approaches. In this way, the problem associated with the asymmetric and nonunique inertia-like matrix, $\tilde{\boldsymbol{M}}$, as in (4.197), can be avoided.

4.12.4 Range-Space Projection Method

As clarified in Section 4.12.3, the essence of Maggi's method is projecting the system dynamics onto the null space of the system constraint matrix. As an alternative, the dynamics can be projected onto the range space of that matrix [115,131,133]. The elimination of the constraint forces is accomplished in accordance with the four steps used to transform the fixed-base manipulator dynamics in Section 4.5.2. First, the system dynamics in the upper part of (4.163) are projected onto $\mathcal{R}(\boldsymbol{J}_c)$ by premultiplication with $\boldsymbol{J}_c\boldsymbol{M}^{-1}$. Second, making use of the second-order motion constraint from the lower part of the same equation, one arrives at

$$\boldsymbol{M}_c^{-1}\boldsymbol{\lambda} + \boldsymbol{J}_c\boldsymbol{M}^{-1}(\boldsymbol{c} + \boldsymbol{g}) - \dot{\boldsymbol{J}}_c\dot{\boldsymbol{q}} = \boldsymbol{J}_c\boldsymbol{M}^{-1}\mathcal{Q}. \tag{4.201}$$

Here $\boldsymbol{M}_c^{-1} = (\boldsymbol{J}_c\boldsymbol{M}^{-1}\boldsymbol{J}_c^T)$ stands for the *system mobility tensor* mapped along the constrained motion directions. This matrix exists at nonsingular postures where $\boldsymbol{J}_c$ has a full row rank. The third step is to obtain Lagrange's multiplier vector (the constraint force), i.e.

$$\boldsymbol{\lambda} = \boldsymbol{J}_c^{-MT}\mathcal{Q} + \boldsymbol{M}_c\dot{\boldsymbol{J}}_c\dot{\boldsymbol{q}} - \boldsymbol{J}_c^{-MT}(\boldsymbol{c} + \boldsymbol{g}). \tag{4.202}$$

Here $\boldsymbol{J}_c^{-M} = \boldsymbol{M}^{-1}\boldsymbol{J}_c\boldsymbol{M}_c$ denotes the inertia-weighted system constraint matrix. In the final step, substitute the constraint force $\boldsymbol{\lambda}$ back into the upper part of (4.163), i.e.

$$\boldsymbol{M}\ddot{\boldsymbol{q}} + \boldsymbol{J}_c^T\boldsymbol{M}_c\dot{\boldsymbol{J}}_c\dot{\boldsymbol{q}} + \boldsymbol{N}^*(\boldsymbol{J}_c)(\boldsymbol{c}+\boldsymbol{g}) = \boldsymbol{N}^*(\boldsymbol{J}_c)\mathcal{Q}. \tag{4.203}$$

The null-space projector $\boldsymbol{N}^*(\boldsymbol{J}_c)$ is given in (4.192).[12] This form of the equation of motion appeared in [133]. The equation can be further simplified as

$$\boldsymbol{M}\ddot{\boldsymbol{q}} = -\boldsymbol{J}_c^T\boldsymbol{M}_c\dot{\boldsymbol{J}}_c\dot{\boldsymbol{q}} + \mathcal{Q}_m. \tag{4.204}$$

This is exactly the same equation as (4.180) and (4.195), obtained with the direct elimination/Gauss and Maggi methods, respectively. It becomes then clear that the range-space projection method is identical to all the other methods discussed so far.

4.12.5 Summary and Conclusions

It has been confirmed that the direct elimination, Gauss' principle of least constraint, Maggi's null-space projection, and the range-space projection methods yield identical equations: (4.168), (4.180), (4.195), and (4.204), respectively. Their equivalence was confirmed under the following conditions:

- the dynamics are projected onto $\mathcal{N}^*(\boldsymbol{J}_c)$,
- the respective null-space projector is parametrized as in (4.192),
- the arbitrary generalized force $\mathcal{Q}_a$ is set as in (4.194).

These conditions are relevant in the case of *ideal* constraints, whereby motion is always in harmony with Gauss' principle of least constraint. With a given generalized input force, the motion is determined in a unique way. This also implies uniqueness of all the components: the Lagrange's multiplier (4.170), the generalized constraint force (4.169), the unconstrained generalized acceleration $\ddot{\boldsymbol{q}}_u$, and the constraint-consistent generalized acceleration with its two components shown in (4.174) (the linear, tangential $\ddot{\boldsymbol{q}}_m$ and the nonlinear, state-dependent component in the normal direction).

In a real system, however, the constraints are never ideal; there is always some friction and compliance at the contact joints. This renders the constraint equations inhomogeneous and calls for active control of the constraint forces. Especially, in multilimb/finger/leg robots, the control of these forces is essential for reaction-based propulsion and manipulation. Such control is achievable in an infinite number of ways since the generalized forces $\mathcal{Q}_u$ and $\mathcal{Q}_a$, appearing in (4.181) and (4.189), respectively, can be chosen freely. The former is relevant to the tangential-force control, the latter ensures the controllability in the normal direction and, thus, of the internal force. Note also that, through the choice of $\mathcal{Q}_u$, Lagrange's multiplier vector (4.177), the constraint force $\mathcal{Q}_c$ (4.179), and the constraint maintaining force $\mathcal{Q}_m$ (4.181) will be determined in a unique way. Furthermore, recall that nonideal constraints will render the motion of the system nonintegrable at the acceleration level. As a consequence, a joint velocity drift may appear, which will necessitate an internal motion (self-motion) control.

[12] This projector is sometimes referred to as the "dynamically consistent" null-space projector [115,131,133].

4.13 REDUCED-FORM REPRESENTATIONS OF THE EQUATION OF MOTION

Reduced-form representations of the equation of motion lead to a system of reduced dimensions. An example of such representation for a space robot model floating in zero gravity, without and with the presence of an external force, was given in (4.127) and (4.133), respectively. In the example, the system dynamics were expressed in terms of the joint-space partial dynamics. Another possibility is to express the system dynamics in terms of the spatial partial dynamics. As will be shown in what follows, these reduced-form representations also result in the elimination of the constraint forces. Another type of reduced-form representation can be obtained via projections onto the end-link (sub)space, yielding dynamic relations in the end-link spatial coordinates.

For clarity but without loss of generality, the derivations will be based on the equation of motion expressed in terms of base quasivelocity, (4.155).

4.13.1 Joint-Space Dynamics–Based Representation

A reduced-form representation of the equation of motion can be obtained by mapping the spatial dynamics component onto the joint space. The joint acceleration is derived from the lower part of (4.155) as

$$\ddot{\boldsymbol{\theta}} = \boldsymbol{M}_{\theta B}^{-1}(\boldsymbol{\tau}_u - \boldsymbol{H}_{BB}^T \dot{\mathcal{V}}_B) - \boldsymbol{M}_{\theta B}^{-1} \boldsymbol{\mathcal{J}}_{cB}^T \boldsymbol{\lambda}. \tag{4.205}$$

Hereby, definitions $\boldsymbol{\lambda} \equiv -\overline{\mathcal{F}}^c$ and $\boldsymbol{\tau}_u \equiv \boldsymbol{\tau} - \boldsymbol{c}_{\theta B} - \boldsymbol{g}_\theta$ were used. To enforce the motion constraints, insert (4.205) into (2.104), under the assumption of hard constraints ($\dot{\overline{\mathcal{V}}}^c = \boldsymbol{0}$). The joint acceleration will then be eliminated from the latter equation. The resultant equation is solved for Lagrange's multiplier vector, i.e.

$$\boldsymbol{\lambda} = \boldsymbol{\mathcal{J}}_{cB}^{-M_{\theta B}T}(\boldsymbol{\tau}_u - \boldsymbol{H}_{BB}^T \dot{\mathcal{V}}_B) + \boldsymbol{M}_{cB}\left(\boldsymbol{h}_{\theta B} + \mathbb{C}_{cB}^T \dot{\mathcal{V}}_B\right), \tag{4.206}$$

where $\boldsymbol{h}_{\theta B} \equiv \dot{\boldsymbol{\mathcal{J}}}_{cB}\dot{\boldsymbol{\theta}} + \dot{\mathbb{C}}_{cB}^T \mathcal{V}_B$. The matrix

$$\boldsymbol{M}_{cB} \equiv \left(\boldsymbol{\mathcal{J}}_{cB} \boldsymbol{M}_{\theta B}^{-1} \boldsymbol{\mathcal{J}}_{cB}^T\right)^{-1} \in \Re^{c\times c} \tag{4.207}$$

stands for the *joint-space inertia tensor* mapped along the constrained motion directions. Substitute this result back into (4.205) to eliminate the constraint forces, so we have

$$\ddot{\boldsymbol{\theta}} = \overline{\boldsymbol{T}}_{\theta B}(\boldsymbol{\tau}_u - \boldsymbol{H}_{BB}^T \dot{\mathcal{V}}_B) - \boldsymbol{\mathcal{J}}_{cB}^{-M_{\theta B}}\left(\boldsymbol{h}_{\theta B} + \mathbb{C}_{cB}^T \dot{\mathcal{V}}_B\right). \tag{4.208}$$

Here $\boldsymbol{\mathcal{J}}_{cB}^{-M_{\theta B}}$ is the inertia-weighted generalized inverse of the joint-space constraint Jacobian (cf. also (4.53)). The matrix

$$\begin{aligned} \overline{\boldsymbol{T}}_{\theta B} &\equiv \boldsymbol{M}_{\theta B}^{-1}\left(\boldsymbol{E} - \boldsymbol{\mathcal{J}}_{cB}^T \boldsymbol{\mathcal{J}}_{cB}^{-M_{\theta B}T}\right) \\ &= \boldsymbol{M}_{\theta B}^{-1} - \boldsymbol{M}_{\theta B}^{-1} \boldsymbol{\mathcal{J}}_{cB}^T \boldsymbol{M}_{cB} \boldsymbol{\mathcal{J}}_{cB} \boldsymbol{M}_{\theta B}^{-1} \end{aligned} \tag{4.209}$$

is symmetric and positive definite, under the assumption of independent constraints. This is the *joint-space mobility tensor* restricted by the null space of the joint-space constraint Jacobian; $\overline{\boldsymbol{T}}_{\theta B}$ will be referred to as the *constraint-consistent joint-space mobility tensor*. Note that, for a given set of independent constraints, $\overline{\boldsymbol{T}}_{\theta B}$ is unique. Premultiply (4.208) by $\boldsymbol{M}_{\theta B}$ to obtain the equation of motion as

$$\boldsymbol{M}_{\theta B}\ddot{\boldsymbol{\theta}} = \left(\boldsymbol{E} - \mathcal{J}_{cB}^T \mathcal{J}_{cB}^{-M_{\theta B}T}\right)(\boldsymbol{\tau}_u - \boldsymbol{H}_{BB}^T \dot{\mathcal{V}}_B) - \mathcal{J}_{cB}^T \left(\mathcal{J}_{cB}\boldsymbol{M}_{\theta B}^{-1}\mathcal{J}_{cB}^T\right)^{-1}\left(\boldsymbol{h}_{\theta B} + \mathbb{C}_{cB}^T \dot{\mathcal{V}}_B\right). \quad (4.210)$$

In this representation, the dimension of the equation of motion has been reduced from $n+6$ to n. The arbitrary joint torque $\boldsymbol{\tau}_u$ can play the role of a control input component. It is filtered by the null-space projector $\mathcal{N}^*(\mathcal{J}_{cB})$ to produce a *constraint maintaining* joint torque, $\boldsymbol{\tau}_m = \left(\boldsymbol{E} - \mathcal{J}_{cB}^T \mathcal{J}_{cB}^{-M_{\theta B}T}\right)\boldsymbol{\tau}_u$, that is useful for motion control along the unconstrained motion directions. This joint torque does not produce any acceleration along the unconstrained motion directions, i.e. it is dynamically consistent.

4.13.2 Spatial Dynamics–Based Representation (Lagrange–d'Alembert Formulation)

The representation of the equation of motion in terms of spatial dynamics is known as Lagrange–d'Alembert's formulation. This formulation has been employed in the field of multifinger grasp modeling ([87], p. 280). Indeed, note that the grasped object is not directly actuated. It is then interesting to observe that the equation of motion of the system (i.e. multiple actuated fingers plus nonactuated object) comprises the same structure as that of a humanoid robot (multiple actuated limbs plus nonactuated base link).

The formulation can be derived from d'Alembert's principle of virtual work. The virtual work of the generalized input and constraint forces along virtual displacement $\delta\boldsymbol{q}_B = \begin{bmatrix}\delta\mathcal{X}_B^T & \delta\boldsymbol{\theta}^T\end{bmatrix}^T$ is expressed as $\delta W = \delta\boldsymbol{q}_B^T(\mathcal{Q} - \mathcal{Q}_{cB})$. According to the principle, the generalized constraint force does no virtual work; $\delta\boldsymbol{q}_B^T\mathcal{Q}_{cB} = \boldsymbol{0}$. Recalling that $\mathcal{Q}_{cB} = \boldsymbol{M}\ddot{\boldsymbol{q}}_B - \mathcal{Q}_u$, $\mathcal{Q}_u$ standing for the generalized force of the unconstrained system (cf. (4.163)), the principle of virtual work can be rewritten as

$$\delta\boldsymbol{q}_B^T\left(\mathcal{Q}_u - \boldsymbol{M}\ddot{\boldsymbol{q}}_B\right) = 0, \quad (4.211)$$

or

$$\begin{bmatrix}\delta\mathcal{X}_B^T & \delta\boldsymbol{\theta}^T\end{bmatrix}\left(\begin{bmatrix}\boldsymbol{0}\\ \mathcal{Q}\end{bmatrix} - \begin{bmatrix}\mathbb{M}_B & \boldsymbol{H}_{BB}\\ \boldsymbol{H}_{BB}^T & \boldsymbol{M}_{\theta B}\end{bmatrix}\begin{bmatrix}\dot{\mathcal{V}}_B\\ \ddot{\boldsymbol{\theta}}\end{bmatrix} - \begin{bmatrix}\mathcal{C}_B\\ \boldsymbol{c}_{\theta B}\end{bmatrix} - \begin{bmatrix}\mathcal{G}_B\\ \boldsymbol{g}_\theta\end{bmatrix}\right) = 0. \quad (4.212)$$

Thus

$$\begin{aligned}0 &= \delta\boldsymbol{\theta}^T\left(\mathcal{Q} - \boldsymbol{M}_{\theta B}\ddot{\boldsymbol{\theta}} - \boldsymbol{H}_{BB}^T\dot{\mathcal{V}}_B - \boldsymbol{c}_{\theta B} - \boldsymbol{g}_\theta\right) - \delta\mathcal{X}_B^T\left(\boldsymbol{H}_{BB}\ddot{\boldsymbol{\theta}} + \mathbb{M}_B\dot{\mathcal{V}}_B + \mathcal{C}_B + \mathcal{G}_B\right)\\ &= \left(\mathcal{J}_{cB}{}^{\#}\mathbb{C}_{cB}^T\delta\mathcal{X}_B\right)^T\left(\mathcal{Q} - \boldsymbol{M}_{\theta B}\ddot{\boldsymbol{\theta}} - \boldsymbol{H}_{BB}^T\dot{\mathcal{V}}_B - \boldsymbol{c}_{\theta B} - \boldsymbol{g}_\theta\right) - \delta\mathcal{X}_B^T\left(\boldsymbol{H}_{BB}\ddot{\boldsymbol{\theta}} + \mathbb{M}_B\dot{\mathcal{V}}_B + \mathcal{C}_B + \mathcal{G}_B\right)\\ &= \left(\mathcal{J}_{cB}{}^{\#}\mathbb{C}_{cB}^T\right)^T\left(\mathcal{Q} - \boldsymbol{M}_{\theta B}\ddot{\boldsymbol{\theta}} - \boldsymbol{H}_{BB}^T\dot{\mathcal{V}}_B - \boldsymbol{c}_{\theta B} - \boldsymbol{g}_\theta\right) - \left(\boldsymbol{H}_{BB}\ddot{\boldsymbol{\theta}} + \mathbb{M}_B\dot{\mathcal{V}}_B + \mathcal{C}_B + \mathcal{G}_B\right).\end{aligned}$$

Hereby, the virtual displacements in the joints were expressed using (2.91) as

$$\delta\boldsymbol{\theta} = \boldsymbol{\mathcal{J}}_{cB}^{\#}\mathbb{C}_{cB}^{T}\,\delta\mathcal{X}_B \tag{4.213}$$

for any virtual displacement of the base link $\delta\mathcal{X}_B$. Finally, substitute the constraint-consistent joint velocity and acceleration, i.e.

$$\dot{\boldsymbol{\theta}} = \boldsymbol{\mathcal{J}}_{cB}^{\#}\mathbb{C}_{cB}^{T}\mathcal{V}_B \tag{4.214}$$

and

$$\ddot{\boldsymbol{\theta}} = \boldsymbol{\mathcal{J}}_{cB}^{\#}\left(\mathbb{C}_{cB}^{T}\dot{\mathcal{V}}_B + \dot{\mathbb{C}}_{c}^{T}\mathcal{V}_B - \dot{\boldsymbol{\mathcal{J}}}_{cB}\dot{\boldsymbol{\theta}}\right) \tag{4.215}$$

(derived from (2.91) and (2.104), respectively), into the above relations to arrive at

$$\widetilde{\mathbb{M}}_B\dot{\mathcal{V}}_B + \widetilde{\mathcal{C}}_B + \widetilde{\mathcal{G}}_B = \mathcal{F}_B. \tag{4.216}$$

Hereby,

$$\begin{aligned}
\widetilde{\mathbb{M}}_B &= \mathbb{M}_B + \mathbb{C}_{cB}\boldsymbol{\mathcal{J}}_{cB}^{\#T}\boldsymbol{M}_{\theta B}\boldsymbol{\mathcal{J}}_{cB}^{\#}\mathbb{C}_{cB}^{T},\\
\widetilde{\mathcal{C}}_B &= \mathcal{C}_B + \mathbb{C}_{cB}\boldsymbol{\mathcal{J}}_{cB}^{\#T}\left\{\boldsymbol{c}_{\theta B} + \boldsymbol{M}_{\theta B}\boldsymbol{\mathcal{J}}_{cB}^{\#}\left(\dot{\mathbb{C}}_{cB}^{T} - \dot{\boldsymbol{\mathcal{J}}}_{cB}\boldsymbol{\mathcal{J}}_{cB}^{\#}\mathbb{C}_{cB}^{T}\right)\mathcal{V}_B\right\},\\
\widetilde{\mathcal{G}}_B &= \mathcal{G}_B + \mathbb{C}_{cB}\boldsymbol{\mathcal{J}}_{cB}^{\#T}\boldsymbol{g}_{\theta},\\
\mathcal{F}_B &= \mathbb{C}_{cB}\boldsymbol{\mathcal{J}}_{cB}^{\#T}\boldsymbol{\tau}.
\end{aligned}$$

With (4.216), the equation of motion of the humanoid robot is expressed in the form of spatial dynamics. The dimension of the system has been significantly reduced, from $n+6$ to six. The forces of constraint appear only implicitly (the $\boldsymbol{\mathcal{J}}_{cB}^{\#T}\boldsymbol{\tau}$-term in the body wrench $\mathcal{F}_B$). Note, however, that with this representation, the partial dynamic relations stemming from the presence of kinematic redundancy cannot be accounted for.

Adjoining the Object Dynamics

Lagrange–d'Alembert's formulation is quite suitable to represent the combined dynamics of the humanoid robot and an object grasped by the robot. The object and the arms form an independent closed loop, the object playing thereby the role of the loop-closure link. The general case of unilateral hand/object contact joints is assumed, $\mathbb{C}_{cH}$ denoting the contact map. The coordinate frame of the object, $\{H\}$, is fixed at its CoM. The object's mass and inertia tensors are denoted as M_H and $\boldsymbol{I}_H$, respectively. Newton–Euler's equation of motion of the object is written as

$$\begin{bmatrix} M_H\boldsymbol{E}_3 & \boldsymbol{0}\\ \boldsymbol{0} & \boldsymbol{I}_H\end{bmatrix}\begin{bmatrix}\dot{\boldsymbol{v}}_H\\ \dot{\boldsymbol{\omega}}_H\end{bmatrix} + \begin{bmatrix}\boldsymbol{0}\\ \boldsymbol{\omega}_H\times\boldsymbol{I}_H\boldsymbol{\omega}_H\end{bmatrix} + \begin{bmatrix}M_H\boldsymbol{g}\\ \boldsymbol{0}\end{bmatrix} = \begin{bmatrix}\boldsymbol{f}_H\\ \boldsymbol{m}_H\end{bmatrix}. \tag{4.217}$$

The compact form representation of this equation is

$$\mathbb{M}_H\dot{\mathcal{V}}_H + \mathcal{C}_H + \mathcal{G}_H = \mathcal{F}_H, \tag{4.218}$$

where $\mathbb{M}_H$ is the constant spatial inertia of the object, $\mathcal{C}_H$ contains the gyroscopic torque term, and $\mathcal{G}_H$ is the gravity wrench. The net wrench, $\mathcal{F}_H$, is in a quasistatic balance with the contact wrenches *impressed* (by the hands) upon the object, i.e.

$$\mathcal{F}_H = -\mathbb{C}_{cH}(\boldsymbol{q}_H)\,\overline{\mathcal{F}}_H^c.$$

Furthermore, adjoin the object dynamics to those of the humanoid robot. For clarity and without loss of generality, the compact form representations (4.162) and (4.218) will be used, the former being expressed in terms of the base quasivelocity. We have

$$\begin{bmatrix} \mathbb{M}_H & \boldsymbol{H}_{HB} \\ \boldsymbol{H}_{HB}^T & \boldsymbol{M}_B \end{bmatrix} \begin{bmatrix} \dot{\mathcal{V}}_H \\ \ddot{\boldsymbol{q}}_B \end{bmatrix} + \begin{bmatrix} \mathcal{C}_H \\ \boldsymbol{c}_B \end{bmatrix} + \begin{bmatrix} \mathcal{G}_H \\ \boldsymbol{g}_B \end{bmatrix} = \begin{bmatrix} \boldsymbol{0} \\ \mathcal{Q} \end{bmatrix} + \begin{bmatrix} -\mathbb{C}_{cH}(\boldsymbol{q}) \\ \boldsymbol{\mathcal{J}}_{cB}^T \end{bmatrix} \overline{\mathcal{F}}^c. \tag{4.219}$$

Here $\boldsymbol{H}_{HB} \in \Re^{6\times(n+6)}$ is a map accounting for the inertial coupling between the object and the hands. Note that $\boldsymbol{H}_{HB}$ and $\mathbb{C}_{cH}(\boldsymbol{q})$ map the joint accelerations of the legs and the contact wrenches at the feet, respectively, at zero since these quantities do not contribute to the object dynamics. Lagrange–d'Alembert's formulation can be derived from the above equation of motion by employing the principle of virtual work with regard to the virtual displacements of the object and the robot. The final result can be written as

$$\widetilde{\mathbb{M}}_H \dot{\mathcal{V}}_H + \widetilde{\mathcal{C}}_H + \widetilde{\mathcal{G}}_H = \mathcal{F}_H, \tag{4.220}$$

where

$$\begin{aligned}
\widetilde{\mathbb{M}}_H &= \mathbb{M}_H + \mathbb{C}_{cH}\boldsymbol{\mathcal{J}}_{cB}^{\#T}\boldsymbol{M}_{\theta B}\boldsymbol{\mathcal{J}}_{cB}^{\#}\mathbb{C}_{cH}^T + \mathbb{C}_{cH}\boldsymbol{\mathcal{J}}_{cB}^{\#T}\boldsymbol{H}_{HB} + \left(\mathbb{C}_{cH}\boldsymbol{\mathcal{J}}_{cB}^{\#T}\boldsymbol{H}_{HB}\right)^T, \\
\widetilde{\mathcal{C}}_H &= \mathcal{C}_H + \mathbb{C}_{cH}\boldsymbol{\mathcal{J}}_{cB}^{\#T}\left\{\boldsymbol{c}_{\theta B} + \boldsymbol{M}_{\theta B}\boldsymbol{\mathcal{J}}_{cB}^{\#}\left(\dot{\mathbb{C}}_{cH}^T - \dot{\boldsymbol{\mathcal{J}}}_{cB}\boldsymbol{\mathcal{J}}_{cB}^{\#}\mathbb{C}_{cH}\right)\mathcal{V}_H\right\} \\
&\quad + \boldsymbol{H}_{HB}^T\boldsymbol{\mathcal{J}}_{cB}^{\#}\left(\dot{\mathbb{C}}_{cH}^T - \dot{\boldsymbol{\mathcal{J}}}_{cB}\boldsymbol{\mathcal{J}}_{cB}^{\#}\mathbb{C}_{cH}\right)\mathcal{V}_H, \\
\widetilde{\mathcal{G}}_H &= \mathcal{G}_H + \mathbb{C}_{cH}\boldsymbol{\mathcal{J}}_{cB}^{\#T}\boldsymbol{g}_\theta, \\
\mathcal{F}_H &= \mathbb{C}_{cH}\boldsymbol{\mathcal{J}}_{cB}^{\#T}\boldsymbol{\tau}.
\end{aligned}$$

4.13.3 Equation of Motion in End-Link Spatial Coordinates

The joint acceleration can be eliminated from the equation of motion to arrive at a dynamic model represented in terms of the end-link spatial coordinates. The motivation behind such an approach for the case of a fixed-base manipulator was clarified in Section 4.5.2. The same motivation is valid in the case of a humanoid robot, as shown in [115] (see also [131, 133]). In these works, the system dynamics were first projected with a dynamically consistent null-space projector along the constrained motion directions at the contacts. With such a model, the *motion control tasks* for the unconstrained motion directions and balance control are achieved within the null space of the projected dynamics. In this way, the *contact control task* can be performed in a dynamically decoupled manner, with the highest task priority. To ensure the performance of the lower-priority (motion) tasks, the system dynamics have to be projected along the unconstrained motion directions, in a subsequent step.

In the remainder of this section, the end-link spatial coordinate representations of the constrained dynamic models derived so far will be obtained by projecting their system dynamics along:

- the constrained motion directions (force-based projection);
- the unconstrained motion directions (motion-based projection);
- both the constrained and the unconstrained motion directions.

Constrained Dynamics Projection Along the Constrained Motion Directions

The projection of the constrained dynamics onto the subspace of constraints in end-link coordinates is achieved in accordance with the four steps used to transform the fixed-base manipulator dynamics in Section 4.5.2 (see also [115]). At the first step, project the constrained equation of motion (e.g. (4.204)) along the constrained motion directions by premultiplication with $\boldsymbol{J}_c\boldsymbol{M}^{-1}$. The second step is to employ the second-order differential kinematics along the constrained motion directions, i.e. $\boldsymbol{J}_c\ddot{\boldsymbol{q}} = \dot{\hat{\mathcal{V}}}^c - \dot{\boldsymbol{J}}_c\dot{\boldsymbol{q}}$. Note that the general case of soft constraints is assumed with a nonzero $\dot{\hat{\mathcal{V}}}^c$. The resultant equation is simple:

$$\begin{aligned}\dot{\hat{\mathcal{V}}}^c &= \boldsymbol{J}_c\overline{\boldsymbol{T}}\mathcal{Q}_m \\ &= \boldsymbol{J}_c\overline{\boldsymbol{T}}(\mathcal{Q} - \boldsymbol{c} - \boldsymbol{g}).\end{aligned} \tag{4.221}$$

Here $\overline{\boldsymbol{T}} = \boldsymbol{M}^{-1}\boldsymbol{N}^*(\boldsymbol{J}_c)$ is the system mobility tensor restricted by the (dual) null space of the system constraint Jacobian; $\overline{\boldsymbol{T}}$ is henceforth referred to as the *constraint-consistent system mobility tensor*. The third step is to employ the quasistatic force relation along the constrained motion directions, i.e.

$$\mathcal{Q} = \boldsymbol{J}_c^T\overline{\mathcal{F}}^c + \boldsymbol{N}^*(\boldsymbol{J}_c)\mathcal{Q}_a, \tag{4.222}$$

$\mathcal{Q}_a$ denoting an arbitrary generalized force. Substituting (4.222) into (4.221) results in

$$\dot{\hat{\mathcal{V}}}^c = \boldsymbol{J}_c\overline{\boldsymbol{T}}\boldsymbol{J}_c^T\overline{\mathcal{F}}^c + \boldsymbol{J}_c\overline{\boldsymbol{T}}(\mathcal{Q}_a - \boldsymbol{c} - \boldsymbol{g}). \tag{4.223}$$

Hereby, the idempotence property of the null-space projector was employed. The final step is to solve for $\overline{\mathcal{F}}^c$. We have

$$\overline{\mathcal{F}}^c = \overline{\boldsymbol{M}}_c\dot{\hat{\mathcal{V}}}^c - (\boldsymbol{J}_c^{-\overline{\boldsymbol{T}}})^T(\mathcal{Q}_a - \boldsymbol{c} - \boldsymbol{g}). \tag{4.224}$$

The matrix $\overline{\boldsymbol{M}}_c \equiv \left(\boldsymbol{J}_c\overline{\boldsymbol{T}}\boldsymbol{J}_c{}^T\right)^{-1}$ is the *constraint-consistent system inertia mapped along the constrained directions* and $\boldsymbol{J}_c^{-\overline{T}}$ is the (right) pseudoinverse of $\boldsymbol{J}_c$ weighted by the constraint-consistent mobility tensor $\overline{\boldsymbol{T}}$.

The last equation represents the constrained dynamics mapped along the constrained motion directions. It is easy to confirm that the same result can be derived from the null space–projected equation of motion (4.196) [78].

System Dynamics Projection Along the Unconstrained Motion Directions

The same procedure as above is applied to project the system dynamics along the unconstrained motion directions. The projection procedure is initialized with premultiplication of

the constrained equation of motion by $\boldsymbol{J}_m\boldsymbol{M}^{-1}$. The second step is to employ the second-order differential kinematics along the unconstrained motion directions, i.e. $\boldsymbol{J}_m\ddot{\boldsymbol{q}} = \dot{\mathcal{V}}^m - \dot{\boldsymbol{J}}_m\dot{\boldsymbol{q}}$. After these steps, the equation of motion assumes the form

$$\dot{\mathcal{V}}^m - \boldsymbol{J}_m\dot{\boldsymbol{q}} + \boldsymbol{J}_m\boldsymbol{J}_c^{-M}\dot{\boldsymbol{J}}_c\dot{\boldsymbol{q}} + \boldsymbol{J}_m\overline{\boldsymbol{T}}(\boldsymbol{c}+\boldsymbol{g}) = \boldsymbol{J}_m\overline{\boldsymbol{T}}\mathcal{Q}. \tag{4.225}$$

In the third step, substitute the quasistatic force relation along the unconstrained motion directions, i.e.

$$\mathcal{Q} = \boldsymbol{J}_m^T\overline{\mathcal{F}}^m + \boldsymbol{N}^*(\boldsymbol{J}_m)\mathcal{Q}_a. \tag{4.226}$$

The term on the r.h.s. of (4.225) then assumes the form

$$\boldsymbol{J}_m\overline{\boldsymbol{T}}\mathcal{Q} = \overline{\boldsymbol{M}}_m\overline{\mathcal{F}}^m + \boldsymbol{J}_m\overline{\boldsymbol{T}}\boldsymbol{N}^*(\boldsymbol{J}_m)\mathcal{Q}_a, \tag{4.227}$$

$\overline{\boldsymbol{M}}_m \equiv \left(\boldsymbol{J}_m\overline{\boldsymbol{T}}\boldsymbol{J}_m{}^T\right)^{-1}$ denoting the *constraint-consistent system inertia mapped along the unconstrained motion directions*. Note that in the second term, the arbitrary generalized force $\mathcal{Q}_a$ is projected onto the null space $\mathcal{N}^*(\boldsymbol{J}) = \mathcal{N}^*(\boldsymbol{J}_c)\cap\mathcal{N}^*(\boldsymbol{J}_m)$. This term will result in zero in the case of a robot with *nonredundant* limbs.

The final step is to solve for the quasistatic force $\overline{\mathcal{F}}^m$, i.e.

$$\overline{\mathcal{F}}^m = \overline{\boldsymbol{M}}_m\dot{\mathcal{V}}^m + \mathcal{C}_m + \mathcal{G}_m - \overline{(\boldsymbol{J}_m^{-\overline{T}})^T}\mathcal{Q}_a. \tag{4.228}$$

Here $\boldsymbol{J}_m^{-\overline{T}}$ is the (right) pseudoinverse of $\boldsymbol{J}_m$ weighted by the constraint-consistent mobility tensor $\overline{\boldsymbol{T}}$ and $\overline{(\boldsymbol{J}_m^{-\overline{T}})^T}$ stands for the restriction of its transpose by the (dual) null space of the mobility Jacobian:

$$\overline{(\boldsymbol{J}_m^{-\overline{T}})^T} = (\boldsymbol{J}_m^{-\overline{T}})^T\boldsymbol{N}^*(\boldsymbol{J}_m).$$

The nonlinear velocity-dependent and gravity terms are

$$\begin{aligned}\mathcal{C}_m &= (\boldsymbol{J}_m^{-\overline{T}})^T\boldsymbol{c} + \overline{\boldsymbol{M}}_m(\boldsymbol{J}_m\boldsymbol{J}_c{}^{-M}\dot{\boldsymbol{J}}_c - \dot{\boldsymbol{J}}_m)\dot{\boldsymbol{q}},\\ \mathcal{G}_m &= (\boldsymbol{J}_m^{-\overline{T}})^T\boldsymbol{g}.\end{aligned}$$

Projection Along the Constrained and Unconstrained Motion Directions

Consider the system dynamics written in terms of the base quasivelocity. The first-order instantaneous motion relation of the humanoid robot, (2.93), can be written as

$$\begin{bmatrix}\mathcal{V}_B\\ \mathcal{V}\end{bmatrix} = \begin{bmatrix}\boldsymbol{E} & \boldsymbol{0}\\ \mathbb{C}_B^T & \mathcal{J}_B\end{bmatrix}\begin{bmatrix}\mathcal{V}_B\\ \dot{\boldsymbol{\theta}}\end{bmatrix}. \tag{4.229}$$

Denote by $\boldsymbol{T}_B$ the 4×4 block matrix on the r.h.s. Assuming a robot with *nonredundant* limbs in a nonsingular configuration, the inverse transformation can be written as

$$\begin{bmatrix}\mathcal{V}_B\\ \dot{\boldsymbol{\theta}}\end{bmatrix} = \begin{bmatrix}\boldsymbol{E} & \boldsymbol{0}\\ -\mathcal{J}_B^{-1}\mathbb{C}_B^T & \mathcal{J}_B^{-1}\end{bmatrix}\begin{bmatrix}\mathcal{V}_B\\ \mathcal{V}\end{bmatrix}, \tag{4.230}$$

the 4×4 block matrix on the r.h.s. standing for the inverse $\boldsymbol{T}_B^{-1}$. The compact form of the equation of motion, (4.162), is projected with the help of $\boldsymbol{T}_B$ as

$$\boldsymbol{M}_B(\boldsymbol{q}) \begin{bmatrix} \dot{\mathcal{V}}_B \\ \dot{\mathcal{V}} \end{bmatrix} + \boldsymbol{C}_B(\boldsymbol{q}, \dot{\boldsymbol{q}}) \begin{bmatrix} \mathcal{V}_B \\ \mathcal{V} \end{bmatrix} + \boldsymbol{g}_B(\boldsymbol{q}) = \begin{bmatrix} -\mathbb{C}_B \\ \boldsymbol{E} \end{bmatrix} \boldsymbol{\mathcal{J}}_B^{-T} \boldsymbol{\tau} + \boldsymbol{T}_B^{-T} \mathcal{Q}_{cB}, \tag{4.231}$$

where $\boldsymbol{M}_B \equiv \boldsymbol{T}_B^{-T} \boldsymbol{M} \boldsymbol{T}_B^{-1}$, $\boldsymbol{C}_B \equiv \boldsymbol{T}_B^{-T} \boldsymbol{c} + \boldsymbol{T}_B^{-T} \boldsymbol{M} \frac{d}{dt}(\boldsymbol{T}_B^{-1})$, and $\boldsymbol{g}_B \equiv \boldsymbol{T}_B^{-T} \boldsymbol{g}$. Since the contact (reaction) wrenches are assumed to act at the contact frames, the last term on the r.h.s. of (4.231) simplifies s.t. the equation of motion becomes

$$\boldsymbol{M}_B(\boldsymbol{q}) \begin{bmatrix} \dot{\mathcal{V}}_B \\ \dot{\mathcal{V}} \end{bmatrix} + \boldsymbol{C}_B(\boldsymbol{q}, \dot{\boldsymbol{q}}) \begin{bmatrix} \mathcal{V}_B \\ \mathcal{V} \end{bmatrix} + \boldsymbol{g}_B(\boldsymbol{q}) = \begin{bmatrix} -\mathbb{C}_B \\ \boldsymbol{E} \end{bmatrix} \boldsymbol{\mathcal{J}}_B^{-T} \boldsymbol{\tau} + \begin{bmatrix} \boldsymbol{0} \\ \boldsymbol{E} \end{bmatrix} \overline{\mathcal{F}}^c. \tag{4.232}$$

Note that there is a duality between this representation and (4.155) [47]. In the above representation, the joint torque appears in all equations while the contact wrenches appear only in the lower part. In (4.155) the situation is just the opposite: the contact wrenches appear in all equations while the joint torque appears only in the lower part. This duality can be useful in balance controller design, as will be clarified in Chapter 5 (see e.g. Section 5.10.6). Note also that the upper part of (4.232) is in the form of Lagrange–d'Alembert's formulation, (4.216). A drawback in the above notation is its limitation to nonredundant systems (because of the appearance of the inverse Jacobian). A balance controller based on the above transformation is presented in Section 5.13.2.

4.13.4 Summary and Discussion

There is a variety of reduced-form representations of the equation of motion. This variety stems from the subspaces and the respective transforms pertinent to both the kinetostatic and the dynamic interrelations. The understanding of these interrelations is quite important in view of a control algorithm design. The interrelations can be represented graphically via a characteristic map for the states of the system. An example of a characteristic map for the states of a dynamic model expressed in terms of the base quasivelocity is shown in Fig. 4.9. This map is actually an extension of Fig. 3.10, appearing at the end of Chapter 3. Recall that three transforms, the Jacobians $\boldsymbol{J}_B, \boldsymbol{\mathcal{J}}_{cB}$ and the contact map $\mathbb{C}_{cB}$, were designated as the fundamental kinetostatic transforms. The latter two transforms appear in both figures (shown with horizontal arrows).

Furthermore, in Fig. 4.9 also dynamic transforms are included (displayed with vertical and diagonal arrows). The vertical arrows reveal three *inertia-type* dynamic transforms, $\boldsymbol{M}_{\theta B}, \mathbb{M}_B$, and $\boldsymbol{M}_{cB}^{-1}$. These transforms act between the dual subspaces of the joint, end-link, and base-link spaces, in the direction from the motion ($\mathcal{M}$) to the force ($\mathcal{F} \equiv \mathcal{M}^*$) domain. They do not induce decompositions of the relevant subspaces. Obviously, $\boldsymbol{M}_{\theta B}$ and $\mathbb{M}_B$ play a fundamental role in the dynamic relations; $\boldsymbol{M}_{cB}$ is a derivative (cf. (4.207)). The diagonal arrows denote coupling inertia–type dynamic transforms (that express *mechanical connection maps* [86,109]). The transform from the joint-motion subspace to the base-link force subspace is represented by the coupling inertia matrix $\boldsymbol{H}_{BB}$. The dual transform, from the base-link motion subspace

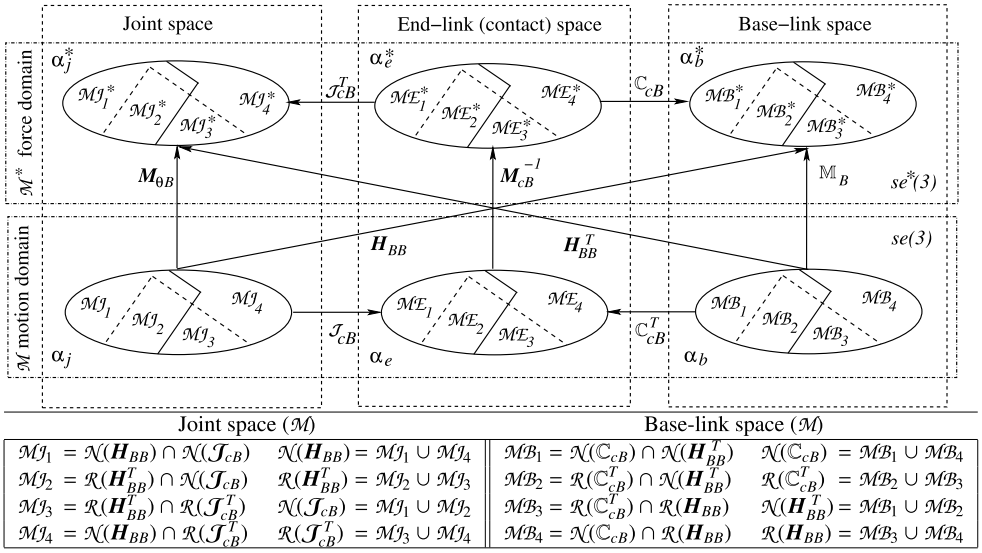

FIGURE 4.9 Characteristic map for the states of a dynamic model expressed in terms of the base quasivelocity. Right angles signify orthogonality decompositions within the motion and force subdomains, stemming from the fundamental transforms $\mathcal{J}_{cB}$, $\boldsymbol{J}$, and $\mathbb{C}_{cB}$ (kinetostatics) and $\boldsymbol{M}_{\theta B}$, $\mathbb{M}_B$, and $\boldsymbol{H}_{BB}$ (dynamics). The αs denote motion elements (velocities/accelerations), the α^*s are their duals (momenta/forces). The horizontal arrows signify the kinetostatic transforms. The vertical arrows denote the inertia-type motion-to-force dynamic transforms across the dual subspaces. The diagonal arrows stand for the coupling inertia–type motion-to-force transforms across the nondual subspaces (i.e. the mechanical connection [86,109]).

to the joint torque subspace, is represented by the transposed coupling inertia, $\boldsymbol{H}_{BB}^T$. The coupling-inertia transform does induce a decomposition of the relevant subspaces, as do the kinetostatic transforms.

To keep the presentation tractable, not all of the range and null spaces of the kinematic, kinetostatic, inertia, and coupling-inertia transforms are shown in Fig. 4.9. In the lower part of the figure, subdomains determined by the range and null spaces of the underlying transforms are shown for the motion subdomains within the joint and base-link subspaces. Similar relations can be obtained for the respective force subdomains. Representative dynamic states within the $\mathcal{MJ}$ domain are:

- $\alpha_{j1} \in \mathcal{MJ}_1$: motion component along the unconstrained motion directions induced by reactionless motion;
- $\alpha_{j2} \in \mathcal{MJ}_2$: motion component along the unconstrained motion directions induced by a motion with maximum inertial coupling;
- $\alpha_{j3} \in \mathcal{MJ}_3$: motion component along the constrained motion directions induced by a motion with maximum inertial coupling;
- $\alpha_{j4} \in \mathcal{MJ}_4$: motion component along the constrained motion directions induced by reactionless motion.

4.14 INVERSE DYNAMICS

A model-based control design makes use of inverse dynamic relations to determine the joint torque as control input. Sought are expressions for the joint torque that explicitly comprise components to be used for the realization of:

- end-link motion/force control,
- internal motion/force control,
- spatial dynamics control (i.e. CoM and angular momentum control).

In Section 4.13, a few ways of representing the equation of motion have been introduced. Depending on the notation, one or more of the above joint torque components may not be exhibited explicitly in the inverse dynamics solution. The following discussion is meant to provide an understanding about the choice of an appropriate notation in controller design.

4.14.1 Based on the Direct Elimination/Gauss/Maggi/Projection Methods

To derive the inverse dynamics solution, recall first that the generalized input force $\mathcal{Q} = \boldsymbol{S}^T \boldsymbol{\tau}$ is one of the components of the unconstrained generalized force $\mathcal{Q}_u$. The latter appears as a projection in the equations (i.e. as constraint maintaining force $\mathcal{Q}_m$ in (4.180) and (4.193)). In other words, the system is singular and underdetermined. To remove the c extra equations, make use of Maggi's approach (the null-space projection method). Applying transformations (4.199) to (4.180) yields

$$\boldsymbol{V}_r^T \mathcal{Q}_u = \boldsymbol{V}_r^T \left(\boldsymbol{M}\ddot{\boldsymbol{q}} + \boldsymbol{J}_c^T \boldsymbol{M}_c \dot{\boldsymbol{J}}_c \dot{\boldsymbol{q}} \right). \tag{4.233}$$

This is an undetermined linear system of $r = n + 6 - c$ equations in $n + 6$ unknowns. The general solution can be written as

$$\mathcal{Q}_u = \boldsymbol{V}_r \boldsymbol{V}_r^T \left(\boldsymbol{M}\ddot{\boldsymbol{q}} + \boldsymbol{J}_c^T \boldsymbol{M}_c \dot{\boldsymbol{J}}_c \dot{\boldsymbol{q}} \right) + \left(\boldsymbol{E} - \boldsymbol{V}_r \boldsymbol{V}_r^T \right) \mathcal{Q}_a, \tag{4.234}$$

whereby identities (4.190) were used. Since $\boldsymbol{N}^*$ is parametrized as in (4.192), the last equation can be rewritten as

$$\mathcal{Q} = \left(\boldsymbol{E} - \boldsymbol{J}_c^T \boldsymbol{J}_c^{-MT} \right) \boldsymbol{M}\ddot{\boldsymbol{q}} + \boldsymbol{J}_c^T \boldsymbol{J}_c^{-MT} \mathcal{Q}_a + \boldsymbol{c} + \boldsymbol{g}, \tag{4.235}$$

whereby the expression $\mathcal{Q}_u = \mathcal{Q} - \boldsymbol{c} - \boldsymbol{g}$ and the orthogonality relation

$$\left(\boldsymbol{E} - \boldsymbol{J}_c^T \boldsymbol{J}_c^{-MT} \right) \boldsymbol{J}_c^T \boldsymbol{M}_c = \boldsymbol{0}$$

were used. The joint torque can be obtained from the last n rows of solution (4.235), via the relation $\mathcal{Q} = \boldsymbol{S}^T \boldsymbol{\tau}$. This solution is characterized by simplicity, dynamic consistency, and instantaneous kinetic energy minimization. The quantities suitable as control inputs are the constraint-consistent generalized acceleration $\ddot{\boldsymbol{q}}$ and the arbitrary generalized force $\mathcal{Q}_a$. The former can be used for internal and/or end-link motion control, via the inverse kinematics.

It can also be used to control the tangential force. The latter is useful for internal and/or end-link force control (e.g. for reactive propulsion/manipulation). In such case, relations (4.194) will be violated, though, which implies a case of imperfect constraints. Note also that there is no explicit control input for the spatial dynamics. Nevertheless, the base link acceleration $\dot{\mathcal{V}}_B$, a component of constraint-consistent generalized acceleration $\ddot{\boldsymbol{q}}$, can be used to control these dynamics indirectly, via (4.99).

If the task of the robot does not require internal force control capability, $\mathcal{Q}_a$ in (4.235) can be set in accordance with (4.194). We have

$$\mathcal{Q} = \left(\boldsymbol{E} - \boldsymbol{J}_c^T \boldsymbol{J}_c^{-MT} \right) \boldsymbol{M}\ddot{\boldsymbol{q}} - \boldsymbol{J}_c^T \boldsymbol{M}_c \dot{\boldsymbol{J}}_c \dot{\boldsymbol{q}} + \boldsymbol{c} + \boldsymbol{g}. \tag{4.236}$$

This is the inverse dynamics solution in the case of ideal constraints. Only $\ddot{\boldsymbol{q}}$ is available as control input, the rest of the terms are nonlinear and state-dependent.

The inverse dynamics solution of a humanoid robot can also be obtained through the null-space projection method [124]. To this end, rewrite (4.200) as

$$\boldsymbol{V}_r^T \left(\boldsymbol{M}\ddot{\boldsymbol{q}} + \boldsymbol{c} + \boldsymbol{g} \right) = \boldsymbol{V}_r^T \boldsymbol{S}^T \boldsymbol{W}^{-\frac{1}{2}} \boldsymbol{W}^{\frac{1}{2}} \boldsymbol{\tau}, \tag{4.237}$$

where $\boldsymbol{W} \in \Re^{n \times n}$ is a p.d. weighting matrix. Solving for the joint torque, one arrives at

$$\boldsymbol{\tau} = \boldsymbol{V}^{\dagger} \boldsymbol{V}_r^T \left(\boldsymbol{M}\ddot{\boldsymbol{q}} + \boldsymbol{c} + \boldsymbol{g} \right) + \left(\boldsymbol{E} - \boldsymbol{V}^{\dagger} \boldsymbol{V}_r^T \boldsymbol{S}^T \right) \boldsymbol{\tau}_a, \tag{4.238}$$

where the generalized inverse $\boldsymbol{V}^{\dagger} = \boldsymbol{W}^{-\frac{1}{2}} \left(\boldsymbol{V}_r^T \boldsymbol{S}^T \boldsymbol{W}^{-\frac{1}{2}} \right)^{+} \in \Re^{n \times r}$ and the relations $\mathcal{Q}_u = \mathcal{Q} - \boldsymbol{c} - \boldsymbol{g}$, $\mathcal{Q} = \boldsymbol{S}^T \boldsymbol{\tau} = \begin{bmatrix} \boldsymbol{0} & \boldsymbol{\tau}^T \end{bmatrix}^T$ were used. The two orthogonal components on the r.h.s. are parametrized by $\boldsymbol{W}$. The normal component is also parametrized by the arbitrary joint torque vector $\boldsymbol{\tau}_a$. The parametrization can be used to minimize the joint torque $\boldsymbol{\tau}$ and, indirectly, the force of the constraint (the reactions). With the latter minimization, the direct handling of the inequality constraints pertinent to the friction cone can be avoided. This can be done either via minimization of the tangential contact forces, or by tracking a suitably designed reaction in the normal direction. No contact joint models thereby need to appear in the equation [124].

In the previous discussion, it was mentioned that the minimum null-space basis operator, $\boldsymbol{V}_r$, can be derived from the SVD of the system constraint matrix $\boldsymbol{J}_c$. It is possible to make use of other known decomposition methods, e.g. the QR factorization. The transpose of the system constraint Jacobian can be factorized as $\boldsymbol{J}_c^T = \boldsymbol{Q} \begin{bmatrix} \boldsymbol{R}^T & \boldsymbol{0} \end{bmatrix}^T$, whereby $\boldsymbol{R} \in \Re^{c \times c}$ and $\boldsymbol{Q} \in \Re^{(n+6) \times (n+6)}$ denote full-rank upper triangular and orthogonal matrices, respectively [77]. The latter can be decomposed as $\boldsymbol{Q} = \begin{bmatrix} \boldsymbol{Q}_c & \boldsymbol{Q}_r \end{bmatrix}$, whereby $\boldsymbol{Q}_r$ provides the minimum null-space basis. With this factorization/decomposition, the inverse dynamics solution attains exactly the same form as (4.238), wherein $\boldsymbol{V}_r$ is just replaced by $\boldsymbol{Q}_r$. Note also that Lagrange's multiplier vector (i.e. the reaction force) can be obtained in a straightforward manner, if needed, as follows:

$$\boldsymbol{\lambda} = \boldsymbol{R}^{-1} \boldsymbol{Q}_c^T \left(\boldsymbol{M}\ddot{\boldsymbol{q}} + \boldsymbol{c} + \boldsymbol{g} - \boldsymbol{S}^T \boldsymbol{\tau} \right). \tag{4.239}$$

Both results, (4.235) and (4.238), comprise two orthogonal components; they provide the base for a dynamic controller design. The latter solution has an advantage though: there is

no need at all to calculate the inverse $\boldsymbol{M}^{-1}$ that appears in the $\boldsymbol{J}_c^{-MT}$-term in (4.235). On the other hand, solution (4.238) does not guarantee the dynamic decoupling and kinetic energy minimization, as does (4.235). Also, solution (4.238) includes explicitly the $\boldsymbol{V}_r$ (or $\boldsymbol{Q}_r$) decomposition component. The decomposition imposes an additional computational burden.

4.14.2 Based on Lagrange–d'Alembert's Formulation

According to Lagrange–d'Alembert's representation of the equation of motion, (4.216), the joint torque can be derived from the following expression:

$$\mathcal{F}_B = \mathbb{C}_{cB}\boldsymbol{\mathcal{J}}_{cB}^{\#T}\boldsymbol{\tau}. \tag{4.240}$$

Solving for the joint torque, one arrives at

$$\begin{aligned}\boldsymbol{\tau} &= \boldsymbol{\mathcal{J}}_{cB}^T\mathbb{C}_{cB}^{\#}\mathcal{F}_B + \boldsymbol{\mathcal{J}}_{cB}^T\overline{\mathcal{F}}^n,\\ \overline{\mathcal{F}}^n &= (\boldsymbol{E} - \mathbb{C}_{cB}^{\#}\mathbb{C}_{cB})\overline{\mathcal{F}}_a^c.\end{aligned} \tag{4.241}$$

The net wrench acting at the base link, $\mathcal{F}_B$, is obtained from Lagrange–d'Alembert's formulation, as in (4.216); $\overline{\mathcal{F}}_a^c$ parametrizes the null space $\mathcal{N}(\mathbb{C}_{cB})$, i.e. the internal-wrench null space (cf. (3.62)). Evaluating this result from the prospective control viewpoint, it becomes apparent that two control components are explicitly present. The spatial dynamics and the internal wrench can be controlled with appropriate choices of $\mathcal{F}_B/\dot{\mathcal{V}}_B$ and $\overline{\mathcal{F}}_a^c$. On the other hand, note that there is no explicit component for the joint/end-link motion control.

4.14.3 Based on the Joint-Space Dynamics Elimination Approach

First, recall that equation of motion (4.210) represents a system of n equations. It is assumed that the number of joints n exceeds the number of constraints c. The difference $r = n - c$ denotes the degree of redundancy. The linear subsystem, determined by the (dual) null-space projection operator $\boldsymbol{N}^*(\boldsymbol{\mathcal{J}}_{cB}) = (\boldsymbol{E} - \boldsymbol{\mathcal{J}}_{cB}^T\boldsymbol{\mathcal{J}}_{cB}^{-M_{\theta B}T})$, is singular ($\text{rank}\boldsymbol{N}^*(\boldsymbol{\mathcal{J}}_{cB}) = r$) and, hence, underdetermined. To obtain the joint torque, the procedure used with the direct elimination approach will be applied. Accordingly, assume that $\boldsymbol{N}^*(\boldsymbol{\mathcal{J}}_{cB})$ is represented by $\boldsymbol{V}_{rB}\boldsymbol{V}_{rB}^T$, with an appropriate modification in the dimensions, i.e.

$$\boldsymbol{V}_{rB}\boldsymbol{V}_{rB}^T(\boldsymbol{\tau}_u - \boldsymbol{H}_{BB}^T\dot{\mathcal{V}}_B) = \boldsymbol{M}_{\theta B}\ddot{\boldsymbol{\theta}} + \boldsymbol{\mathcal{J}}_{cB}^T\left(\boldsymbol{\mathcal{J}}_{cB}\boldsymbol{M}_{\theta B}^{-1}\boldsymbol{\mathcal{J}}_{cB}^T\right)^{-1}\left(\boldsymbol{h}_{\theta B} + \mathbb{C}_{cB}^T\dot{\mathcal{V}}_B\right). \tag{4.242}$$

Then, reduce the dimension of the above equation to r by annihilating the extra c equations. This is accomplished by premultiplication with $\boldsymbol{V}_{rB}^T$. The resultant equation is solved for the joint torque of the unconstrained system, $\boldsymbol{\tau}_u$. We have

$$\begin{aligned}\boldsymbol{\tau}_u - \boldsymbol{H}_{BB}^T\dot{\mathcal{V}}_B &= \boldsymbol{V}_{rB}\boldsymbol{V}_{rB}^T\boldsymbol{M}_{\theta B}\ddot{\boldsymbol{\theta}}\\ &\quad + \boldsymbol{V}_{rB}\boldsymbol{V}_{rB}^T\boldsymbol{\mathcal{J}}_{cB}^T\left(\boldsymbol{\mathcal{J}}_{cB}\boldsymbol{M}_{\theta B}^{-1}\boldsymbol{\mathcal{J}}_{cB}^T\right)^{-1}\left(\boldsymbol{h}_{\theta B} + \mathbb{C}_{cB}^T\dot{\mathcal{V}}_B\right) + \boldsymbol{\mathcal{J}}_{cB}^T\boldsymbol{\mathcal{J}}_{cB}^{-M_{\theta B}T}\boldsymbol{\tau}_a,\end{aligned} \tag{4.243}$$

where $\boldsymbol{V}_{rB}^{+T} = \boldsymbol{V}_{rB}$ and $\boldsymbol{E} - \boldsymbol{V}_{rB}\boldsymbol{V}_{rB}^{T} = \boldsymbol{\mathcal{J}}_{cB}^{T}\boldsymbol{\mathcal{J}}_{cB}^{-M_{\theta B}T}$ were used. The input joint torque is then finally obtained as

$$\boldsymbol{\tau} = (\boldsymbol{E} - \boldsymbol{\mathcal{J}}_{cB}^{T}\boldsymbol{\mathcal{J}}_{cB}^{-M_{\theta B}T})\boldsymbol{M}_{\theta B}\ddot{\boldsymbol{\theta}} + \boldsymbol{H}_{BB}^{T}\dot{\mathcal{V}}_{B} + \boldsymbol{\mathcal{J}}_{cB}^{T}\overline{\mathcal{F}}_{a}^{c} + \boldsymbol{c}_{\theta B} + \boldsymbol{g}_{\theta}. \tag{4.244}$$

Hereby, the orthogonality relation $(\boldsymbol{E} - \boldsymbol{\mathcal{J}}_{cB}^{T}\boldsymbol{\mathcal{J}}_{cB}^{-M_{\theta B}T})\boldsymbol{\mathcal{J}}_{cB}^{T}(\boldsymbol{\mathcal{J}}_{cB}\boldsymbol{M}_{\theta B}^{-1}\boldsymbol{\mathcal{J}}_{cB}{}^{T})^{-1} = \boldsymbol{0}$ was used and the term $\boldsymbol{\mathcal{J}}_{cB}^{-M_{\theta B}T}\boldsymbol{\tau}_{a}$ was replaced with an arbitrary contact wrench $\overline{\mathcal{F}}_{a}^{c}$. The normal joint torque component $\boldsymbol{\mathcal{J}}_{cB}^{T}\overline{\mathcal{F}}_{a}^{c}$ can be used for reaction/internal and/or end-link force control. The constraint-consistent joint acceleration $\ddot{\boldsymbol{\theta}}$ is available for tangential force and/or internal motion control. It can also be used for the end-link motion control, via the inverse kinematic relations. Furthermore, it is apparent that $\boldsymbol{H}_{BB}^{T}\dot{\mathcal{V}}_{B}$, $\boldsymbol{c}_{\theta B}$, and $\boldsymbol{g}_{\theta}$ comprise both normal and tangential components. The latter two are usually compensated in the controller. The former term, on the other hand, represents a prospective control input for the base-link motion/spatial dynamics.

4.14.4 Summary and Conclusions

The inverse dynamics solutions are determined under the assumption that the state $(\boldsymbol{q}, \dot{\boldsymbol{q}}_{(\circ)})$, the generalized acceleration $\ddot{\boldsymbol{q}}_{(\circ)} = \begin{bmatrix} \dot{\mathcal{V}}_{(\circ)}^{T} & \ddot{\boldsymbol{\theta}}^{T} \end{bmatrix}^{T}$, and the contact forces $\overline{\mathcal{F}}^{c}$ are known. The state can be obtained either from the calculations during the previous time step in a simulator, or from sensor signals in the real robot. The generalized acceleration and the contact forces are usually determined as reference values that include feedforward and feedback terms in the controller. There are two major issues that need to be tackled. First, since humanoid robots are usually subjected to multiple motion/force task constraints, the system quite frequently may arrive at an overconstrained state (cf. the discussion in Section 2.8). At such a state, no solution to the inverse dynamics problem can be found. Second, the inequality constraints pertinent to the friction cone cannot be handled directly. There are a few ways to deal with these two problems. Two of them, the assignment of priorities (fixed or variable) among the tasks and the use of general solvers to handle inequality constraints, have been discussed in Chapter 2 from the kinetostatic point of view. Others, that are based on dynamic relations, will be introduced in Section 5.14.

Concluding this section, it should be noted that due to the significant computational cost, the complete model of a humanoid robot is most often used in off-line algorithms, mainly in simulators. Complete models also appear in both off-line and on-line motion generators. In the former case, for example, the so-called "dynamics filter" has been introduced to transform the captured (complex) whole-body movements of an actor into motions of a real robot [165,169,172]. In the latter case, the complete model can be used to confirm the correctness of the motion [155] or to compensate the errors generated when using a simple dynamic model [149]. Furthermore, complete models have also been used in the field of parameter identification [156,79,7]. Readers interested in an on-line implementation of a whole-body control approach with a resolved acceleration type controller are referred to [27].

References

[1] F. Aghili, A unified approach for inverse and direct dynamics of constrained multibody systems based on linear projection operator: applications to control and simulation, IEEE Transactions on Robotics 21 (2005) 834–849.
[2] A. Albu-Schaffer, O. Eiberger, M. Grebenstein, S. Haddadin, C. Ott, T. Wimbock, S. Wolf, G. Hirzinger, Soft robotics, IEEE Robotics & Automation Magazine 15 (2008) 20–30.
[3] A. Albu-Schaffer, C. Ott, U. Frese, G. Hirzinger, Cartesian impedance control of redundant robots: recent results with the DLR-light-weight-arms, in: 2003 IEEE International Conference on Robotics and Automation, IEEE, 2003, pp. 3704–3709 (Cat. No. 03CH37422).
[4] H. Arai, S. Tachi, Position control of manipulator with passive joints using dynamic coupling, IEEE Transactions on Robotics and Automation 7 (1991) 528–534.
[5] S. Arimoto, Control Theory of Non-Linear Mechanical Systems: A Passivity-Based and Circuit-Theoretic Approach, Clarendon Press, 1996.
[6] D. Asmar, B. Jalgha, A. Fakih, Humanoid fall avoidance using a mixture of strategies, International Journal of Humanoid Robotics 09 (2012) 1250002.
[7] K. Ayusawa, G. Venture, Y. Nakamura, Identifiability and identification of inertial parameters using the underactuated base-link dynamics for legged multibody systems, The International Journal of Robotics Research 33 (2014) 446–468.
[8] A. Balestrino, G. De Maria, L. Sciavicco, Adaptive control of manipulators in the task oriented space, in: 13th Int. Symp. Ind. Robots, 1983, pp. 131–146.
[9] E. Bayo, R. Ledesma, Augmented Lagrangian and mass-orthogonal projection methods for constrained multibody dynamics, Nonlinear Analysis 9 (1996) 113–130.
[10] B.J. Benda, P.O. Riley, D.E. Krebs, Biomechanical relationship between center of gravity and center of pressure during standing, IEEE Transactions on Rehabilitation Engineering 2 (1994) 3–10.
[11] W. Blajer, A geometric unification of constrained system dynamics, Multibody System Dynamics 1 (1997) 3–21.
[12] D.J. Block, K.J. Åström, M.W. Spong, The Reaction Wheel Pendulum, Morgan & Claypool Publishers, 2007.
[13] W. Book, O. Maizza-Neto, D. Whitney, Feedback control of two beam, two joint systems with distributed flexibility, Journal of Dynamic Systems, Measurement, and Control 97 (1975) 424.
[14] A. Bowling, S. Harmeyer, Repeatable redundant manipulator control using nullspace quasivelocities, Journal of Dynamic Systems, Measurement, and Control 132 (2010) 031007.
[15] R. Brockett, Asymptotic stability and feedback stabilization, in: R.W. Brockett, R.S. Millmann, H.J. Sussmann (Eds.), Differential Geometric Control Theory, Birkhäuser, Boston, Basel, Stuttgart, 1983, pp. 181–191.
[16] H. Bruyninckx, O. Khatib, Gauss' principle and the dynamics of redundant and constrained manipulators, in: IEEE International Conference on Robotics and Automation, 2000, pp. 2563–2568.
[17] M. Carpenter, M.A. Peck, Reducing base reactions with gyroscopic actuation of space-robotic systems, IEEE Transactions on Robotics 25 (2009) 1262–1270.
[18] M. Cefalo, G. Oriolo, M. Vendittelli, Planning safe cyclic motions under repetitive task constraints, in: IEEE International Conference on Robotics and Automation, 2013, pp. 3807–3812.
[19] K.-S. Chang, O. Khatib, Efficient algorithm for extended operational space inertia matrix, in: IEEE/RSJ International Conference on Intelligent Robots and Systems, 1999, pp. 350–355.
[20] N.a. Chaturvedi, N.H. McClamroch, D.S. Bernstein, Asymptotic smooth stabilization of the inverted 3-D pendulum, IEEE Transactions on Automatic Control 54 (2009) 1204–1215.
[21] C. Chevallereau, E. Westervelt, J.W. Grizzle, Asymptotically stable running for a five-link, four-actuator, planar bipedal robot, The International Journal of Robotics Research 24 (2005) 431–464.
[22] Y. Choi, D. Kim, Y. Oh, B.-j. You, Posture/walking control for humanoid robot based on kinematic resolution of CoM Jacobian with embedded motion, IEEE Transactions on Robotics 23 (2007) 1285–1293.
[23] Y. Choi, B.-j. You, S.-r. Oh, On the stability of indirect ZMP controller for biped robot systems, in: IEEE/RSJ International Conference on Intelligent Robots and Systems (IROS), 2004, pp. 1966–1971.
[24] J. Craig, Introduction to Robotics: Mechanics & Control, 3rd edition, Prentice Hall, 2004.
[25] R.H. Crompton, L. Yu, W. Weijie, M. Günther, R. Savage, The mechanical effectiveness of erect and "bent-hip, bent-knee" bipedal walking in Australopithecus afarensis, Journal of Human Evolution 35 (1998) 55–74.
[26] H. Dai, A. Valenzuela, R. Tedrake, Whole-body motion planning with centroidal dynamics and full kinematics, in: IEEE-RAS International Conference on Humanoid Robots, Madrid, Spain, 2014, pp. 295–302.
[27] B. Dariush, G.B. Hammam, D. Orin, Constrained resolved acceleration control for humanoids, in: IEEE/RSJ International Conference on Intelligent Robots and Systems, 2010, pp. 710–717.

[28] V. De Sapio, O. Khatib, Operational space control of multibody systems with explicit holonomic constraints, in: IEEE International Conference on Robotics and Automation, 2005, pp. 2950–2956.
[29] A. Dietrich, C. Ott, A. Albu-Schaffer, Multi-objective compliance control of redundant manipulators: hierarchy, control, and stability, in: IEEE/RSJ International Conference on Intelligent Robots and Systems, IEEE, 2013, pp. 3043–3050.
[30] J. Englsberger, A. Werner, C. Ott, B. Henze, M.A. Roa, G. Garofalo, R. Burger, A. Beyer, O. Eiberger, K. Schmid, A. Albu-Schaffer, Overview of the torque-controlled humanoid robot TORO, in: IEEE-RAS International Conference on Humanoid Robots, IEEE, Madrid, Spain, 2014, pp. 916–923.
[31] I. Fantoni, R. Lozano, M.W. Spong, Energy based control of the pendubot, IEEE Transactions on Automatic Control 45 (2000) 725–729.
[32] R. Featherstone, Rigid Body Dynamics Algorithms, Springer Science+Business Media, LLC, Boston, MA, 2008.
[33] R. Featherstone, O. Khatib, Load independence of the dynamically consistent inverse of the Jacobian matrix, The International Journal of Robotics Research 16 (1997) 168–170.
[34] C. Fitzgerald, Developing baxter, in: IEEE Conference on Technologies for Practical Robot Applications, 2013, pp. 1–6.
[35] Y. Fujimoto, A. Kawamura, Simulation of an autonomous biped walking robot including environmental force interaction, IEEE Robotics & Automation Magazine 5 (1998) 33–42.
[36] M. Gajamohan, M. Merz, I. Thommen, R. D'Andrea, The Cubli: a cube that can jump up and balance, in: IEEE/RSJ International Conference on Intelligent Robots and Systems, 2012, pp. 3722–3727.
[37] C.F. Gauß, Über ein neues allgemeines Grundgesetz der Mechanik, Journal für die Reine und Angewandte Mathematik 4 (1829).
[38] J.M. Gilbert, Gyrobot: control of multiple degree of freedom underactuated mechanisms using a gyrating link and cyclic braking, IEEE Transactions on Robotics 23 (2007) 822–827.
[39] A. Goswami, Postural stability of biped robots and the foot-rotation indicator (FRI) point, The International Journal of Robotics Research 18 (1999) 523–533.
[40] A. Goswami, V. Kallem, Rate of change of angular momentum and balance maintenance of biped robots, in: IEEE International Conference on Robotics and Automation, New Orleans, LA, USA, 2004, pp. 3785–3790.
[41] J. Grizzle, Planar bipedal robot with impulsive foot action, in: IEEE Conf. on Decision and Control, Atlantis, Paradise Island, Bahamas, 2004, pp. 296–302.
[42] M. Hara, D. Nenchev, Body roll reorientation via cyclic arm motion in zero gravity, Robotic Life Support Laboratory, Tokyo City University, 2017 (Video clip), https://doi.org/10.1016/B978-0-12-804560-2.00011-0.
[43] M. Hara, D. Nenchev, Object tracking with a humanoid robot in zero gravity (asynchronous leg motion in two phases), Robotic Life Support Laboratory, Tokyo City University, 2017 (Video clip), https://doi.org/10.1016/B978-0-12-804560-2.00011-0.
[44] M. Hara, D. Nenchev, Object tracking with a humanoid robot in zero gravity (asynchronous leg motion), Robotic Life Support Laboratory, Tokyo City University, 2017 (Video clip), https://doi.org/10.1016/B978-0-12-804560-2.00011-0.
[45] M. Hara, D. Nenchev, Object tracking with a humanoid robot in zero gravity (synchronous leg motion), Robotic Life Support Laboratory, Tokyo City University, 2017 (Video clip), https://doi.org/10.1016/B978-0-12-804560-2.00011-0.
[46] J. Hauser, R.M. Murray, Nonlinear controllers for non-integrable systems: the Acrobot example, in: 1990 American Control Conference, 1990, pp. 669–671.
[47] B. Henze, M.A. Roa, C. Ott, Passivity-based whole-body balancing for torque-controlled humanoid robots in multi-contact scenarios, The International Journal of Robotics Research 35 (2016) 1522–1543.
[48] G. Hirzinger, N. Sporer, A. Albu-Schaffer, M. Hahnle, R. Krenn, A. Pascucci, M. Schedl, DLR's torque-controlled light weight robot III-are we reaching the technological limits now?, in: IEEE International Conference on Robotics and Automation, 2002, pp. 1710–1716.
[49] N. Hogan, Impedance control: an approach to manipulation, in: American Control Conference, 1984, pp. 304–313.
[50] N. Hogan, Impedance control: an approach to manipulation: Part I–theory, Journal of Dynamic Systems, Measurement, and Control 107 (1985) 1.
[51] J.M. Hollerbach, Ki C. Suh, Redundancy resolution of manipulators through torque optimization, IEEE Journal on Robotics and Automation 3 (1987) 308–316.

[52] K. Iqbal, Y.-c. Pai, Predicted region of stability for balance recovery: motion at the knee joint can improve termination of forward movement, Journal of Biomechanics 33 (2000) 1619–1627.
[53] A. Jain, G. Rodriguez, An analysis of the kinematics and dynamics of underactuated manipulators, IEEE Transactions on Robotics and Automation 9 (1993) 411–422.
[54] S. Kajita, H. Hirukawa, K. Harada, K. Yokoi, Introduction to Humanoid Robotics, Springer Verlag, Berlin, Heidelberg, 2014.
[55] S. Kajita, F. Kanehiro, K. Kaneko, K. Fujiwara, K. Harada, K. Yokoi, H. Hirukawa, Biped walking pattern generation by using preview control of zero-moment point, in: IEEE International Conference on Robotics and Automation, 2003, pp. 1620–1626.
[56] S. Kajita, F. Kanehiro, K. Kaneko, K. Fujiwara, K. Harada, K. Yokoi, H. Hirukawa, Resolved momentum control: humanoid motion planning based on the linear and angular momentum, in: IEEE/RSJ International Conference on Intelligent Robots and Systems, Las Vegas, Nevada, 2003, pp. 1644–1650.
[57] S. Kajita, F. Kanehiro, K. Kaneko, K. Fujiwara, K. Harada, K. Yokoi, H. Hirukawa, Resolved momentum control: motion generation of a humanoid robot based on the linear and angular momenta, Journal of the Robotics Society of Japan 22 (2004) 772–779.
[58] S. Kajita, T. Yamaura, A. Kobayashi, Dynamic walking control of a biped robot along a potential energy conserving orbit, IEEE Transactions on Robotics and Automation 8 (1992) 431–438.
[59] R.E. Kalaba, F.E. Udwadia, Equations of motion for nonholonomic, constrained dynamical systems via Gauss's principle, ASME Journal of Applied Mechanics 60 (1993) 662–668.
[60] O. Khatib, A unified approach for motion and force control of robot manipulators: the operational space formulation, IEEE Journal on Robotics and Automation 3 (1987) 43–53.
[61] O. Khatib, Inertial properties in robotic manipulation: an object-level framework, The International Journal of Robotics Research 14 (1995) 19–36.
[62] T. Komura, H. Leung, J. Kuffner, S. Kudoh, J. Kuffner, A feedback controller for biped humanoids that can counteract large perturbations during gait, in: IEEE International Conference on Robotics and Automation, 2005, pp. 1989–1995.
[63] A. Konno, M. Uchiyama, M. Murakami, Configuration-dependent vibration controllability of flexible-link manipulators, The International Journal of Robotics Research 16 (1997) 567–576.
[64] T. Koolen, T. de Boer, J. Rebula, A. Goswami, J. Pratt, Capturability-based analysis and control of legged locomotion, Part 1: theory and application to three simple gait models, The International Journal of Robotics Research 31 (2012) 1094–1113.
[65] C. Lanczos, The Variational Principles of Mechanics, Dover Publications, 1970, 4th, 1986 edition.
[66] A. Laulusa, O.A. Bauchau, Review of classical approaches for constraint enforcement in multibody systems, Journal of Computational and Nonlinear Dynamics 3 (2008) 011004.
[67] S.-H. Lee, A. Goswami, Reaction Mass Pendulum (RMP): an explicit model for centroidal angular momentum of humanoid robots, in: IEEE International Conference on Robotics and Automation, 2007, pp. 4667–4672.
[68] S.-H. Lee, A. Goswami, The reaction mass pendulum (RMP) model for humanoid robot gait and balance control, in: B. Choi (Ed.), Humanoid Robots, InTech, 2009, p. 396, chapter 9.
[69] S.-H.H. Lee, A. Goswami, A momentum-based balance controller for humanoid robots on non-level and non-stationary ground, Autonomous Robots 33 (2012) 399–414.
[70] L. Lilov, M. Lorer, Dynamic analysis of multirigid-body system based on the gauss principle, ZAMM – Zeitschrift für Angewandte Mathematik und Mechanik 62 (1982) 539–545.
[71] H.-o. Lim, Y. Kaneshima, A. Takanishi, Online walking pattern generation for biped humanoid robot with trunk, in: IEEE International Conference on Robotics and Automation, Washington, DC, USA, 2002, pp. 3111–3116.
[72] J. Luh, M. Walker, R. Paul, Resolved-acceleration control of mechanical manipulators, IEEE Transactions on Automatic Control 25 (1980) 468–474.
[73] S. Ma, D.N. Nenchev, Local torque minimization for redundant manipulators: a correct formulation, Robotica 14 (1996) 235–239.
[74] A. Maciejewski, Kinetic limitations on the use of redundancy in robotic manipulators, IEEE Transactions on Robotics and Automation 7 (1991) 205–210.
[75] R. Marino, M.W. Spong, Nonlinear control techniques for flexible joint manipulators: a single link case study, in: 1986 IEEE International Conference on Robotics and Automation, 1986, pp. 1030–1036.

[76] J. Mayr, F. Spanlang, H. Gattringer, Mechatronic design of a self-balancing three-dimensional inertia wheel pendulum, Mechatronics 30 (2015) 1–10.
[77] M. Mistry, J. Buchli, S. Schaal, Inverse dynamics control of floating base systems using orthogonal decomposition, in: IEEE International Conference on Robotics and Automation, IEEE, Anchorage, AK, USA, 2010, pp. 3406–3412.
[78] M. Mistry, L. Righetti, Operational space control of constrained and underactuated systems, in: H. Durrant-Whyte, N. Roy, P. Abbeel (Eds.), Robotics: Science and Systems VII, MIT Press, 2012, pp. 225–232.
[79] M. Mistry, S. Schaal, K. Yamane, Inertial parameter estimation of floating base humanoid systems using partial force sensing, in: IEEE-RAS International Conference on Humanoid Robots, Paris, France, 2009, pp. 492–497.
[80] K. Mitobe, G. Capi, Y. Nasu, Control of walking robots based on manipulation of the zero moment point, Robotica 18 (2000) 651–657.
[81] K. Mitobe, G. Capi, Y. Nasu, A new control method for walking robots based on angular momentum, Mechatronics 14 (2004) 163–174.
[82] S. Miyahara, D. Nenchev, Walking in zero gravity, Robotic Life Support Laboratory, Tokyo City University, 2017 (Video clip), https://doi.org/10.1016/B978-0-12-804560-2.00011-0.
[83] M. Muehlebach, G. Mohanarajah, R. D'Andrea, Nonlinear analysis and control of a reaction wheel-based 3D inverted pendulum, in: 52nd IEEE Conference on Decision and Control, Florence, Italy, 2013, pp. 1283–1288.
[84] A. Müller, Motion equations in redundant coordinates with application to inverse dynamics of constrained mechanical systems, Nonlinear Dynamics 67 (2011) 2527–2541.
[85] M.P. Murray, A. Seireg, R.C. Scholz, Center of gravity, center of pressure, and supportive forces during human activities, Journal of Applied Physiology 23 (1967) 831–838.
[86] R.M. Murray, Nonlinear control of mechanical systems: a Lagrangian perspective, Annual Reviews in Control 21 (1997) 31–42.
[87] R.M. Murray, Z. Li, S.S. Sastry, A Mathematical Introduction to Robotic Manipulation, CRC Press, 1994.
[88] Y. Nakamura, T. Suzuki, M. Koinuma, Nonlinear behavior and control of a nonholonomic free-joint manipulator, IEEE Transactions on Robotics and Automation 13 (1997) 853–862.
[89] N. Naksuk, Y. Mei, C. Lee, Humanoid trajectory generation: an iterative approach based on movement and angular momentum criteria, in: IEEE/RAS International Conference on Humanoid Robots, Los Angeles, CA, USA, 2004, pp. 576–591.
[90] C. Natale, B. Siciliano, L. Villani, Spatial impedance control of redundant manipulators, in: IEEE International Conference on Robotics and Automation, 1999, pp. 1788–1793.
[91] B. Nemec, L. Zlajpah, Null space velocity control with dynamically consistent pseudo-inverse, Robotica 18 (2000) 513–518.
[92] D. Nenchev, Restricted Jacobian matrices of redundant manipulators in constrained motion tasks, The International Journal of Robotics Research 11 (1992) 584–597.
[93] D. Nenchev, A controller for a redundant free-flying space robot with spacecraft attitude/manipulator motion coordination, in: IEEE/RSJ International Conference on Intelligent Robots and Systems, 1993, pp. 2108–2114.
[94] D. Nenchev, Y. Umetani, K. Yoshida, Analysis of a redundant free-flying spacecraft/manipulator system, IEEE Transactions on Robotics and Automation 8 (1992) 1–6.
[95] D. Nenchev, K. Yoshida, Impact analysis and post-impact motion control issues of a free-floating space robot subject to a force impulse, IEEE Transactions on Robotics and Automation 15 (1999) 548–557.
[96] D. Nenchev, K. Yoshida, M. Uchiyama, Reaction null-space based control of flexible structure mounted manipulator systems, in: 5th IEEE Conference on Decision and Control, Kobe, Japan, 1996, pp. 4118–4123.
[97] D. Nenchev, K. Yoshida, Y. Umetani, Introduction of redundant arms for manipulation in space, in: IEEE International Workshop on Intelligent Robots, 1988, pp. 679–684.
[98] D. Nenchev, K. Yoshida, Y. Umetani, Analysis, design and control of free-flying space robots using fixed-attitude-restricted Jacobian matrix, in: The Fifth International Symposium on Robotics Research, MIT Press, Cambridge, MA, USA, 1990, pp. 251–258.
[99] D. Nenchev, K. Yoshida, P. Vichitkulsawat, M. Uchiyama, Reaction null-space control of flexible structure mounted manipulator systems, IEEE Transactions on Robotics and Automation 15 (1999) 1011–1023.
[100] D.N. Nenchev, Reaction null space of a multibody system with applications in robotics, Mechanical Sciences 4 (2013) 97–112.
[101] D.N. Nenchev, A. Nishio, Ankle and hip strategies for balance recovery of a biped subjected to an impact, Robotica 26 (2008) 643–653.

[102] A. Nishio, K. Takahashi, D. Nenchev, Balance control of a humanoid robot based on the reaction null space method, in: IEEE/RSJ Int. Conf. on Intelligent Robots and Systems, Beijing, China, 2006, pp. 1996–2001.
[103] K. Nishizawa, D. Nenchev, Body roll reorientation via cyclic foot motion in zero gravity, Robotic Life Support Laboratory, Tokyo City University, 2017 (Video clip), https://doi.org/10.1016/B978-0-12-804560-2.00011-0.
[104] R. Olfati-Saber, Nonlinear Control of Underactuated Mechanical Systems with Application to Robotics and Aerospace Vehicles, Ph.D. thesis, MIT, 2001.
[105] K. O'Neil, Divergence of linear acceleration-based redundancy resolution schemes, IEEE Transactions on Robotics and Automation 18 (2002) 625–631.
[106] D.E. Orin, A. Goswami, Centroidal momentum matrix of a humanoid robot: structure and properties, in: IEEE/RSJ International Conference on Intelligent Robots and Systems, IROS, Nice, France, 2008, pp. 653–659.
[107] D.E. Orin, A. Goswami, S.H. Lee, Centroidal dynamics of a humanoid robot, Autonomous Robots 35 (2013) 161–176.
[108] V. Ortenzi, M. Adjigble, J.A. Kuo, R. Stolkin, M. Mistry, An experimental study of robot control during environmental contacts based on projected operational space dynamics, in: IEEE-RAS International Conference on Humanoid Robots, Madrid, Spain, 2014, pp. 407–412.
[109] J.P. Ostrowski, Computing reduced equations for robotic systems with constraints and symmetries, IEEE Transactions on Robotics and Automation 15 (1999) 111–123.
[110] K. Osuka, T. Nohara, Attitude control of torque unit manipulator via trajectory planning – treatment as a nonholonomic system, Journal of the Robotics Society of Japan 18 (2000) 612–615 (in Japanese).
[111] K. Osuka, K. Yoshida, T. Ono, New design concept of space manipulator: a proposal of torque-unit manipulator, in: 33rd IEEE Conference on Decision and Control, 1994, pp. 1823–1825.
[112] C. Ott, A. Kugi, Y. Nakamura, Resolving the problem of non-integrability of nullspace velocities for compliance control of redundant manipulators by using semi-definite Lyapunov functions, in: IEEE International Conference on Robotics and Automation, 2008, pp. 1999–2004.
[113] Y.-c. Pai, J. Patton, Center of mass velocity-position predictions for balance control, Journal of Biomechanics 30 (1997) 347–354.
[114] J.G. Papastavridis, Maggi's equations of motion and the determination of constraint reactions, Journal of Guidance, Control, and Dynamics 13 (1990) 213–220.
[115] J. Park, Control Strategies for Robots in Contact, Ph.D. thesis, Stanford University, USA, 2006.
[116] J. Park, W. Chung, Y. Youm, On dynamical decoupling of kinematically redundant manipulators, in: IEEE/RSJ International Conference on Intelligent Robots and Systems, 1999, pp. 1495–1500.
[117] E. Popov, A. Vereschagin, S. Zenkevich, Manipulating Robots. Dynamics and Algorithms, Nauka, Moscow, USSR, 1978 (in Russian).
[118] M. Popovic, A. Hofmann, H. Herr, Angular momentum regulation during human walking: biomechanics and control, in: IEEE International Conference on Robotics and Automation, 2004, pp. 2405–2411.
[119] M. Popovic, A. Hofmann, H. Herr, Zero spin angular momentum control: definition and applicability, in: IEEE/RAS International Conference on Humanoid Robots, 2004, pp. 478–493.
[120] M.B. Popovic, A. Goswami, H. Herr, Ground reference points in legged locomotion: definitions, biological trajectories and control implications, The International Journal of Robotics Research 24 (2005) 1013–1032.
[121] J. Pratt, J. Carff, S. Drakunov, A. Goswami, Capture point: a step toward humanoid push recovery, in: IEEE-RAS International Conference on Humanoid Robots, Genoa, Italy, 2006, pp. 200–207.
[122] R.D. Quinn, J. Chen, C. Lawrence, Redundant manipulators for momentum compensation in a micro-gravity environment, in: AIAA Guidance, Navigation and Control Conference, 1988, AIAA PAPER 88-4121.
[123] M. Reyhanoglu, A. van der Schaft, N.H. McClamroch, I. Kolmanovsky, Dynamics and control of a class of underactuated mechanical systems, IEEE Transactions on Automatic Control 44 (1999) 1663–1671.
[124] L. Righetti, J. Buchli, M. Mistry, M. Kalakrishnan, S. Schaal, Optimal distribution of contact forces with inverse-dynamics control, The International Journal of Robotics Research 32 (2013) 280–298.
[125] L. Righetti, J. Buchli, M. Mistry, S. Schaal, Inverse dynamics control of floating-base robots with external constraints: a unified view, in: IEEE International Conference on Robotics and Automation, IEEE, 2011, pp. 1085–1090.
[126] N. Rotella, M. Bloesch, L. Righetti, S. Schaal, State estimation for a humanoid robot, in: IEEE/RSJ International Conference on Intelligent Robots and Systems, 2014, pp. 952–958.
[127] H. Sadeghian, L. Villani, M. Keshmiri, B. Siciliano, Dynamic multi-priority control in redundant robotic systems, Robotica 31 (2013) 1–13.

[128] A. Sano, J. Furusho, Realization of natural dynamic walking using the angular momentum information, in: IEEE International Conference on Robotics and Automation, Tsukuba, Japan, 1990, pp. 1476–1481.
[129] A. Sano, J. Furusho, Control of torque distribution for the BLR-G2 biped robot, in: Fifth International Conference on Advanced Robotics, vol. 1, IEEE, 1991, pp. 729–734.
[130] A.K. Sanyal, A. Goswami, Dynamics and balance control of the reaction mass pendulum: a three-dimensional multibody pendulum with variable body inertia, Journal of Dynamic Systems, Measurement, and Control 136 (2014) 021002.
[131] L. Sentis, Synthesis and Control of Whole-Body Behaviors in Humanoid Systems, Ph.D. thesis, Standford University, 2007.
[132] L. Sentis, O. Khatib, Control of free-floating humanoid robots through task prioritization, in: IEEE International Conference on Robotics and Automation, IEEE, 2005, pp. 1718–1723.
[133] L. Sentis, O. Khatib, Compliant control of multicontact and center-of-mass behaviors in humanoid robots, IEEE Transactions on Robotics 26 (2010) 483–501.
[134] J.S.J. Shen, A. Sanyal, N. Chaturvedi, D. Bernstein, H. McClamroch, Dynamics and control of a 3D pendulum, in: 43rd IEEE Conference on Decision and Control, Nassau, Bahamas, 2004, pp. 323–328.
[135] N.E. Sian, K. Yokoi, S. Kajita, F. Kanehiro, K. Tanie, Whole body teleoperation of a humanoid robot – a method of integrating operator's intention and robot's autonomy, in: IEEE International Conference on Robotics and Automation, 2003, pp. 1613–1619.
[136] M.W. Spong, Underactuated mechanical systems, in: Control Problems in Robotics and Automation, Springer-Verlag, London, 1998, pp. 135–150.
[137] M.W. Spong, D.J. Block, The Pendubot: a mechatronic system for control research and education, in: 1995 34th IEEE Conference on Decision and Control, New Orleans, LA, USA, 1995, pp. 555–556.
[138] M.W. Spong, P. Corke, R. Lozano, Nonlinear control of the reaction wheel pendulum, Automatica 37 (2001) 1845–1851.
[139] M.W. Spong, S. Hutchinson, M. Vidyasagar, Robot Modeling and Control, Wiley, 2006.
[140] M.W.M. Spong, Partial feedback linearization of underactuated mechanical systems, in: IEEE/RSJ International Conference on Intelligent Robots and Systems, IEEE, 1994, pp. 314–321.
[141] K. Sreenath, A.K. Sanyal, The reaction mass biped: equations of motion, hybrid model for walking and trajectory tracking control, in: IEEE International Conference on Robotics and Automation, 2015, pp. 5741–5746.
[142] L. Stirling, K. Willcox, D. Newman, Development of a computational model for astronaut reorientation, Journal of Biomechanics 43 (2010) 2309–2314.
[143] L.A. Stirling, Development of Astronaut Reorientation Methods, Ph.D. thesis, MIT, 2008.
[144] T. Sugihara, Y. Nakamura, H. Inoue, Real-time humanoid motion generation through ZMP manipulation based on inverted pendulum control, in: IEEE Int. Conf. on Robotics and Automation, Washington, DC, 2002, pp. 1404–1409.
[145] A. Takanishi, M. Ishida, Y. Yamazaki, I. Kato, The realization of dynamic walking by the biped walking robot WL-10RD, Journal of the Robotics Society of Japan 3 (1985) 325–336.
[146] A. Takanishi, H.-o. Lim, M. Tsuda, I. Kato, Realization of dynamic biped walking stabilized by trunk motion on a sagittally uneven surface, in: IEEE International Workshop on Intelligent Robots and Systems, 1990, pp. 323–330.
[147] T. Takenaka, T. Matsumoto, T. Yoshiike, Real time motion generation and control for biped robot – 3rd report: dynamics error compensation, in: IEEE/RSJ International Conference on Intelligent Robots and Systems, St. Louis, USA, 2009, pp. 1594–1600.
[148] T. Takenaka, T. Matsumoto, T. Yoshiike, T. Hasegawa, S. Shirokura, H. Kaneko, A. Orita, Real time motion generation and control for biped robot – 4th report: integrated balance control, in: IEEE/RSJ Int. Conf. on Intelligent Robots and System, 2009, pp. 1601–1608.
[149] T. Takenaka, T. Matsumoto, T. Yoshiike, S. Shirokura, Real time motion generation and control for biped robot – 2nd report: running gait pattern generation, in: IEEE/RSJ International Conference on Intelligent Robots and Systems, 2009, pp. 1092–1099.
[150] N.G. Tsagarakis, S. Morfey, G. Medrano Cerda, Z. Li, D.G. Caldwell, COMpliant huMANoid COMAN: optimal joint stiffness tuning for modal frequency control, in: 2013 IEEE International Conference on Robotics and Automation, 2013, pp. 673–678.
[151] F.-C. Tseng, Z.-D. Ma, G.M. Hulbert, Efficient numerical solution of constrained multibody dynamics systems, Computer Methods in Applied Mechanics and Engineering 192 (2003) 439–472.

[152] B. Ugurlu, A. Kawamura, Bipedal trajectory generation based on combining inertial forces and intrinsic angular momentum rate changes: Eulerian ZMP resolution, IEEE Transactions on Robotics 28 (2012) 1406–1415.
[153] Y. Umetani, K. Yoshida, Resolved motion rate control of space manipulators with generalized Jacobian matrix, IEEE Transactions on Robotics and Automation 5 (1989) 303–314.
[154] Z. Vafa, S. Dubowsky, On the dynamics of manipulators in space using the virtual manipulator approach, in: IEEE International Conference on Robotics and Automation, 1987, pp. 579–585.
[155] B. Vanderborght, B. Verrelst, R. Van Ham, M. Van Damme, D. Lefeber, Objective locomotion parameters based inverted pendulum trajectory generator, Robotics and Autonomous Systems 56 (2008) 738–750.
[156] G. Venture, K. Ayusawa, Y. Nakamura, Dynamics identification of humanoid systems, in: CISM-IFToMM Symp. on Robot Design, Dynamics, and Control, ROMANSY, 2008, pp. 301–308.
[157] M. Vukobratović, Contribution to the study of anthropomorphic systems, Kybernetika 8 (1972) 404–418.
[158] M. Vukobratovic, B. Borovac, Zero-moment point – thirty five years of its life, International Journal of Humanoid Robotics 01 (2004) 157–173.
[159] M. Vukobratović, A.A. Frank, D. Juricić, On the stability of biped locomotion, IEEE Transactions on Bio-Medical Engineering 17 (1970) 25–36.
[160] P.M. Wensing, L.R. Palmer, D.E. Orin, Efficient recursive dynamics algorithms for operational-space control with application to legged locomotion, Autonomous Robots 38 (2015) 363–381.
[161] P.-B. Wieber, Holonomy and nonholonomy in the dynamics of articulated motion, in: M. Diehl, K. Mombaur (Eds.), Fast Motions in Biomechanics and Robotics, Springer-Verlag, Berlin, Heidelberg, 2006, pp. 411–425, Lecture no edition.
[162] D. Winter, Human balance and posture control during standing and walking, Gait & Posture 3 (1995) 193–214.
[163] Y. Xu, T. Kanade (Eds.), Space Robotics: Dynamics and Control, The Kluwer International Series in Engineering and Computer Science, vol. 188, Springer US, Boston, MA, 1993.
[164] K. Yamada, K. Tsuchiya, Force control of a space manipulator, in: i-SAIRAS, Kobe, Japan, 1990, pp. 255–258.
[165] K. Yamane, Y. Nakamura, Dynamics filter – concept and implementation of online motion generator for human figures, IEEE Transactions on Robotics and Automation 19 (2003) 421–432.
[166] R. Yang, Y.-Y. Kuen, Z. Li, Stabilization of a 2-DOF spherical pendulum on X-Y table, in: IEEE International Conference on Control Applications, 2000, pp. 724–729.
[167] K. Yoshida, D. Nenchev, A general formulation of under-actuated manipulator systems, in: S. Hirose, Y. Shirai (Eds.), Robotics Research: The 8th International Symposium, Springer, London, New York, 1997, pp. 72–79.
[168] Y. Yoshida, K. Takeuchi, Y. Miyamoto, D. Sato, D.N. Nenchev, Postural balance strategies in response to disturbances in the frontal plane and their implementation with a humanoid robot, IEEE Transactions on Systems, Man, and Cybernetics: Systems 44 (2014) 692–704.
[169] Y. Zheng, K. Yamane, Human motion tracking control with strict contact force constraints for floating-base humanoid robots, in: IEEE-RAS International Conference on Humanoid Robots, IEEE, Atlanta, GA, USA, 2013, pp. 34–41.
[170] Y. Zhang, D. Guo, S. Ma, Different-level simultaneous minimization of joint-velocity and joint-torque for redundant robot manipulators, Journal of Intelligent & Robotic Systems 72 (2013) 301–323.
[171] Y. Zhao, L. Sentis, A three dimensional foot placement planner for locomotion in very rough terrains, in: IEEE-RAS International Conference on Humanoid Robots, Humanoids 2012, IEEE, 2012, pp. 726–733.
[172] Y. Zheng, K. Yamane, Adapting human motions to humanoid robots through time warping based on a general motion feasibility index, in: IEEE International Conference on Robotics and Automation, IEEE, 2015, pp. 6281–6288.